การพัฒนาระบบการวิเคราะห์แบบย่อส่วน
เพื่อการตรวจวัดสารประกอบอินทรีย์และโลหะหนัก

นายภูมิรัตน์ รัตนรัตน

วิทยานิพนธ์นี้เป็นส่วนหนึ่งของการศึกษาตามหลักสูตรปริญญาวิทยาศาสตรดุษฎีบัณฑิต
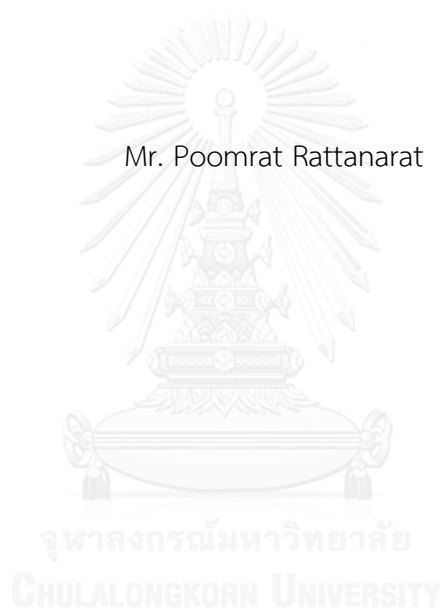สาขาวิชาเคมี ภาควิชาเคมี
คณะวิทยาศาสตร์ จุฬาลงกรณ์มหาวิทยาลัย
ปีการศึกษา 2557
ลิขสิทธิ์ของจุฬาลงกรณ์มหาวิทยาลัย

DEVELOPMENT OF MINIATURIZED ANALYTICAL SYSTEMS

FOR DETERMINATION OF ORGANIC COMPOUNDS AND HEAVY METALS

Mr. Poomrat Rattanarat

A Dissertation Submitted in Partial Fulfillment of the Requirements

for the Degree of Doctor of Philosophy Program in Chemistry

Department of Chemistry

Faculty of Science

Chulalongkorn University

Academic Year 2014

Thesis Title	DEVELOPMENT OF MINIATURIZED ANALYTICAL SYSTEMS FOR DETERMINATION OF ORGANIC COMPOUNDS AND HEAVY METALS
By	Mr. Poomrat Rattanarat
Field of Study	Chemistry
Thesis Advisor	Professor Orawon Chailapakul, Ph.D.

Accepted by the Faculty of Science, Chulalongkorn University in Partial Fulfillment of the Requirements for the Doctoral Degree

⋯⋯⋯⋯⋯⋯⋯⋯⋯⋯⋯⋯⋯⋯⋯Dean of the Faculty of Science

(Professor Supot Hannongbua, Dr.rer.nat.)

THESIS COMMITTEE

⋯⋯⋯⋯⋯⋯⋯⋯⋯⋯⋯⋯⋯Chairman

(Assistant Professor Warinthorn Chavasiri, Ph.D.)

⋯⋯⋯⋯⋯⋯⋯⋯⋯⋯⋯⋯⋯Thesis Advisor

(Professor Orawon Chailapakul, Ph.D.)

⋯⋯⋯⋯⋯⋯⋯⋯⋯⋯⋯⋯⋯Examiner

(Assistant Professor Suchada Chuanuwatanakul, Ph.D.)

⋯⋯⋯⋯⋯⋯⋯⋯⋯⋯⋯⋯⋯Examiner

(Associate Professor Nattaya Ngamrojanavanich, Ph.D.)

⋯⋯⋯⋯⋯⋯⋯⋯⋯⋯⋯⋯⋯External Examiner

(Assistant Professor Weena Siangproh, Ph.D.)

ภูมิรัตน์ รัตนรัตน : การพัฒนาระบบการวิเคราะห์แบบย่อส่วนเพื่อการตรวจวัดสารประกอบ อินทรีย์และโลหะหนัก (DEVELOPMENT OF MINIATURIZED ANALYTICAL SYSTEMS FOR DETERMINATION OF ORGANIC COMPOUNDS AND HEAVY METALS) อ.ที่ ปรึกษาวิทยานิพนธ์หลัก: ศ. ดร.อรวรรณ ชัยลภากุล, 137 หน้า.

วิทยานิพนธ์ฉบับนี้มุ่งเน้นการพัฒนาระบบการวิเคราะห์ขนาดเล็กสำหรับการหาปริมาณ ของสารที่สนใจซึ่งสามารถแบ่งออกได้ 2 ส่วน โดยส่วนแรกคือ การพัฒนาวิธีทางเลือกใหม่สำหรับการ ตรวจวัดสารประกอบอินทรีย์โดยใช้อุปกรณ์วิเคราะห์บนกระดาษ/พอลิเมอร์ควบคู่ไปกับการตรวจวัด เชิงเคมีไฟฟ้า สารประกอบอินทรีย์ที่สนใจในส่วนนี้ประกอบด้วย สารประกอบโดปามีน น้ำตาลกลูโคส และ 4-อะมิโนฟีนอล ในส่วนที่สองคือ การพัฒนาอุปกรณ์ปฏิบัติการบนกระดาษเชิงสี/เคมีไฟฟ้า สำหรับการหาปริมาณโลหะหนักหลายชนิดในคราวเดียวกัน (ได้แก่ โครเมียม นิกเกิล ทองแดง เหล็ก ตะกั่ว และแคดเมียม) ซึ่งระบบขนาดเล็กชนิดนี้ได้รับการออกแบบมาเพื่อให้มีรูปทรงเรขาคณิตที่ เหมาะสมสำหรับแต่ละการทดสอบ พารามิเตอร์ของระบบตรวจวัดได้รับการปรับให้เหมาะสมเพื่อให้ ได้ภาวะที่ให้การวิเคราะห์ที่ดีที่สุด โดยมีการศึกษากลยุทธ์ในการปรับปรุงความจำเพาะเจาะจงและ ความไวในการตรวจวิเคราะห์ รวมถึงมีการศึกษาประสิทธิภาพการทำงานของระบบอันประกอบด้วย ช่วงความเป็นเส้นตรง ขีดจำกัดในการตรวจวัด ขีดจำกัดในการหาปริมาณ การผลิตซ้ำ ความแม่นยำ ในการตรวจวัดภายในวันเดียวกันและระหว่างวัน ความจำเพาะเจาะจงของระบบนี้ได้ถูกทดสอบ สำหรับการตรวจวัดสารที่สนใจต่อสารรบกวนที่พบได้ทั่วไปในสารตัวอย่าง พบว่าความถูกต้องและ ความเที่ยงของระบบวิเคราะห์มีประสิทธิภาพที่ดีให้ผลการวิเคราะห์ที่ยอมรับได้ คือน้อยกว่า 5 เปอร์เซ็นต์ และให้ขีดจำกัดต่ำสุดในการตรวจวัดอยู่ในระดับต่ำมาก (เช่น 14.8 พิโคโมล และ 5.8 นา โนโมล สำหรับการตรวจวัดโดปามีนและน้ำตาลกลูโคส ตามลำดับ) นอกจากนี้ระบบที่พัฒนาขึ้นนี้ยัง ประสบความสำเร็จในการหาปริมาณของสารที่สนใจในสารตัวอย่าง (เช่น ตัวอย่างทางชีวภาพ ตัวอย่างยา และสิ่งแวดล้อม) มีผลที่น่าพอใจและสอดคล้องกับผลการทดลองที่ได้จากเทคนิคการ วิเคราะห์แบบดั้งเดิม

ภาควิชา	เคมี	ลายมือชื่อนิสิต	....
สาขาวิชา	เคมี	ลายมือชื่อ อ.ที่ปรึกษาหลัก	....
ปีการศึกษา	2557		

5272651023 : MAJOR CHEMISTRY

KEYWORDS: LAB-ON-PAPER, 137 METALS

POOMRAT RATTANARAT: DEVELOPMENT OF MINIATURIZED ANALYTICAL SYSTEMS FOR DETERMINATION OF ORGANIC COMPOUNDS AND HEAVY METALS. ADVISOR: PROF. ORAWON CHAILAPAKUL, Ph.D., pp.

This dissertation focused on the development of novel miniaturized analytical systems for the determination of several analytes of interest, which can be divided into 2 sections. The first section is the development of alternative methods for the measurement of organic compounds using paper-based/polymer-based analytical device coupled with electrochemical detection. Various target organic compounds including dopamine, glucose, and 4-aminophenol were determined by the proposed systems. The second section is the development of paper-based colorimetric/electrochemical device for the simultaneous quantification of heavy metals (e.g. chromium, nickel, copper, iron, lead, and cadmium). Miniaturized systems were initially designed to allow the appropriate geometry for each assay. Experimental parameters in the detection mode were optimized and selected in order to determine the best analytical conditions. Strategies to improve the selectivity and sensitivity in analysis were discussed. An analytical performance of the system comprising of linearity, limit of detection, limit of quantification, reproducibility, accuracy, intra-day, and inter-day precision, was investigated. Selectivity for the detection of analytes of interest was demonstrated for common interferences. The results showed that the accuracy and precision of these proposed systems were reported in an acceptable range lower than 5%. A low detection limit was achieved (e.g. 14.8 pmol and 5.8 nmol for detection dopamine and glucose, respectively). In addition, the developed systems were successfully applied to the determination of target analytes in samples (e.g. relevant biological, pharmaceutical, and environmental samples) with satisfactory results, correlating to those obtained from the conventional analytical techniques.

Department: Chemistry   Student's Signature ....

Field of Study: Chemistry   Advisor's Signature ....

Academic Year: 2014

ACKNOWLEDGEMENTS

I would like to express my deepest appreciation to my advisor, Professor Dr. Orawon Chailapakul, for giving me a great opportunity to pursue my Ph.D. She continuously conveyed her supports in regards to research and dissertation during my 6 years with her. She always inspired my ideas with her timely advice, scholarly advice, and scientific approach that helped me accomplishes my research. Without her guidance, this would not have been possible.

I take this opportunity to thank to Professor Dr. Charles S. Henry and my colleagues in his research group from Colorado State University. I am extremely grateful for their kind supports and affectionate encouragement throughout my 1 year in United States. Thanks to all members in his laboratory for friendship and remarkable experiences. I also express my warm gratitude to Professor Dr. Toshihiko Imato for his suggestion and constructive advice and thus enabling me to complete my work in a very limited, yet efficient timely manner in Japan.

I would also like to thank Assistant Professor Dr. Warinthorn Chavasiri, Assistant Professor Dr. Suchada Chuanuwatanakul, and Associate Professor Dr. Nattaya Ngamrojanavanich for serving on my committee.

Special thanks to Assistance Professor Dr. Weena Siangproh. She advised me to start my Ph.D. in Chulalongkorn University. This was a first step of making my dream come true. She constantly provided contribution and excellent advice with kindness and enthusiasm from time to time. I would like to thank Dr.Wijitar Dungchai and Dr.Amara Apilux who gave me the advice and also taught me a preliminary laboratory skill.

To my lovely friends at Electrochemistry and Optical Spectroscopy Research Unit (EOSRU), it has been enjoyable moment with you all. I am thank you for providing necessary supports and helpful advice during difficult time. I appreciated friendship and every single meaningful suggestion of you all.

I would like to give special thanks to Mr. Dittaporn Linananda and his family for motivation, optimism, and encouragement. Thanks for not letting me give up and pushing me farther than I thought I could be.

Last but definitely not least, I would like to thank the most important persons in my life. Without my family, Mr. Udon Rattanarat, Mrs. Ranee Rattanarat, Ms. Benjarat Rattanarat, and Chayapa Rattanarat, I would not have been accomplished anything in my life. I always treasure your blessing, encouragement and unconditional love.

CONTENTS

LIST OF TABLES

LIST OF FIGURES

LIST OF ABBREVIATIONS AND SYMBOLS

4-AP	4-aminophenol
1,5-DPC	1,5-diphenylcarbazide
A	ampere
A	electrode area
AA	ascorbic acid
ASV	anodic stripping voltammetry
AE	auxiliary electrode
Ag/AgCl	silver/silver chloride
Bi	bismuth
BSA	bovine serum albumin
Ce	cerium
CoPc	cobalt phthalocyanine
C_O	concentration of oxidized species
C_R	concentration of reduced species
CE	counter electrode
Cd	cadmium
Cys	cysteine
CNT	carbon nanotube
CPE	carbon paste electrode
Cr	chromium
Cu	copper
CV	cyclic voltammetry
CZE	capillary zone electrophoresis

D	diffusion coefficient
DA	dopamine
DPV	differential-pulse voltammetry
E^0	standard potential
E_p	peak potential (V)
$E_{p,a}$	anodic peak potential
$E_{p,c}$	cathodic peak potential (V)
E_{app}	applied potential (V)
E_{dep}	deposition potential (V)
eCD	electrochemical compact-disk
F	faraday constant (96487 coulombs)
$Fe(CN)_6^{3-}$	ferricyanide
$Fe(CN)_6^{4-}$	ferrocyanide
Fe	iron
g	gram
G	graphene
Glu	glucose
GOx	glucose oxidase
Hg	mercury
h	hour
i.d.	inter diameter
ICP-MS	inductively-coupled plasma-mass spectrometry
i_p	peak current (A)
$i_{p,a}$	anodic peak current (A)

$i_{p,c}$	cathodic peak current (A)
LOD	limit of detection
LOQ	limit of quatification
MCE	microchip capillary electrophoresis
mol	mole
mV	millivolt
min	minute
M	molar
mM	millimolar
mL	milliliter
nm	nanometer
nM	nanomolar
n	number of electron
Ni	nickel
NE	norepinephrine
o.d.	outer diameter
OSHA	The Occupational Health Administration
PA	paracetamol
PAD	paper-based analytical device
PANI	polyaniline
PBS	phosphate buffer saline
PDDA	polydiallyldimethylammonium chloride
PDMS	poly(dimethylsiloxane)
Pb	lead

PELs	permissible exposure limits
ppm	part per million
ppb	part per billion
PM	particular matter
R^2	coefficient
RE	reference electrode
RSD	relative standard deviation
rpm	round per minute
SD	standard deviation
SDS	sodium dodecyl sulfate
SPCE	screen-printed carbon electrode
S/B	signal to background
S/N	signal to noise
SEM	scanning electron microscopy
SWV	square-wave voltammetry
W_f	water fraction
WE	working electrode
T	Kelvin temperature
TCA	trichloroacetic acid
TEM	transmission electron microscopy
TTAB	tetradecyltrimethylammonium bromide
TWEEN-20	polyoxyethylene (20) sorbitan monolaurate
UA	uric acid
UV-Vis	ultraviolet-visible

V	volt
v	scan rate
°C	degree Celsius
μL	microliter
μM	micromolar
μg	microgram
μm	micrometer (micron)
μPAD	microfluidic paper-based analytical device

CHAPTER I

INTRODUCTION

1.1 Introduction

Over the past several years, miniaturized analytical systems (e.g. paper test kits and polymer microfluidics) have emerged as an important analytical system in numerous research fields including biotechnology, medical science, forensics, and environmental studies [1]. Up to this date, some devices are now commercially available and can conveniently integrate the necessary steps for rapid assays in order to detect some biomarkers in the clinical analysis of blood and also measure metal contaminants in the environmental monitoring. These devices can act as a preliminary screening tool which would decrease a tendency of potential threats from numerous hazardous diseases, leading to improve the quality of human being in resource-poor and remote areas. Therefore, these miniaturized portable analytical tools are particularly important for the people who have no direct access to test clinical assays in medical laboratories. Furthermore, these devices offer a proper solution which can be used even by untrained person under challenging environmental conditions and limited power.

Microfluidic is a class of miniaturized system which process or manipulate small amounts of fluids within channels in sub-millimeter scale [2]. The capability to perform laboratory operations on small scales using these systems has several advantages. For instance, they require smaller volume of sample/chemicals and are therefore faster, cheaper, and less hazardous to use than those of conventional analytical methods. Moreover, if the propose of device is to use in scarce resource settings, the cost of device would be as low as possible. To accomplish lower production cost, using cost-effective materials coupled with the mass production of devices is favorable. Although classical materials (e.g. silicon and glass) have been previously introduced for device fabrication, which have outstanding properties for capillary electrophoresis and organic solvent-involved application, the costs from

required manufacturing processes are inappropriate to produce these devices for rural communities with limited resources [3, 4].

Currently, elastomer [5, 6] and paper [7, 8] are promising materials which are affordable, portable, disposable, and have low manufacturing for large-scale fabrication of miniaturized systems. Elastomers enable inexpensive rapid prototyping and can integrate with valves, allowing complicated or parallel fluid manipulation within a microchip. Moreover, paper-based devices have been recently introduced, which are extremely low-cost to prepare and easy to use. For detection modes in these systems, various common analytical measurements comprising of fluorescence [9], UV-Visible spectroscopy [10], and mass spectrometry [11, 12] have been used. The main disadvantages of detection systems are their high cost, complicated instrument, and difficulty to couple with miniaturized systems for fieldwork applications. Thus, there is a strong need for new approaches which are considerably less expensive and can be simply performed by minimally trained people or even mutual citizens.

In this research, various miniaturized analytical systems with low cost and simple operation were developed for determination of analyte of interest in relevant real samples. The development of miniaturized system in this work can be divided into 2 sections which these systems were designed for the determination of organic compounds and heavy metals. 5 developed systems are described as follows;

1. Sodium dodecyl sulfate modified electrochemical paper-based analytical device for determination of dopamine levels in biological samples.

2. An electrochemical compact disk-type microfluidics platform for use as an enzymatic biosensor.

3. High-throughput determination of 4-aminophenol using a graphene-polyaniline modified electrochemical droplet-based microfluidic sensor.

4. A microfluidic paper-based analytical device for rapid quantification of particulate chromium.

5. Multilayer paper-based device for colorimetric and electrochemical quantification of metals

These developed systems were successfully used to quantify each analyte selectively and sensitively. Various optimal conditions were investigated to achieve the best performance of analytical measurement. Selectivity for the detection of analytes of interest in the presence of common interference was tested. Lastly, the successful applications of these proposed device for the detection of analyte in a real sample were carried out.

1.2 Research Objective

The three main goals of this dissertation are as below:

1. To develop new miniaturized device with inexpensive operation and rapidity for selective and sensitive detection of organic compounds and heavy metals.

2. To investigate the unique strategy to improve sensitivity and selectivity in each system.

3. To use these proposed devices for the determination of target analyte in relevant biological/environmental samples.

1.3 Scope of Research

To accomplish the research objectives in this dissertation, the device platform was initially designed to obtain the suitable platform for each assay. Experimental conditions affecting the performance of detection were optimized. Using optimal conditions, the analytical figures of merit of each system including linear working range, limits of detection and quantification, repeatability, and reproducibility, were examined. Various common interferences were investigated to test the selectivity in these systems. In addition, the developed systems were then validated with the conventional analytical techniques. To demonstrate the potential application, these systems were then applied to measure analyte concentration in relevant samples. Finally, all the results were discussed in the dissertation.

CHAPTER II

THEORY

2.1 Miniaturized Analytical System

Over the past decade, the field of miniaturized device has attached much interest, particularly in the area of chemical and biochemical analysis systems. Microfluidic is a class of miniaturized analytical system which is geometrically created in micrometer scale [2]. With its capability including low cost of operation, fast response time, and easy to handle, these devices would be beneficial for on-site application in rural areas. Currently, there are various types of materials for microchip fabrications as shown in the Table 2.1.1.

Table 2.1.1 Overview of materials for fabrication of miniaturized device [13, 14]

Property	Silicon/glass	PDMS Elastomer	Paper
common technique for device fabrication	photolithography	casting	photolithography and wax-printing
multilayer channel	hard	easy	easy
dimension of smallest channel	<100 nm	<1 µm	～200 µm
thermo-stability	very high	medium	medium
organic solvent compatibility	very high	low	medium
resistance to oxidizer	excellent	moderate	low
hydrophobicity	hydrophilic	hydrophobic	amphiphilic
surface charge	very stable	not stable	N/A
material cost	high	low	low
optical transparency	no/high	high	low

This dissertation focuses on the development of cost-effective miniaturized system for rapid and on-site analysis; therefore, the inexpensive materials consisting of paper and poly(dimethylsiloxane) were selected to use as a substrate material for the fabrication of these devices.

2.1.1 Polymer-based Microchip

Device fabrication by using polymers is an interesting method which is easy to operate and low cost of prototyping and manufacturing. Poly(dimethylsiloxane) (PDMS) is one of the most attractive elastomeric polymer to use as a substrate material. PDMS is a silicon-based organic polymer which is light weight, inexpensive material, flexibility, and optical transparency. It can be used in the biology and chemistry studies because of its high hydrophobicity, gas permeability, and biological nontoxicity. Moreover, PDMS is chemical inert and can be easily bonded to glass or other layers of PDMS to form complex PDMS device containing multiple layers of PDMS [15].

Previously, wet chemical-etching of glass and silicon have been introduced for conventional fabrication methods of microfluidic devices [16, 17]. Fabrication of PDMS microfluidic devices by soft lithography provides less expensive and more rapid than those conventional methods. These soft-lithographic methods are based on fast replica molding procedure and do not need to be fabricated in a cleanroom. The PDMS comprises of methylated linear siloxane structure (Figure 2.1.1) consisting of repeating $-OSi(CH_3)_2-$ units [18].
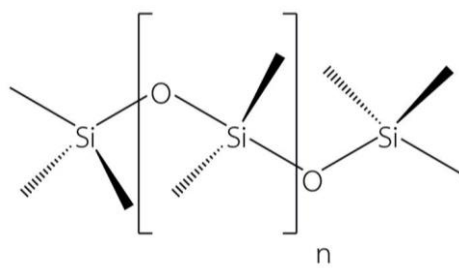
Figure 2.1.1 Poly(dimethylsiloxane) structure

Figure 2.1.2 displays the variety of PDMS microfluidic platforms which have been reported including simple flow-injection [6, 19], droplet-based system [20-23], compact disk (CD)-type microchip [24, 25] and microchip capillary electrophoresis [5, 26-28]. In each platform, it requires different liquid propulsion method. For example, droplet-based systems and simple-flow injection remain to use traditional mechanical pumping systems (e.g. syringe and peristaltic pumps). The capillary electrophoresis is commonly performed within microchannel by using electroosmotic system. For CD microfluidics, the rotating system is used to generate centrifugal force which is a major driving force for fluid movement.
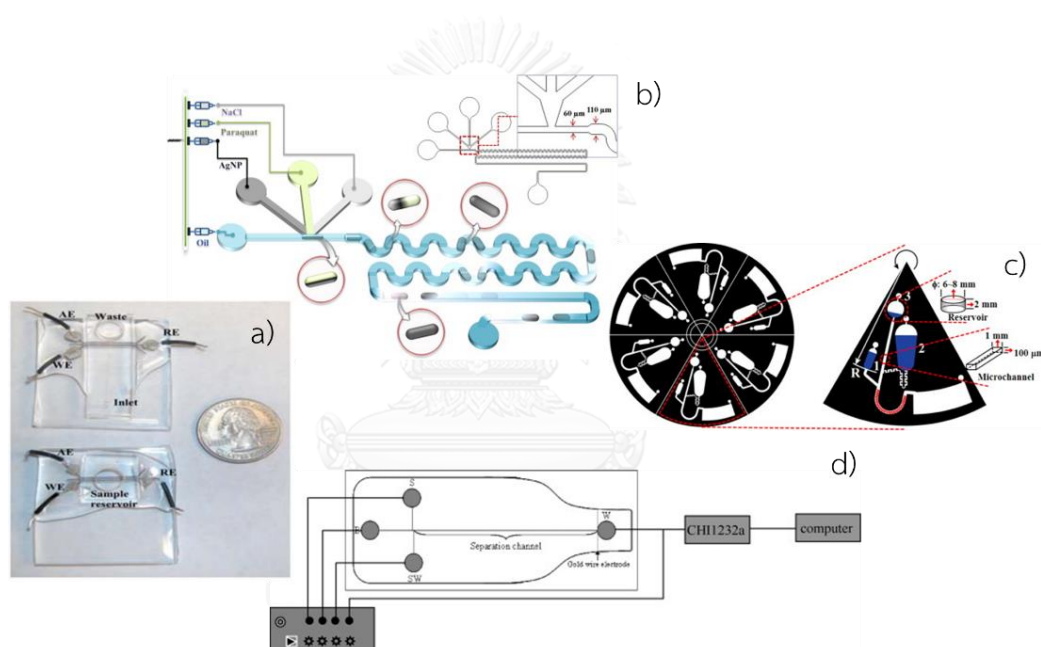
Figure 2.1.2 Various designs of PDMS microfluidics for different application; (a) simple flow-injection, (b) droplet-based system, (c) CD-type microfluidics, and (d) microchip capillary electrophoresis.

2.1.2 Paper-based Device

Another attractive material for the fabrication of microfluidic device is paper. Paper-based device has also become an alternative rapid method for various potential applications including environmental monitoring, food safety, and particularly health

diagnosis [13, 29, 30]. There are numerous advantages of paper which is suitable to use as a base material for the fabrication as summarized below;

Table 2.1.2 Advantages of the use of paper for the fabrication of device

Paper properties	Advantages towards the fabrication of paper-based device
inexpensive and abundant	can be mass production of cost-effective devices
commercially available in a wide range of thicknesses and porosity	can control the flow rate of the solution by selecting a type of paper
easy to flow aqueous solution via capillary force	no need to use external pumping system
numerous units of –OH on the cellulose surface	easy to modify the paper surface to immobilize
White	can easily observe the color change for colorimetric measurement
flammable and biodegradable	disposable and environmentally friendly product

Nowadays, paper test kits are commercially available and widely used in daily human life. For instance, pregnancy test strips are the fastest way to monitor early pregnancy [31]. The principle of pregnancy test kit is antibody-antigen interaction between human chorionic gonadotropin (hCG) and its antibody. After the kits are immersed into the urine sample, testing solution flows onto the device by capillary force. The visible color obviously occurs on the test line when the target hCG is present in the urine sample.

In 2007, the next generation of paper testing device was introduced by Whitesides research group [8]. The paper was patterned to provide multiple millimeter-sized channel on a single paper device. Colorimetric detection in paper-based device was performed to determine biomarkers (e.g. glucose and protein) level

simultaneously in urine. Similarly to the traditional paper test strips, the testing solution can easily flow through the channel by capillary action without requirement of external pumping system. After the color product was completely generated, the mobile phone camera was used to capture to measure the color intensity related to concentration of target analyte.
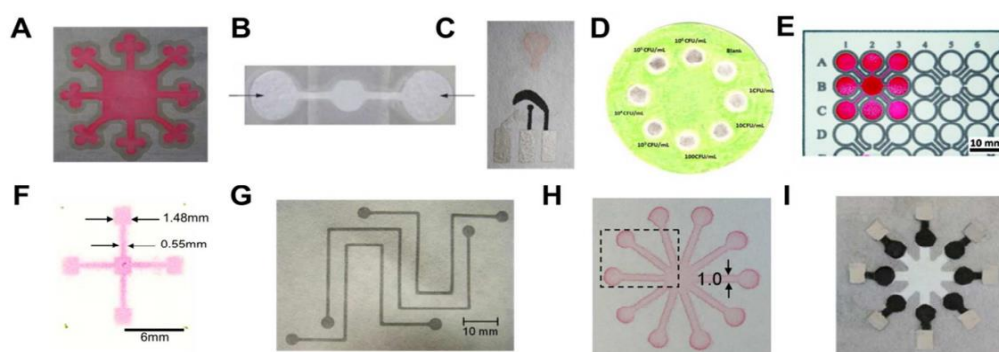
Figure 2.1.3 Various paper-based devices fabricated from different fabrication techniques; (a) wax stamping, (b) wax dipping, (c) wax screen-printing, (d) wax drawing, (e) wax printing, (f) inkjet etching, (g) inkjet printing, (h) flexographic printing polystyrene, and (i) photolithography

2.2 Detection Method

The detection technique has also played an important role in the development and application of miniaturized systems. These analytical detection techniques have been reported as a detection mode in miniaturized systems as follows;

1. Colorimetry [32, 33]
2. Fluorescence [34, 35]
3. Absorption detection [10, 36, 37]
4. Raman spectroscopy [30, 38]
5. Nuclear magnetic resonance (NMR) spectroscopy [23]
6. Electrochemistry [26, 39]
7. Mass spectrometry [11, 40, 41]

8. Chemiluminescence [42, 43]

Although these techniques provide outstandingly selective and sensitive detection, the main disadvantages are high equipment cost and difficulty to use for on-site analysis. In this dissertation, colorimetric and electrochemical detections were selected to use as a detection mode in miniaturized systems. These techniques are easy, portable, and inexpensive way in order to couple with the proposed device which can be used for the preliminary testing in the remote areas.

2.2.1 Colorimetric detection

Colorimetric detection is the most common detection mode which is used in various miniaturized analytical systems because of its simplicity in terms of operation and visual interpretation. The principle of this method is formation of colored product obtained from chemical reactions between the analytes and colorimetric reagents. The changes in color intensity can be monitored by using camera phones or scanners [33, 44].
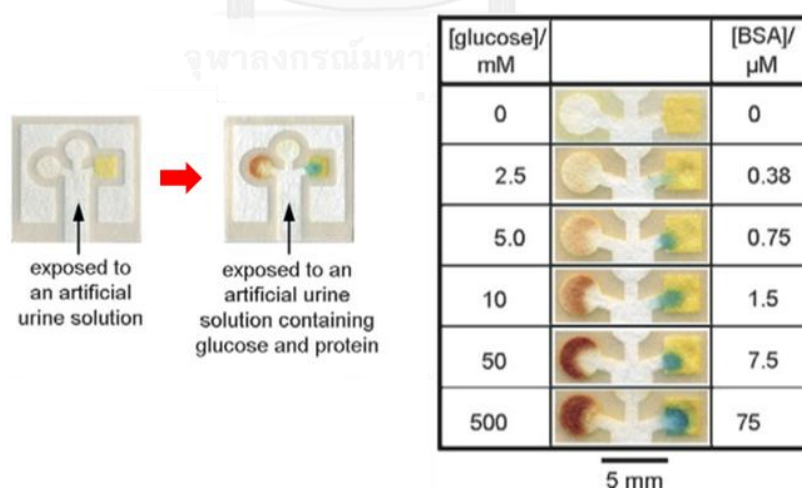
Figure 2.2.1 The overall experimental procedure and colorimetric results for the determination of glucose and bovine serum albumin (BSA) using paper-based microfluidic device.

2.2.2 Electrochemical detection

Electrochemical detection is a well-known detection technique which has been widely integrated in miniaturized system because of its low cost, small size, high sensitivity, high speed operation, easy miniaturization, and low power requirements [45, 46]. In this detection mode, electrodes are used to investigate the relationship between analyte of interest and electrical response (current, potential, or charge).

There are two types of electrochemical cells which are (i) galvanic and (ii) electrolytic. Galvanic cell (potentiometric technique) uses a spontaneous reaction to provide electrical work while electrolytic cell (potentiostatic technique) consumes electrical energy from an external source. Both galvanic and electrolytic cells consist of 2 main components including

(i) Supporting electrolyte: a medium containing inert chemical species which which do not react with analyte. It is usually used to keep a constant ionic strength, to decrease the solution resistance and electromigration effect within electrochemical cell.

(ii) Electrodes: an electrical conductor immersed in the sample solution which is required at least 2 types of electrode. The working electrode (WE) is used for the detection of analyte, and the reference electrode (RE) serves a constant and reproducible potential. In some cases, the counter electrode (CE) might be used in the electrochemical cell to reduce the electrical flowing through the RE. A simple redox reaction at electrode surface is shown below (equation 2.1)

$$O + ne^- \leftrightarrow R \qquad\qquad (2.1)$$

Where O and R are oxidized and reduced forms of the electroactive species which either are soluble in solution or absorbed on the electrode surface and are transported by diffusion. The relationship between the concentrations of electroactive species can be described by Nernst Equation (equation 2.2) [47-49].

$$E = E^0 + 2.3(RT/nF) \log (C_O/C_R) \qquad\qquad (2.2)$$

Where E^0: Standard potential of the redox reaction

    C_O: Concentration of oxidized form

    C_R: Concentration of reduced form

    R: Gas constant ($8,314$ J K^{-1} mol^{-1})

    T: Temperature (Kelvin, K)

    n: number of electrons

    F: Faraday constant (96487 C/mol))

In this dissertation, some potentiostatic methods were used as an electrochemical detection method in the miniaturized system such as cyclic voltammetry, square-wave voltammetry, and amperometry. This chapter attempts to provide an overview of these techniques.

2.2.2.1 Voltammetry

Voltammetry is a controlled-potential (potentiostatic) technique which is based on a dynamic (nonzero-current) situation. This technique deals with charge transfer processes at the interface between electrode and solution. An electrochemical information about the thermodynamics and kinetics of chemical reactions is obtained which can be used to identify and quantitate different species in solution [48]. In general, a potentiostat instrument is used in this technique to apply a potential across a pair of electrodes, and the current response obtained from oxidation/reduction process of analyte is measured simultaneously. The common potential waveforms are shown in Figure 2.2.2 [50].
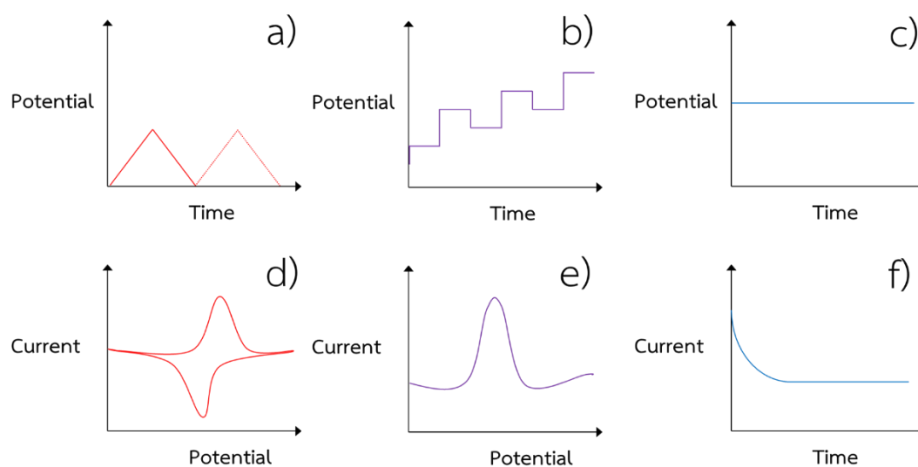
Figure 2.2.2 Potential excitation waveforms (upper) and their output electrochemical responses (bottom) for cyclic voltammetry (a, d), square-wave voltammetry (b, e), and chronoamperometry (c, f)

2.2.2.1.1 Cyclic Voltammetry (CV)

Cyclic voltammetry is commonly used to acquire qualitative electrochemical information about oxidation/reduction reactions of electroactive species. This technique is the most encountered technique to provide electrochemical information on the thermodynamics and kinetics of heterogeneous electron transfer reactions, and coupled chemical reactions. Using a triangular potential waveform (Figure 2.2.2a), the potential of WE is linearly scanned in both forward and reverse directions. The resulting plot between current (vertical axis) and potential (horizontal axis) is termed as cyclic voltammogram (Figure 2.2.2d) which is related to many important parameters. The peak currents (cathodic peak current ($i_{p,c}$) and anodic peak current ($i_{p,a}$)) dependence on scan rate can be described by Randles-Sevick equation (equation 2.3) [51].

$$i_p = (2.69 \times 10^5)\, n^{3/2}\, A\, F\, C\, D^{1/2}\, \nu^{1/2} \tag{2.3}$$

Where   n: number of electrons

A: electrode surface area (cm^2)

F: Faraday constant (96487 C/mol))

C: concentration (mol cm^{-3})

D: diffusion coefficient (cm^2 s^{-1})

v: scan rate (mV s^{-1})

For reversible redox couple, well-defined cyclic voltammogram is observed. The ratio of cathodic-to-anodic peak current ($i_{p,c}/i_{p,a}$) is unity approximately. The peak separation (between anodic peak potential ($E_{p,a}$) and cathodic peak potential ($E_{p,c}$)) is approximately equal to

$$\Delta E_p = E_{p,a} - E_{p,c} = 59/n \qquad (2.4)$$

Where ΔE_p: peak separation (mV)

Moreover, the formal potential (E^O) value should be centered between $E_{p,a}$ and $E_{p,c}$:

$$E^O = (E_{p,a} + E_{p,c})/2 \qquad (2.5)$$

For irreversible reaction process, ΔE_p between $E_{p,a}$ and $E_{p,c}$ is widely separated and the reverse peak in the cyclic voltammogram might be disappeared. Furthermore, a shift of the peak potential is observed while the scan rate is varied.

2.2.2.1.2 Square-wave Voltammetry (SWV)

Square-wave voltammetry (SWV) is one of the pulse technique which is known for its higher electrochemical sensitivity than other pulse techniques [52]. The potential waveform of SWV is shown in Figure 2.2.2b. A square wave is imposed on a staircase waveform. The forward pulse of square wave is coincident with the staircase step in the time and polarity while the reverse cycle of the square wave occurs half way through the staircase step. The current is sampled twice at the beginning of a

pulse and the end of a pulse. The resulting plot as shown in Figure 2.2.2e is termed as square-wave voltammogram. The SWV response (e.g. peak height and peak width) depends on the exact optimization of experimental parameters (i.e. scan rate and staircase step).

2.2.2.2 Amperometry

Amperometric detection has been widely used as an electrochemical detector in flow-based analysis and chromatographic systems. Amperometry is an electrochemical technique which the electrode potential is maintained at a constant value, and the resulting current is measured as a function of time [53]. The potential waveform and chronoamperogram are shown in the Figure 2.2.2c and f, respectively. At fixed potential, oxidation or reduction of electroactive species at electrode surface is occurred. The current output is directly proportional to the analyte concentration. Selectivity is accomplished by the selecting an applied potential while minimizing the background and interference responses. The optimization of applied potential is obtained by constructing hydrodynamic voltammograms. The applied potential which provides the highest signal/background (S/B) ratio is selected to use as an optimal applied potential.

2.2.2.3 Stripping techniques

Stripping voltammetry has become an attractive electrochemical technique for sensitive detection of trace metals and some organic compounds. There are at least 2 steps which are preconcentration and stripping steps.

(i) <u>Pre-concentration or accumulation step</u>: analyte is deposited at the electrode surface by either an anodic or cathodic or an adsorptive process.

(ii) <u>Stripping step</u>: The voltammetric response is then generated where the voltage is scanned in order to strip out the deposited or adsorbed analyte from the electrode surface.

If the accumulation potential of electrode is fixed at negative value to occur reduction of analyte on the electrode surface before potential is scanned to more positive direction, this technique is termed as "anodic stripping voltammetry".

2.3 Fabrication Method

2.3.1 Photolithography

Photolithography is a technique to produce high-resolution micrometer-scale structures. The principle is based on the radiation of ultra-violet (UV) light on a photoactive material which undergoes a chemical reaction to form a liquid-solid transition [54]. As shown in Figure 2.3.1, photoresist is coated onto a glass or silicon substrate using spin-coater device. The photoresist-coated substrate is subsequently exposed to UV light through a transparency mask containing with the desired microfluidic pattern. After baking in the oven or hot plate, the un-, or exposed layer of the photoresist is removed.
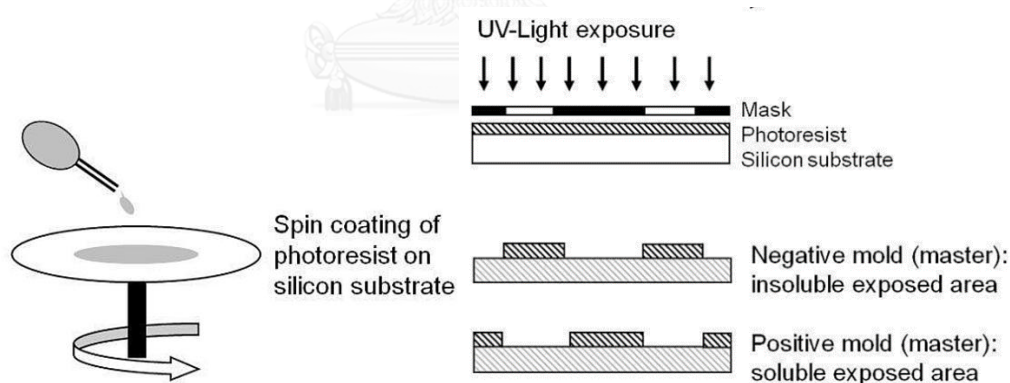
Figure 2.3.3 Photolithography procedure for the fabrication of microfluidic devices. (i) A photoresist is deposited on a silicon wafer substrate using spin coater, (ii) The coated substrate is exposed to UV light through a mask; (iii) , the non-crosslinked material is removed after baking and chemical development steps. Finally, a negative or a positive mold is obtained.

The desired pattern remains on the substrate forming a positive or negative mold. The light-exposed areas on the positive photoresist are usually soluble. For

the negative photoresist, the areas are insoluble. The negative photoresist is often used to create a mold for PDMS-based miniaturized devices replicated by soft lithography.

2.3.2 Soft Lithography

PDMS-based microfluidic is formed by replicating against a negative mold of the desired microfluidic pattern.   The PDMS is commercially supplied in two components, a base and a curing agent [55]. A typical PDMS fabrication procedure is described in Figure 2.3.4.
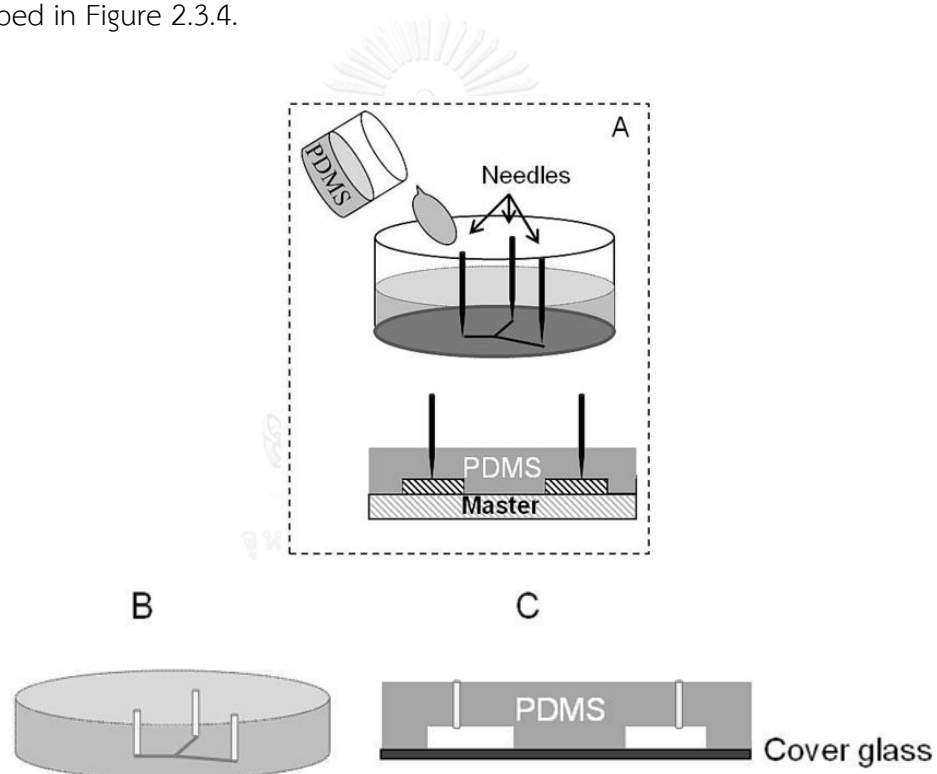
Figure 2.3.4 Replication of PDMS based microfluidic devices produced by soft lithography.

To produce a PDMS replica, the mixture between base and curing agent in a ratio of 10:1 is prepared and then poured over the template, and cure it by baking at 65 $^\circ$C. In the curing step, crosslinking reaction (Figure 2.3.5) between silicon hydride

groups and vinyl groups (present in the base) is occurred. Finally, a cross-linked elastomeric solid is formed.
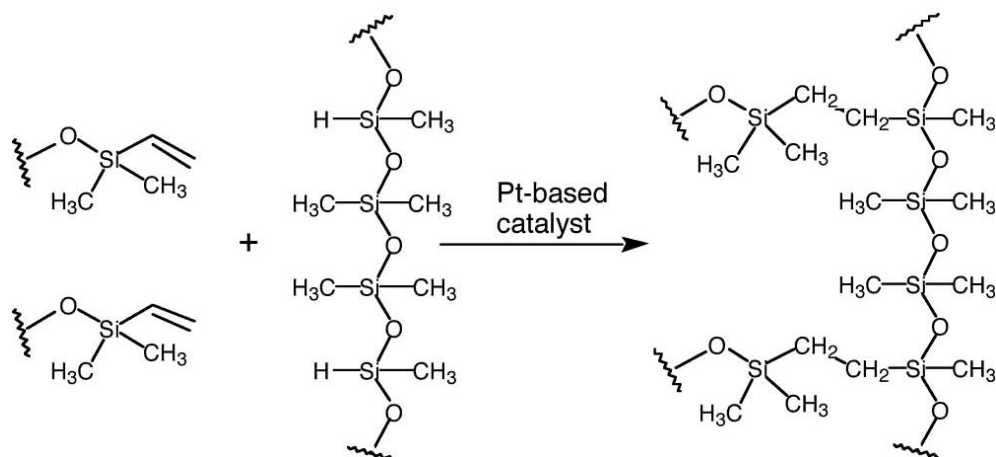
Figure 2.3.5 Crosslinking reaction to produce elastomeric PDMS during curing.

2.3.3 Wax-printing Method

Normally, paper-based device are fabricated by penetration of hydrophobic material into the hydrophilic cellulose paper [56]. Usually, photoresist and wax have been used as preferred hydrophobic materials to create these hydrophobic barriers in the paper (Figure 2.3.6). For the fabrication using photolithography, the similar procedure as described above (section 2.3.1) was performed on paper instead of silicon wafer or glass substrates [57].

The wax-printing method has been frequently used for fast mass production of paper-based device. In this technique, the hydrophobic platform is printed onto a paper using a commercial wax printer. Then, the wax-printed paper is heated, which allows the penetration of wax into the paper pores, generating hydrophobic barrier within the paper.
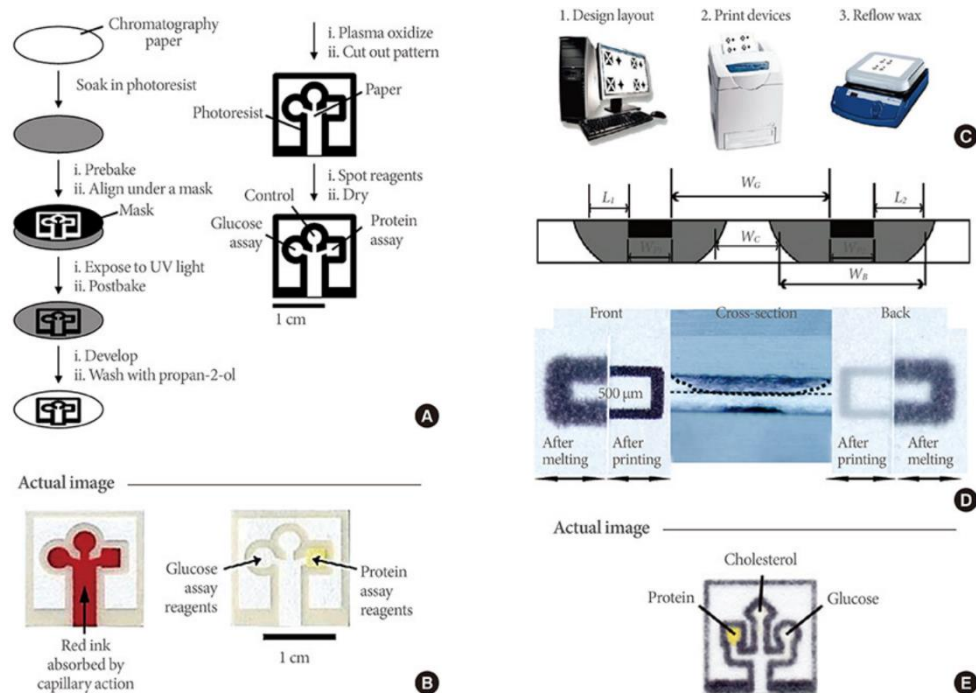
Figure 2.3.6 Fabrication of two-dimensional paper-based devices: (a) Fabrication procedure and (b) actual image of paper-based device using photolithography method, (c) Wax-printing step for fabrication of paper-based device by wax-printing method. (d) Schematic illustration of the spreading of molten wax during printing or the thermal process on paper, and (e) Actual image of paper-based device fabricated by wax-printing method.

CHAPTER III

DEVELOPMENT OF MINIATURAIZED DEVICE BASED ON PAPER/POLYMER FOR ELECTROCHEMICAL DETERMINATION OF ORGANIC COMPOUNDS

3.1 Sodium Dodecyl Sulfate Modified Electrochemical Paper-Based Analytical Device for Determination of Dopamine Levels in Biological Samples

Poomrat Rattanarat[a], Wijitar Dungchai[b], Weena Siangproh[c], Orawon Chailapakul[a,d,*], Charles S. Henry[e, f, *]

[a]Department of Chemistry, Faculty of Science, Chulalongkorn University, Patumwan, Bangkok 10330, Thailand

[b]Department of Chemistry, Faculty of Science, King Mongkut's University of Technology Thonburi, 91 Prachautid Road, Thungkru, Bangkok 10140, Thailand

[c]Department of Chemistry, Faculty of Science, Srinakharinwirot University, Sukhumvit 23, Wattana, Bangkok 10110, Thailand

[d]National Center of Excellence for Petroleum, Petrochemicals and Advanced Materials, Chulalongkorn University, Patumwan, Bangkok 10330, Thailand

[e]Department of Chemistry, Colorado State University, Fort Collins, Colorado 80523

[f]Department of Chemical and Biological Engineering, Colorado State University, Fort Collins, Colorado 80523

*Corresponding authors

Abstract

We report the development of an electrochemical paper-based analytical device (ePAD) for the selective determination of dopamine (DA) in model serum sample. The ePAD device consists of three layers. In the top layer, SU-8 photoresist defines a hydrophilic sample application spot on the filter paper. The middle layer was made from transparency film and contained two holes, one for sample preconcentration and the other for the surfactant to allow transfer to the third layer. A screen-printed carbon electrode formed the bottom layer and was used for electrochemical measurements. In the absence of the anionic surfactant, sodium dodecyl sulfate (SDS), the oxidation peaks of DA, ascorbic acid (AA) and uric acid (UA) overlapped. With the addition of SDS, the DA oxidation peak shifted to more negative values and was clearly distinguishable from AA and UA. The oxidation potential shift was presumably due to preferential electrostatic interactions between the cationic DA and the anionic SDS. Indeed, whilst the SDS-modified paper improved the DA current five-fold, the non-ionic Tween-20 and cationic tetradecyltrimethylammonium bromide surfactants had no effect or reduced the current, respectively. Furthermore, only the SDS-modified paper showed the selective shift in oxidation potential for DA. DA determination was carried out using square-wave voltammetry between -0.2 and 0.8 V *vs*. Ag/AgCl, and this ePAD was able to detect DA over a linear range of 1-100 μM with a detection limit (S/N = 3) of 0.37 μM. The ePAD seems suitable as a low cost, easy-to-use, portable device for the selective quantitation of DA in human serum samples.

3.1.1 Introduction

Dopamine (DA) is an important catecholamine that is involved in neurotransmission within the central and peripheral nervous systems [58] and plays a prominent role in the function of human metabolism, cardiovascular, renal, and hormonal systems [59]. In a healthy human, DA is found in the brain at ~50 nmol g^{-1} and in extracellular fluids at 0.01-1 μM. Abnormally low levels are associated with Parkinson's disease [60] and Alzheimer's disease [61] while abnormally high levels of DA are found in Attention-Deficit Hyperactivity Disorder, Huntington's disease [58] and Schizophrenia [62]. Because of the clinical significance of DA in these diseases a number of analytical methods have been developed with the goal of providing fast but sensitive, selective and reliable detection in complex biological samples. A variety of methods for DA detection have been reported previously, and include liquid chromatography [61], capillary electrophoresis [63], spectrofluorometry [64], electrogenerated chemiluminescence [65], mass spectrometry [66], microchip electrophoresis [67] and surface plasmon resonance [68]. These methods, however, are generally time-consuming, require complicated expensive instrumentation, and can only be carried out in the laboratory.

Of the common analytical methods for DA detection, electrochemical measurements have attracted increasing interest due to their speed, low cost, portability, high sensitivity and ability to make direct measurements in biological systems [69, 70]. However, a significant problem for electrochemical-based DA detection is the presence of ascorbic acid (AA) and uric acid (UA) since both AA and UA oxidize at similar potentials as DA and both are typically found at higher levels than DA, making it difficult to obtain selective quantification [71]. Various methods for electrode modification have been explored to improve DA selectivity. For instance, catalytic molecularly imprinted polymers [72], silanized graphene [73], carbon nanotube/magnetic particles [74], single-stranded DNA/poly(anilineboronic acid)/carbon nanotubes , and 2,4,6-triphenylpyrylium/zeolite Y [75] have been used to chemically modify electrodes. These methods; however, require expensive materials, as well as complicated and tedious fabrication steps. An alternative method

to gain selectivity is through the use of surfactants. The use of surfactants for electrode modification [76] has previously been investigated for DA determination, where the cationic cetylpyridinium chloride [77], cetyltrimethylammonium bromide [78], and tetraoctylammonium bromide [79] were reported to enable the separation and simultaneous determination of AA and DA at micromolar levels in pharmaceutical samples. Sodium dodecyl sulphate (SDS) has been reported to improve DA detection selectivity when directly assembled into the electrode material [80, 81] as well as when used as a masking agent [78] or molecular spacer [82]. The negatively charged SDS film formed on the electrode surface has been shown to improve the sensitivity and lower the detection limit as well as shift the oxidation potential for DA detection.

Here, a paper-based analytical device (PAD) is used to determine DA in the presence of SDS. PADs represent a new trend in analytical chemistry that builds on the combination of age old lateral flow immunoassays and paper-spot tests with modern abilities to perform photolithography to define small structures on a monolithic substrate [8]. PADs have several advantages, including low cost of materials, lightweight, flexibility, disposability, biodegradability, and power-free flow generation using capillary action. While the majority of work with PADs has used colorimetric detection [44, 83-85], other detection modes, such as chemiluminescence [43], electrochemiluminescence [43], mass spectrometry [11] and surface enhanced Raman spectroscopy [30], have been demonstrated. Electrochemical detection has also been used in this format. Dungchai et al. [86] demonstrated PADs with electrochemical detection (or ePADs) for the determination of glucose, lactate and UA in serum using oxidase enzymes to produce hydrogen peroxide for electrochemical detection. Nie et al. [87] reported a new design of ePADs for biosensors and metal detection applications, whilst Dossi et al. [88] proposed an amperometric gas sensor as a detector in flow injection analysis using paper-based screen-printed carbon electrodes (SPCE) with room temperature ionic liquids for the determination of 1-butanethiol vapors. Tan et al. [89] reported the use of a paper disk that was impregnated with zinc as an internal standard and bismuth for *in situ* electrode

modification, respectively, for a more sensitive determination of Pb (II) levels in drinking water than the commercial SPCE without modified paper disk.

Here, we report the development of an ePAD-based assay for DA detection that possesses an enhanced selectivity and sensitivity through the use of the anionic surfactant SDS, impregnated in one layer of the device. The potential benefits of this device, including ease of operation, small sample volume, low cost, high selectivity for DA via electrostatic interactions with the negatively charged SDS, low detection limits from sample preconcentration, and a high reproducibility using a commercial SPCE, were evaluated. The time required to measure DA, the limit of detection (LOD) and the effect of biologically relevant interfering compounds were evaluated. Finally, this device was used for the determination of DA in human control serum samples.

3.1.2 Experimental

3.1.2.1 Materials and Equipment

SU-8 negative photoresist and developer were purchased from MicroChem Corp. (Newton, MA). For square-wave voltammetry (SWV), a commercially available potentiostat (ED201 e-corder, eDAQ) was used. Disposable SPCEs on a ceramic substrate with a 4-mm disk carbon working electrode were obtained from Dropsens and connected to the potentiostat through a standard edge connector (Llanera, Spain). Electrochemical measurements were made in a Faraday cage to reduce electronic noise. All experiments were done at room temperature (22 ± 2 °C). Filter paper (No. 1, 11 cm diameter) was obtained from Whatman. 18 MΩ cm^{-1} resistance water was obtained from a Millipore Milli-Q water system. The supporting phosphate buffered saline (PBS) electrolyte was prepared as 0.8% (w/v) NaCl, 0.02% (w/v) KCl, 0.144% (w/v) Na$_2$HPO$_3$, 0.024% (w/v) KH$_2$PO$_4$ in Milli-Q water. All reagents, including DA, norepinephrine-bitartrate salt (NE), SDS, tetradecyltrimethylammonium bromide (TTAB) Sigma) and polyoxyethylene (20) sorbitan monolaurate (Tween-20) from Sigma, trichloroacetic acid (TCA), KH$_2$PO$_4$ and KCl from Fisher, Na$_2$HPO$_4$ (Mallinckrodt) and NaCl (Macron), were used as received without further purification. For the determination of

DA levels in real serum samples, lyophilized human control serum sample (level I) was obtained from Pointe Scientific (Canton, MI). Prior to use, deionized water (5.0 mL) was added to rehydrate the human serum. All samples with TCA precipitation and sample pH adjustment as indicated were analyzed using electrochemical detection.

3.1.2.2 Fabrication of the Paper-Based Analytical Device (ePAD)

Patterned papers were fabricated using previously described methods [7]. Briefly, the transparency film photomask was designed with Adobe Illustrator CS5 software (Adobe Systems, Inc.) and printed by Chaiyaboon Co. (Bangkok, Thailand). The filter paper was coated with 4 g of SU-8 negative photoresist using a spin coater (G3P-8). After baking at 95 °C for 10 min, the photomask was placed above the coated paper and exposed to ultraviolet (UV) light with 100% intensity for 10 s (Intelli-ray 400). Areas exposed with UV light remained hydrophobic while unexposed areas were hydrophilic. The exposed paper was baked at 95 °C for 10 min followed by soaking in the SU-8 developer and then isopropanol for 3 min each, respectively. Finally, the patterned paper was dried in a hood at room temperature (22±2 °C). Prior to use, paper microfluidic devices were exposed to air plasma (Harrick PDC-32G) for 2 min.

3.1.2.3 Electroanalytical Procedure for the Selective Determination of DA levels

The device consisted of three layers; (i) a layer of patterned paper containing a 7 mm diameter hydrophilic area for sample preconcentration, (ii) a 50 mm x 25 mm transparency film connector layer with two 5-mm diameter holes 5 mm apart, the second of which contains the selective, SDS-modified, transfer paper to wick the sample to (iii) a commercial SPCE for electrochemical detection of DA (Figure 3.1.1a). The two holes in the transparency were designed to allow for sample preconcentration, by repeated 20 μL sample applications and drying, in the first hole

followed by selective sample transfer through the second hole containing treated filter paper to the SPCE (third layer) (Figure 3.1.1b).

3.1.2.4 ePAD Operation

For operation, the selective transfer paper was prepared by adding 20 μL of 1 mM SDS in PBS adjusted to pH 2 with 3 M HCl and the paper was then placed into the second hole of the connector layer (Figure 3.1.1b). Preconcentration of the analyte on the spot assay was first performed by adding 20-μL aliquots of the test sample to the hydrophilic circle (7 mm diameter) on the first layer, aligned above the first hole of the middle layer, and allowed to dry between applications. The hydrophobic barrier prevents the sample from spreading out and dispersing the analyte across the paper, whilst the first hole (without paper disk) of the middle layer prevents the leakage of the solution from the bottom of the patterned paper through to the third layer (SPCE) by making a space between the patterned paper and the commercial SPCE. This procedure was repeated two more times (unless otherwise noted) so as to non-specifically concentrate the sample. Next, the patterned paper was moved manually from first hole to the second hole of the connector (middle) layer, and 60 μL of the selective wicking solution (1 mM SDS in PBS at pH 2 except where specified otherwise) was added to the patterned paper. The solution was then transferred by wicking from the patterned paper to the SPCE (third layer) and SWV was performed without oxygen removal. The use of a commercial SPCE was chosen as the third layer because of the cost, stability, and availability of these electrodes.

The optimum parameters for SWV measurement were found in preliminary trials (data not shown) to be a pulse amplitude of 0.15 V, square wave frequency of 30 Hz, and a step height of 0.005 V for scanning the potential between -0.2 V to 0.8 V *vs*. Ag/AgCl, and so these parameters were used throughout this study. Protein precipitation using TCA was used for serum sample preparation [90]. The sample was vortexed for 5 min following TCA addition to 0.6 M followed by centrifugation at 1073 rcf for 10 min and harvesting of the supernatant.
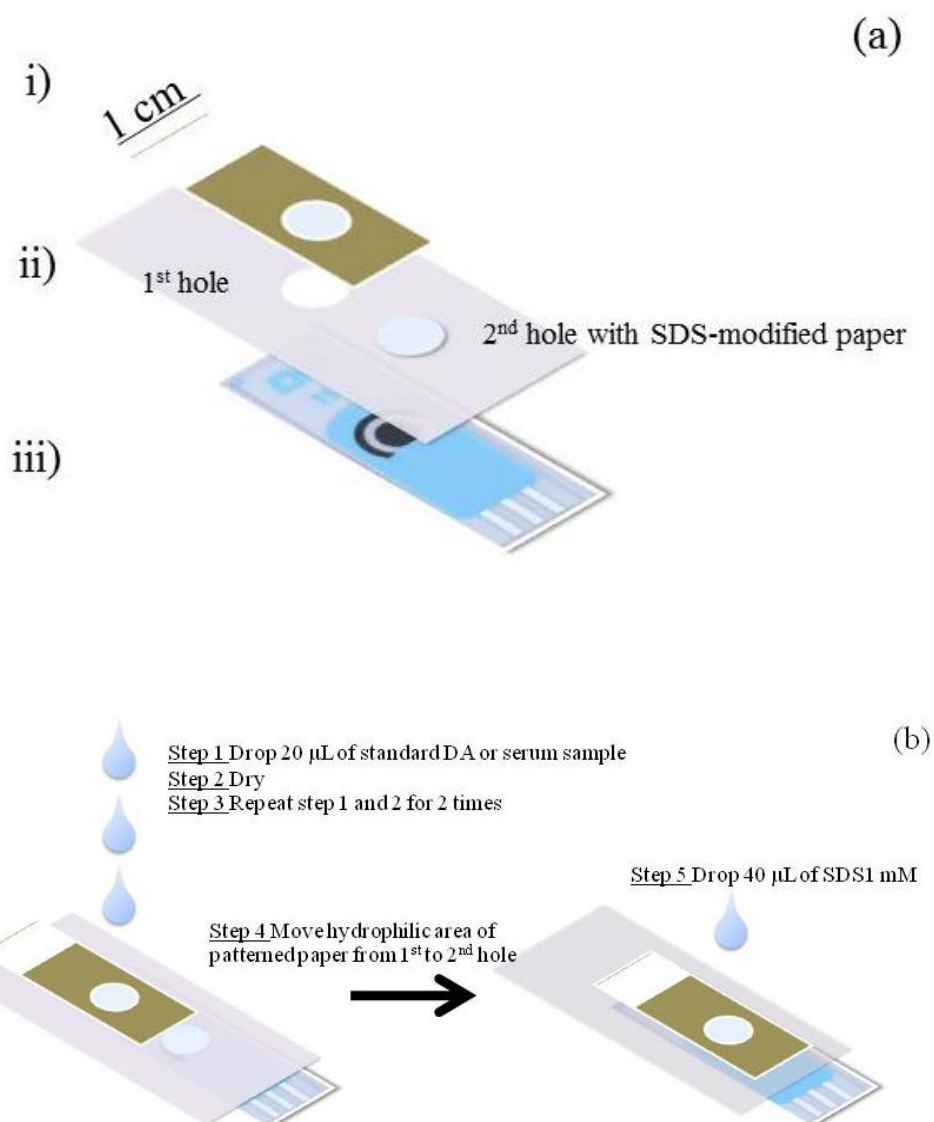
Figure 3.1.1 (a) Schematic representation of the paper-based analytical device for determination of DA consisting of: (i) the patterned paper for sample preconcentration, (ii) the transparency film connector with two holes for sample preconcentration and for selective transport of DA using a SDS-modified paper disk and wicking solution, respectively, and (iii) a commercial SPCE. (b) Sequence of operation steps for the selective determination of DA in human serum.

3.1.3. Results and Discussion

3.1.3.1 Electrochemical Characterization of DA

Prior reports have shown that SDS can improve the specificity and sensitivity of DA detection in the presence of interfering analytes, such as AA and UA, through electrostatic interactions between the surfactant film on the electrode surface and the cationic DA [80, 81, 91]. In the presence of SDS, the electrode surface becomes negatively charged and preconcentrates the cationic catecholamines [82]. At the same time, the negatively charged surface of the electrode rejects common anionic interferences. To show this concept worked with the designed combination of a paper-spot device and a commercial SPCE, the detection of DA with and without SDS was investigated. The peak current for DA increased by approximately two-fold relative to a single sample application when three 20-µL (80 µM DA) sample applications (4.8 nmol total) were applied when no SDS was present in the wicking PBS buffer. However, 1 mM SDS was present in the same wicking solution the DA current increased approximately five-fold compared to the system without preconcentration and SDS (Figure 3.1.2).

This increase in peak current is believed to be the result of an increase in the mass of DA transported from the top layer to the middle layer contacted to electrode surface as well as the ability of the anionic surfactant to preconcentrate the DA at the electrode surface. The peak potential shift is most likely the result of favorable interactions between the anionic head groups of the surfactant and the cationic DA [82].

Next, the quantity of 20-µL sample applications and the SDS concentration in the selective wicking solution were optimized. The highest numerical DA current response was observed after five 20-µL sample applications (8 pmol total) were applied to the preconcentration spot, but there was no statistically significant difference in the obtained current responses obtained from three to five sample applications (Figure 3.1.3). That additional applications did not significantly increase the peak current any further is most likely due to surface saturation.
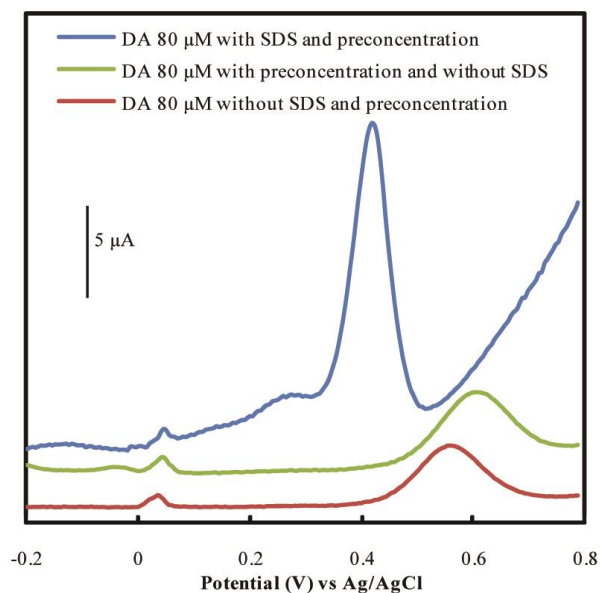
Figure 3.1.2 Representative DA voltammograms with or without preconcentration (three or one 20-μL applications of an 80 μM sample, respectively, yielding 4.8 or 1.6 nmol DA total) and with or without 1 mM SDS wicking solution. SWV detection conditions: pulse amplitude = 0.15 V, square wave frequency = 30 Hz, and step height = 0.005 V.
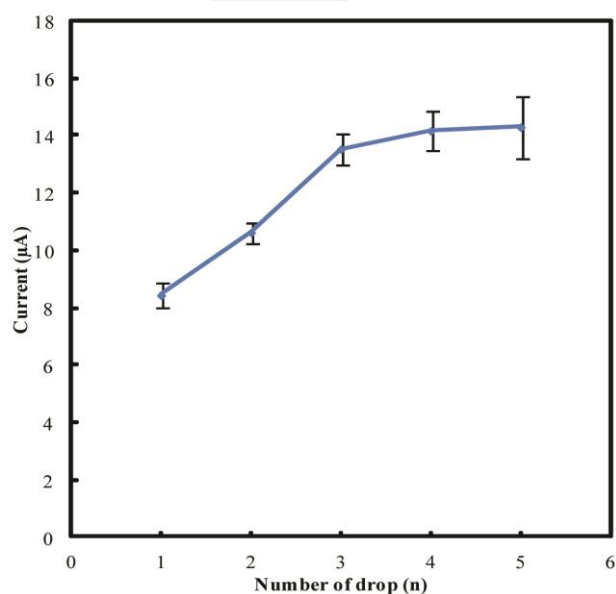
Figure 3.1.3 Effect of the application number (sample preconcentration by repeated 20-μL applications) of an 80 μM DA sample solution using the spot assay on the paper-based analytical device.

The SDS concentration in the wicking solution also had a significant effect on the DA peak current. When the SDS concentration was higher than 1 mM, electrode fouling occurred and the peak current decreased (Figure 3.1.4c). In contrast, if the SDS concentration was less than 1 mM, the AA and DA oxidation peaks overlapped (Figure 3.1.4b). Thus, SDS at 1 mM gave the optimal DA detection and so three 20-μL sample applications and a 40 μL PBS/ 1 mM SDS wicking solution were used for all remaining studies.
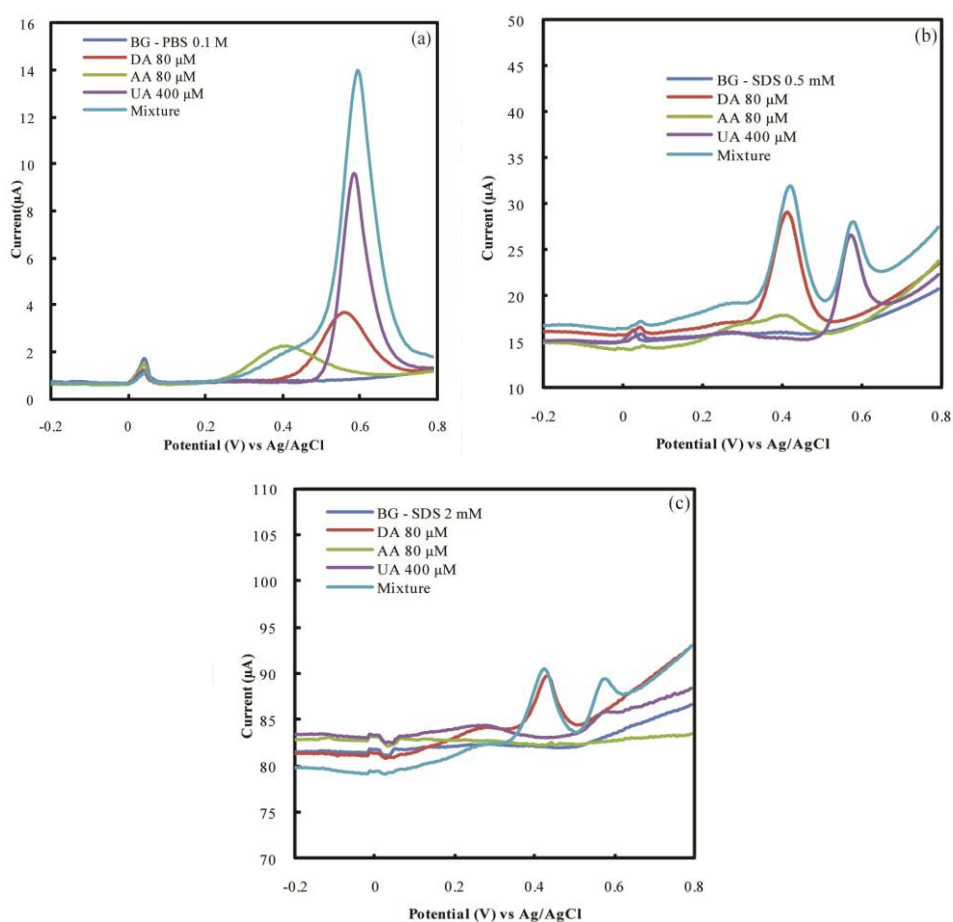
Figure 3.1.4 Representative square-wave voltammograms for either no sample application (BG; background) or with three 20-μL applications (preconcentration) of AA (80 μM), DA (80 μM) and UA (400 μM) (representing 4.8, 4.8 and 24 nmol total for AA, DA and UA, respectively) applied individually or as a mixture of all three, but in the (a) absence of SDS , in the (b) presence of 0.5 mM SDS, and (c) 2 mM SDS in the PBS wicking solution.

3.1.3.2 Analytical Performance and Interferences

AA and UA are generally present in biological samples at concentrations of 100- to 1000- fold higher than DA [82], whilst the highest AA and UA levels in normal human serum are 80 μM and 400 μM, respectively. Therefore, the ability to selectively determine DA in the presence of AA and UA was studied using the highest anticipated serum concentrations for AA (80 μM) and UA (400 μM). In the absence of SDS in the wicking solution, the response of these compounds completely overlapped at ~ 600 mV (Figure 3.1.4a).
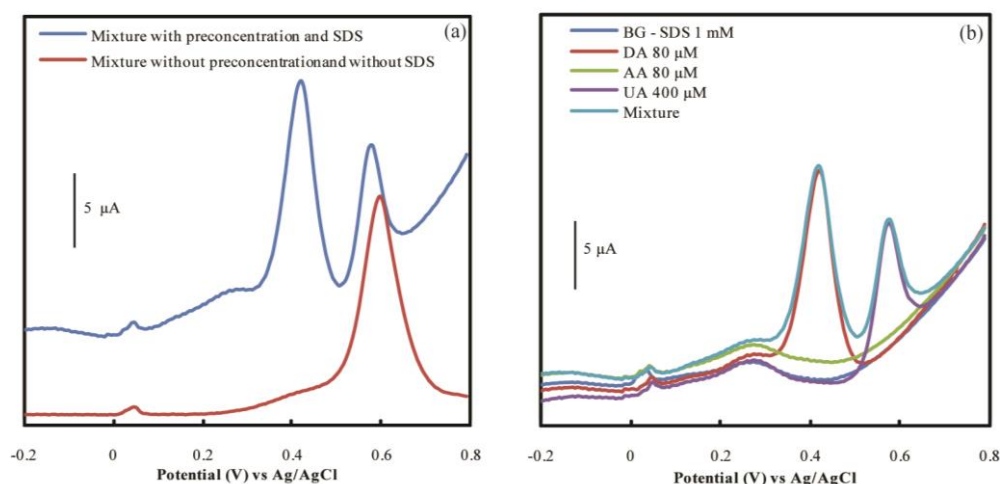
Figure 3.1.5 (a) Discrimination of the SDS enhancement effect between square-wave voltammograms for the mixture of samples of AA (80 μM), DA (80 μM) and UA (400 μM) with or without preconcentration (three or one 20-μL application, respectively) in presence or absence of 1 mM SDS in the wicking solution. (b) Representative voltammograms of no sample application (background; BG) or samples of AA (80 μM), DA (80 μM) and UA (400 μM) (4.8, 4.8 and 24 nmol total for AA, DA and UA, respectively) alone or a mixture of all three, using this system with optimum conditions.

In contrast, their responses in the presence of 1 mM SDS in the wicking solution showed separate peaks at ~400 and 600 mV and a potential difference ($E_{UA} - E_{DA}$) of around 200 mV (Figure 3.1.5a). The individual voltammograms for DA, AA and UA, as well as the mixture of all three compounds, revealed that the anodic peak of AA was not observed under these conditions (Figure 3.1.5b). At pH 2, the separation of well-

defined peaks with oxidation potentials for DA (red line) and UA (purple line) were 400 mV and 600 mV, respectively. These results clearly show the ability of the SDS-containing wicking solution and paper to provide selective determination of DA in the presence of AA and UA.

The linear range was found to be 1-100 µM, with a correlation coefficient (r^2) of 0.9949 and RSD of 4.32% (n = 3) (Figure 3.1.6a and b). The LOD, evaluated using a signal-to-noise (S/N) ratio of three, was found to be 0.37 µM, which is similar to previously published studies using surfactant-modified electrodes. However, the limit of quantitation (LOQ), evaluated using a S/N ratio of 10, was 1.22 µM, which is lower than some previously published results using modified carbon electrodes [77, 79, 92]. Although the LOD and LOQ values reported here are higher than those obtained with a modified Pt electrode, the CPSE based e-PAD reported here does not require the complicated electrode modification strategies to achieve detection at physiologically relevant levels [82].
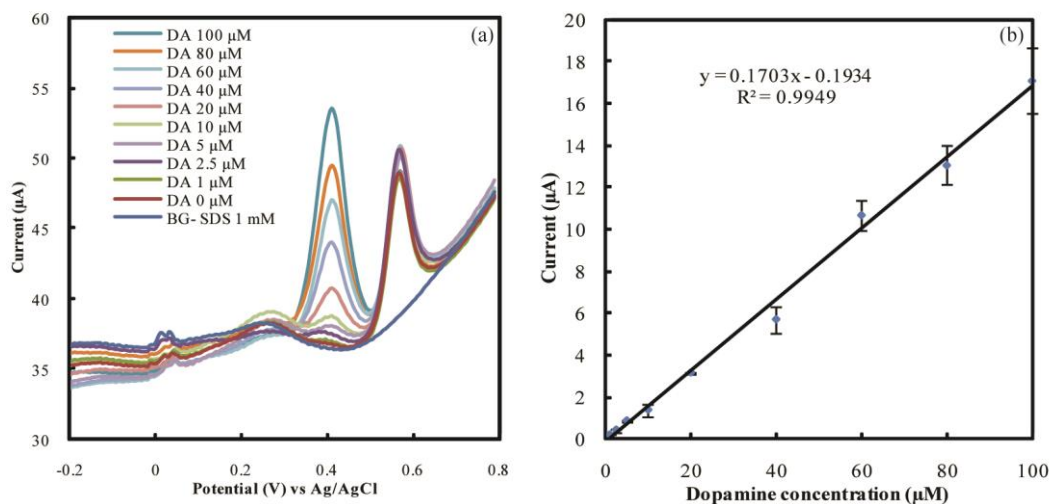
Figure 3.1.6 (a) Representative square-wave voltammograms and (b) the derived calibration curve for DA detection over a concentration range of 1 to 100 µM in the copresence of AA and UA at 80 µM and 400 µM (4.8 and 24 nmol total), respectively, and with 1 mM SDS in the PBS pH 2 wicking solution.

3.1.3.3 Analytical Application

To evaluate the performance of this system on complex biological samples, DA was analyzed in control serum samples. Control serum samples are used to standardize clinical assays and so to validate new diagnostic assays. Known concentrations of DA were added to the serum and then the protein precipitated by TCA and centrifugation. The protein-free serum supernatant was then added to the ePAD as three 20-µL applications as described previously. The resulting voltammograms revealed a dose-dependent DA response (Figure 3.1.7a), from which the standard curve (Figure 3.1.7b) showed acceptable linearity with a correlation coefficient (r^2) of 0.9979 (n = 3). These results clearly indicate the ability to measure DA levels in a biologically relevant sample.
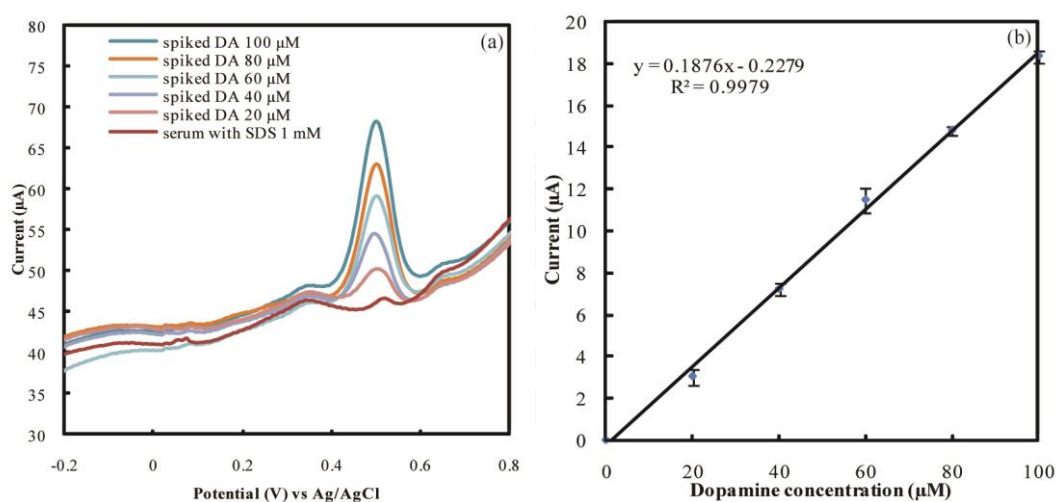
Figure 3.1.7 (a) Representative square-wave voltammograms and (b) the derived calibration curve of different spiked DA concentrations (20-100 µM; 1.2-6 nmol total) in human serum after the TCA protein precipitation step.

3.1.3.4 Mechanism for Enhancement and Selective Detection of DA

The effect of surfactant chemistry on the performance of the ePAD was studied using the anionic SDS in comparison to the cationic TTAB and nonionic Tween-20 as representative members of the three charge classes of surfactants in the wicking solution. At pH 2, the anodic UA peak was barely visible at 600 mV in the TTAB-

containing wicking solution and AA and DA signals were not detected (Figure 3.1.8). This is due to repulsion between the positively charged compounds and the positively charged surfactant. In the case of Tween-20, the AA, DA and UA signals were not seen at any surfactant concentration, most likely due to electrode fouling [93].
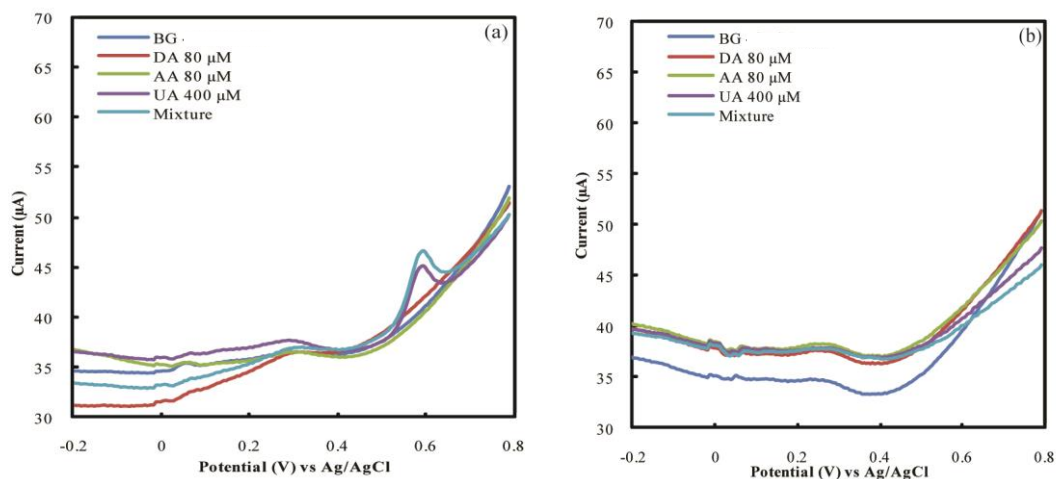
Figure 3.1.8 Representative voltammograms of preconcentrated (three 20-µL applications) DA (80 µM), AA (80 µM) and UA (400 µM) (4.8, 4.8 and 24 nmol total for AA, DA and UA, respectively), applied individually or as a mixture of all three, and with no sample application (background; BG), using PBS pH 2 with (a) the cationic TTAB or (b) the nonionic Tween-20 surfactant as the wicking solution.

Next, NE (pK$_a$ = 8.6 [94]), a structurally similar catecholamine to DA, was studied with these surfactants to determine if structural variations in the analyte had any effect on the results. The anodic peak of NE was seen in the SDS system but not with TTAB or Tween-20 (Figure 3.1.9), suggesting that the selectivity mechanism is primarily governed by the electrostatic interactions and not the structure of the compound.

Finally, the impact of the pH of the wicking solution on the subsequent detection of DA was evaluated between pH 2 and 10 in the presence of 1 mM SDS. The peak potentials of DA and UA were dependent on the pH, whilst at 80 µM AA (4.8 nmol total applied DA) was not detectable at any tested pH (Figure 3.1.10). This is because at a low pH, the generation of two protons during the electrooxidation is

unfavorable [95], while at a higher pH, the negatively charged AA is difficult to oxidize because of the repulsion at the negative SDS film. In the presence of SDS, the DA response was highest and lowest at pH 2.0 and 5.0, respectively, with a current difference of 10.82 µA, while the peak current for UA was highest and lowest at pH 2.0 and 10.0, respectively, with a current difference of 7.63 µA. The trend in response was attributed to the ionization of DA and UA in the cationic form at a lower pH value Figure 3.1.10).
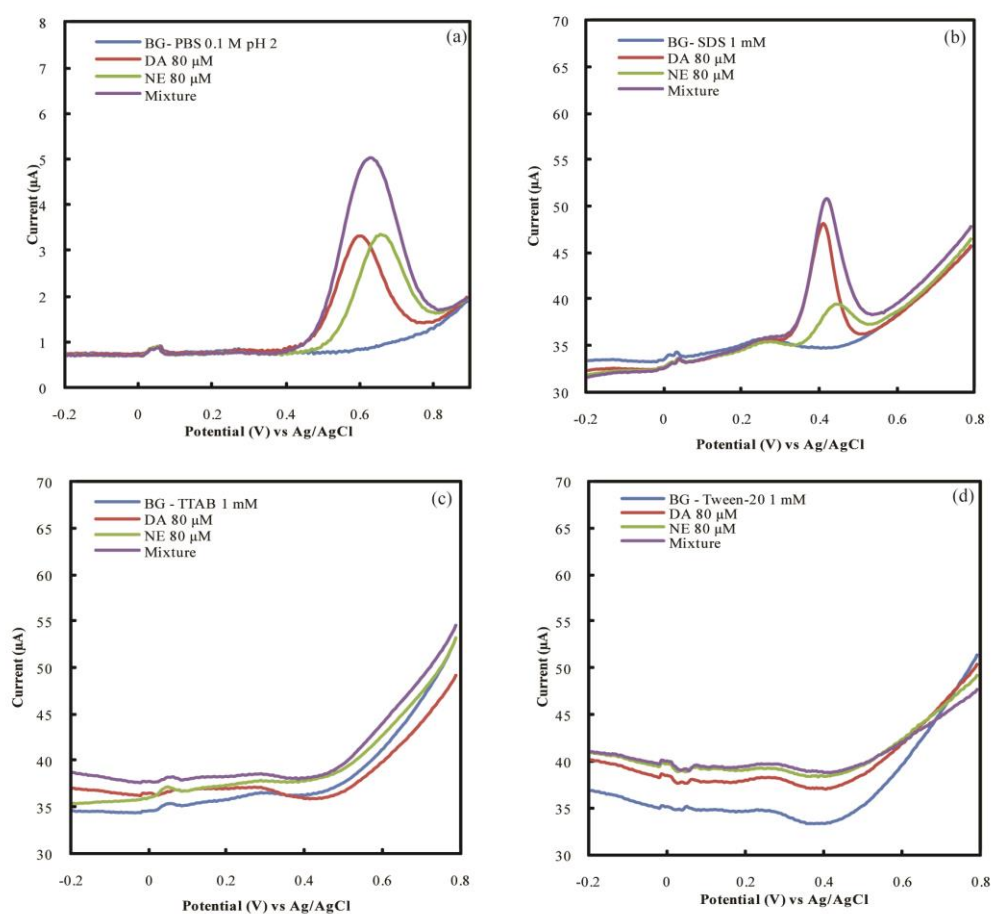
Figure 3.1.9 Representative square-wave voltammograms for either no sample amplification (BG; background) or with three 20-µL applications (preconcentration) of DA (80 µM) or NE (80 µM) (representing 4.8, 4.8 and 24 nmol total of AA, DA and UA, respectively) applied individually or as a mixture of both, in the (a) absence of any surfactant or (b-d) with 1 mM of (b) SDS, (c) TTAB or (d) Tween-20 as the surfactant in the PBS wicking solution.
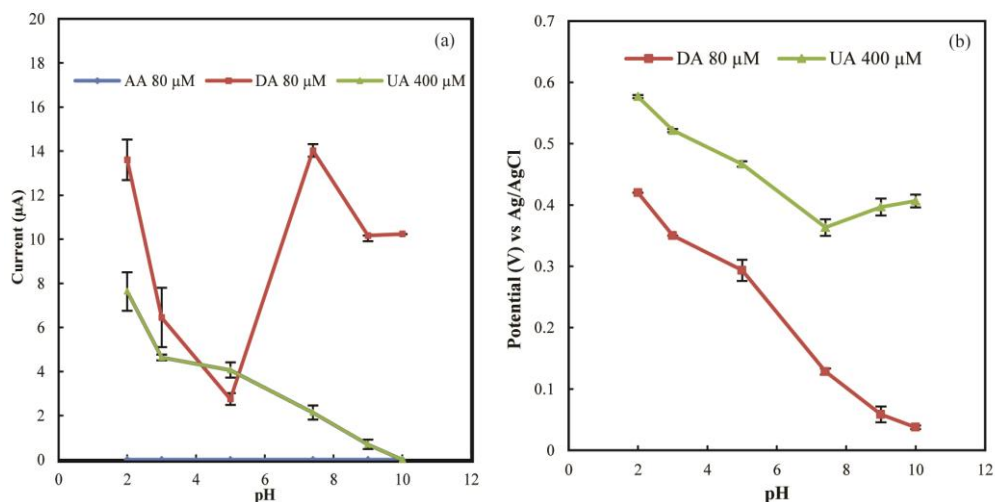
Figure 3.1.10. The effect of the pH value on (a) the peak current of AA (blue line), DA (red line) and UA (green line); and on (b) the oxidation peak potential of DA (red line) and UA (green line). Samples were preconcentrated as three 20-μL applications (DA and AA at 80 μM (4.8 nmol total), UA at 400 μM (24 nmol total)) and wicked with 1 mM SDS in PBS at the indicated pH values.

3.1.4. Conclusions

Here, a novel ePAD was demonstrated for determination of DA levels in serum that made use of a multilayer paper device coupled with selective transport of the cationic DA to the working electrode. Using a series of paper membranes and the addition of multiple aliquots of the test DA-containing sample, a significant preconcentration was achieved, along with an increase in the selectivity due to a shift in the oxidation potential. The system was tested with human serum, and the serum was shown to have a negligible effect on DA determination. The mechanism behind the selective enhancement of the signal is primarily the result of electrostatic interactions of the analytes with the anionic SDS.

3.2 An Electrochemical Compact Disk-type Microfluidics Platform for Use as an Enzymatic Biosensor

Poomrat Rattanarat[a], Prinjaporn Teengam[b], Weena Siangproh[c], Ryoichi Ishimatsu[d], Koji Nakano[d], Orawon Chailapakul[a,e,*], Toshihiko Imato[d,*]

[a]*Electrochemistry and Optical Spectroscopy Research Unit, Department of Chemistry, Faculty of Science, Chulalongkorn University, Patumwan, Bangkok 10330, Thailand*

[b]*Petrochemistry, Faculty of Science, Chulalongkorn University, Patumwan, Bangkok 10330, Thailand*

[c]*Department of Chemistry, Faculty of Science, Srinakharinwirot University, Sukhumvit 23, Wattanna, Bangkok, 10110, Thailand*

[d]*Department of Applied Chemistry, Graduate School of Engineering, Kyushu University, Fukuoka, 819-0395, Japan*

[e]*National Center of Excellence for Petroleum, Petrochemicals, and Advanced Materials, Chulalongkorn University, Bangkok 10330, Thailand*

*Corresponding authors

Abstract

A novel centrifuge-based microfluidic device coupled with an electrochemical detector for the determination of glucose in control human serum is described. The electrochemical compact disk (eCD) platform was based on a poly(dimethylsiloxane) (PDMS) material containing reservoir, a mixing chamber, a spiral channel, a carbon-paste electrode (CPE) detector, and a waste reservoir. For electrode fabrication, a mixture consisting of cobalt phthalocyanine (CoPC), graphite powder, PDMS, and mineral oil was printed and formulated into a PDMS-based electrode pattern. To enhance electrochemical sensitivity, a graphene-polyaniline (G-PANI) nanocomposite solution was cast onto the working electrode surface. During the rotation of the eCD platform at a rotation speed of ~1000 rpm, a glucose solution and a glucose oxidase solution in separate reservoirs were mixed in a spiral channel to produce hydrogen peroxide by an enzymatic reaction. The produced hydrogen peroxide was determined using the electrode detector set at an applied potential of +0.4 V vs. CPE (pseudo reference electrode). Under optimal conditions, a linear calibration ranging from 1 to 10 mM with a limit of detection (LOD) of 0.29 mM (S/N=3) and a limit of quantitation (LOQ) of 0.97 mM (S/N=10) was obtained. Various common interference compounds including ascorbic acid, uric acid, paracetamol, and L-cysteine were tested. Finally, glucose in control serum samples containing certified concentrations were amperometrically determined and validated. Glucose levels measured using the eCD system matched actual values for the certified reference serum samples with satisfactory accuracy.

Keywords: compact disk-type microfluidics, electrochemical detection, glucose oxidase, human serum

3.2.1 Introduction

Miniaturized systems including test strips and microfluidic devices continuously used in numerous applications such as point of care testing, agricultural quality control, food analysis, and environmental monitoring [26, 71, 96, 97]. With its capability, which including portability, prompt response time, and low cost of manufacturing, miniaturized testing devices have proven to be beneficial for handling on-site analysis in remote areas. In terms of clinical diagnosis, the devices can act as a preliminary screening tool which would be able to reduce potential risks associated with aggressive diseases and improve the quality of life for many people. Microfluidics is an innovative technology platform which is geometrically designed in sub-millimeter scale. This device is frequently fabricated on glass [39] or a polymer [5] containing a micropattern platform. In general, the flow of liquids through their channels can be controlled using liquid mechanical pumping or a high voltage power supply for normal flow injection and electrokinetic systems [3, 28], respectively. For detection, various common analytical measurements comprising of optical imaging [98], absorbance [27] and fluorescence spectroscopy [99], and mass spectrometry [100] have been used. The main disadvantages of complicated propulsion and detection systems are their high cost and difficulty to couple with miniaturized systems for fieldwork applications. Therefore, all of these developments present novel analytical challenges which need to be addressed.

Compact disk (CD)-based microfluidics is a new class of miniaturized high-throughput screening systems incorporate various laboratory functionalities such as sampling, mixing, reaction, and detection [101, 102]. The testing and reagent solutions are allowed to flow by centrifugal force. Furthermore, the flow rate can be varied by adjustment of the speed of rotation of the disk via the use of a portable rotary motor system. The solution from the reservoir located at the center of the disk is pumped through the channels and then flows towards to outer perimeter of disk. The advantageous centrifugal pumping is that it is relatively insensitive to physicochemical properties such as pH, ionic strength or chemical composition (in contrast to electroosmotic pumping). The utility of CD technology has progressed and is not used

in applications in biomedical diagnosis, food safety, and environmental monitoring. Some reports [24, 25, 101, 103, 104] have concentrated on measuring several analyte of interest using CD microfluidics. For example, various applications have been reported including enzyme-linked immunosorbent assay (ELISA) for rat immunoglobulin G (IgG) [25] and immunoglobulin A (IgA) [24], cultivation and behavioural observation of *Caenorhabditis elegans* [104], a label-free haptoglobin assay [101], and simultaneous determination of cationic and anionic nutrients (nitrite, nitrate and nitrite, ammonium, orthophosphate, and silicate) in water samples [103]. All of these analyses used spectrophotometric detection. To the best of our knowledge, only a few publications concerning electrochemical detection in centrifugal CD-based microfluidics have appeared.

Electrochemical detection offers great promise with excellent features including remarkable sensitivity, inherent miniaturization of both the detector and control instrumentation [45, 46, 71, 105]. Moreover, this technique is independence of sample turbidity or optical path length, is low cost, and power demands are minimal. Among the electrochemical enzymatic sensors, glucose sensors have been broadly developed because their effectiveness in the point-of-care testing of diabetic human subjects. Over the past five decades, the classical glucose biosensor was based on the consumption of oxygen due to an enzymatic reaction between glucose and glucose oxidase (GOx) and measurement of hydrogen peroxide (H_2O_2), the product of the reaction [106]. Unfortunately, a high applied potential value of H_2O_2 electro-oxidation for amperometric detection is required [107].

As a result, the objective of this research was to develop a novel CD-based microfluidics instrument coupled with a screen-printed electrode for the determination of glucose. To accomplish this, a screen-printed carbon paste electrode was first incorporated onto a CD-based microfluidics platform for in-microchannel detection within the CD-flow pattern. Outstanding electrode modifiers consisting of graphene-polyaniline (G-PANI) nanocomposite and cobalt phthalocyanine (CoPc) electrocatalyst were selected to reduce the applied potential to 0.4 V. vs. CPE for monitoring the H_2O_2 product produced in the enzymatic reaction. This modified

electrode also enhanced the electrochemical response of produced H_2O_2 [108, 109]. Due to the centrifugal force, a test sample solution and a glucose oxidase (GOx) (an enzyme) solution were physically mixed at the mixing chamber of the CD microfluidics platform. Significant parameters including rotating speed, applied potential, GOx concentration were then optimized. Common interfering substances at the highest levels that are present in in human serum (except paracetamol) have a negligible effect towards glucose detection. Finally, our proposed method was applied to the quantitation of glucose in human serum and the results were found to be acceptable.

3.2.2 Experimental

3.2.2.1 Chemicals and Reagent

The SU-8 negative photoresist and developer were purchased from MicroChem Corp. (Newton, MA). All chemicals were analytical grade. The following materials and chemicals were used as received: mineral oil (Perkin Elmer, Thailand), graphite powder ($\leq$20 μm, Sigma-Aldrich, Singapore), and poly(dimethylsiloxane) (PDMS) Sylgard 184 elastomer kit (Dow Corning, USA). Sodium chloride (NaCl), disodium hydrogen phosphate (Na_2HPO_4), potassium dihydrogen phosphate (KH_2PO_4), potassium chloride (KCl) and albumin were purchased from Wako Pure Chemicals Industry (Japan) for preparation of phosphate buffer saline (PBS) 0.1 M pH 7.4. Glucose oxidase (GOx) and potassium ferricyanide ($K_3[Fe(CN)_6]$) were obtained from Sigma-Aldrich (Singapore). Glucose (Glu), dopamine hydrochloride (DA), ascorbic acid (AA), uric acid (UA), paracetamol (PA), cysteine (Cys), citric acid, fructose, glycine, urea, and albumin were purchased from Wako Pure Chemicals Industry (Japan). Polyaniline and camphor-10-sulfonic acid ($C_{10}H_{16}O_4S$) were purchased from Merck (Darmstadt, Germany). Graphene (G) was purchased from A.C.S (Medford, USA). Control human serum samples consisting of level I and II were obtained from Aalto Scientific, Ltd. (San Marcos, CA, USA). Millipore filtered water on a Milli-Q system (Nihon Millipore, Tokyo, Japan) was used throughout this experiment.

3.2.2.2 Fabrication of Electrochemical Compact-disk (eCD system)

3.2.2.2.1. Compact-disk microfluidic platform

Figure 3.2.1a shows the conceptual design of the compact-disk microfluidics set up, comprised of 2 layers of PDMS-based microchannel and electrode. The configuration of eCD platform was described as follows; for upper PDMS layer, microchannel width was 500 µm while the thickness was 100 µm. The reservoir diameter on the CD platform was 5 mm. The radius between each reservoir and the center of the compact disk was 35 mm and 27 mm for testing solution and washing solution, respectively.
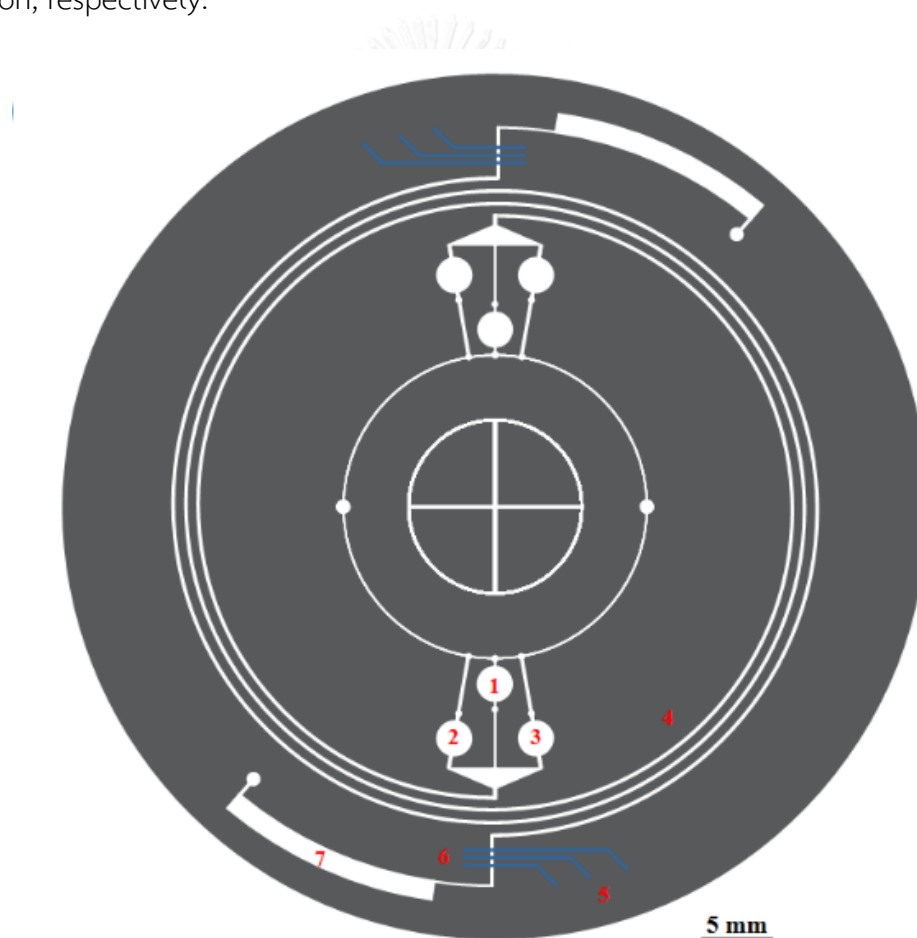
Figure 3.2.1 Concept design of eCD microchip consisting of 1: washing solution reservoir, 2: enzyme reservoir, 3: sample reservoir, 4, spiral mixing channel, 5, G-PANI/CoPc-CPE, 6: detection zone, and 7: waste reservoir.

Microchannel was constructed of PDMS using a soft lithography method as follows [55]. Briefly, the SU-8 negative photoresist was coated onto a silicon wafer substrate using a spin coater (K-359S1, Kyowariken, Tokyo, Japan) at 500 rpm for 20 s and 2000 rpm for 30 s, respectively. The silicon substrate was baked at 65 ^{o}C for 5 min and 95 ^{o}C for 45 min. The transparent films containing the microchannel and electrode design (Figure 3.2.1a) were aligned onto the baked silicon wafer. The baked silicon wafer was then exposed to ultra-violet (UV) light using UV exposure device (BOX-W98, Sunhayato, Tokyo, Japan). The SU-8 master template of CD microfluidic was obtained after treating by SU-8 developer and isopropanol, respectively. Next, the mixture between PDMS and a curing agent in a 10:1 ratio was prepared and degassed under vacuum conditions to remove air bubbles in the PDMS mixture. The clear PDMS mixture was poured over both SU-8 masters and baked in an oven at 65 ^{o}C for at least 2 h. The cross-linked PDMS was peeled off the mold and punched by using a circular punch to create the reservoirs.

3.2.2.2.2. Graphene-polyaniline nanocomposite modified cobalt phthalocyanide-carbon paste electrode (G-PANI/CoPc-CPE)

We followed the previous procedures reported by Sameenoi et al. [6] to fabricate the screen-printed carbon-paste electrode for in-channel detection within the CD microfluidics platform. First, CoPC and a graphite composite (10% w/w) was prepared by adding CoPc to graphite powder and mixing with diethylether to provide a well homogenized CoPc-graphite mixture. The diethylether was completely evaporated to produce a dehydrated powder of 10% (w/w) CoPc-graphite composite. Next, a paste comprised of CoPc-graphite powder, PDMS, and mineral oil in a ratio of 2:1:1 was extensively mixed and then spread onto the PDMS electrode channel. Excess carbon paste was removed using Scotch Magic TapeTM until a clear carbon paste electrode was obtained.

For the electrode modifier, graphene-polyaniline (G-PANI) nanocomposite was prepared using a liquid/liquid interfacial polymerization method [110]. Briefly,

graphene powder was dispersed in a hydrochloric acid solution containing $FeCl_3$, which was used as the water phase. The oil phase was prepared by dissolving aniline monomer in chloroform. Both solutions consisting of an oil and a water phase were transferred to a beaker and the polymerization of polyaniline was allowed to proceed for 2 days. Finally, the product was collected by filtration and rinsed with distilled water, following drying step in a vacuum oven at 60 ^{o}C for 1 day. A JEM-2100 transmission electron microscope (Japan Electron Optics Laboratory Co., Ltd, Japan) was used for the electrode characterization.

In the next step, the G-PANI nanocomposite was redispersed in an NMP solution and carefully cast onto surface area of the carbon-paste working electrode. The cast CPE was baked in an oven at 65 ^{o}C. For both electrochemical sensing in batch and eCD systems, a second PDMS layer (consisting of 8 mm diameter hole or CD microchannel) was plasma-sealed to PDMS layer containing G-PANI/CoPc-CPE. The actual working electrode area for the batch system was 4 mm^2 while the eCD system was 0.25 mm^2. Finally, copper wires were connected to the end of the CPE using silver paint (SPI supplies, West Chester, PA) and epoxy glue, respectively.

3.2.2.3 Centrifugal Rotating Procedure

The eCD microchip was set on a turn table fabricated by Kyusgu Keisoku Co., Ltd., Japan. Prior to the analysis, 10 μL of 0.1 M PBS was added to reservoir No. 1 used as the washing solution while 10 μL aliquots of 100 U/mL GOx and the test solution were dropped into reservoirs No. 2 and 3, respectively. Scotch Magic Tape^{TM} was also used to cover all reservoirs and the waste area to prevent the leakage of solution during rotation of the CD microchip. The LabView software was used to control the rotating speed of the CD microchip by adjusting the applied voltage. In order to observe flow characteristic in the CD microchannel, a high speed camera (VW-Z1, Keyence, Co., Japan) was used to indicate the required rotating speed to provide the optimal centrifugal force to initiate solution flow. Figure 3.2.2 shows a captured photograph using a pink Rose Bengal solution for visible observation within the CD microchannel. The speed of rotation was increased to 957 rpm within 30 s and

maintained at the same speed for 390 s to generate a solution flow via centrifugal force. The mixing solution from reservoir No. 2, 3 and the flow of the washing solution were generated, respectively. All solutions had completely flowed to the waste reservoir within 400 s.

3.2.2.4 Electrochemical Detection of Glucose

For cyclic voltammetry and amperometry, a commercially available potentiostat (ALS/chi Electrochemical Analyzer Model 715AN, CH instruments, Austin, TX, USA) was used. The working electrode was either a G-PANI/CoPC-CPE or a CPE. The auxiliary and reference electrodes were CPE. All experiments were conducted at room temperature. For the batch system, cyclic voltammetry was used to characterize the electrochemical performance of the bare CPE and the G-PANI/CoPc-CPE. A cyclic voltammogram of hydrogen peroxide (H_2O_2) was recorded in the range of -0.2 to 1.0 V vs. CPE at scan rate of 100 mV/s.

An amperometric method was used for the detection of produced H_2O_2 in the eCD microchip system. To optimize the amperometric applied potential, hydrodynamic voltammetry in a range of 0.2–0.8 V vs. CPE was examined. The hydrodynamic voltammogram was plotted between the peak current and applied potential. The amperometric measurements were performed at the potential of 0.4 V vs. CPE which obtained from the maximum signal-to-background (S/B) ratio in the hydrodynamic voltammograms. A calibration graph between the anodic current and glucose concentration was created using the linear least square regression method. The limit of detection (LOD) and the limit of quantitation (LOQ) were calculated from $3SD_{bl}/S$ to $10SD_{bl}/S$, respectively, where SD_{bl} is the standard deviation of the blank measurement ($n = 7$) and S is the slope of the linearity or sensitivity of the method. In addition, the selectivity in this work was examined by observing whether any electroactive interference, present as a main component in normal human serum was an issue. For glucose determination in control human serum, all samples were directly tested using the eCD microchip system without any pre-treatment procedure.
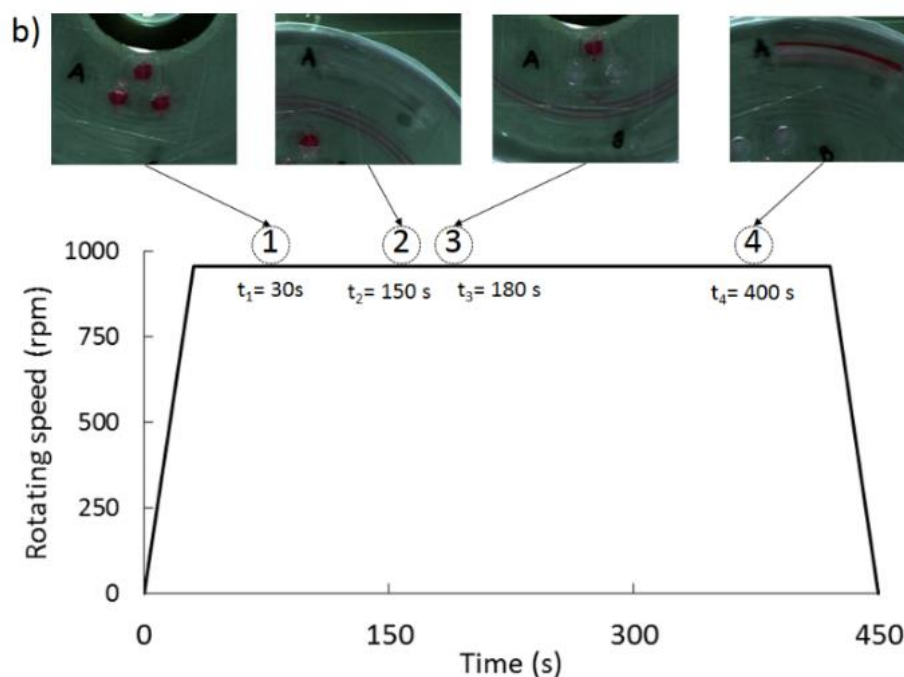
Figure 3.2.2 Rotating speed set up to centrifugal force for controlling the solution delivery system inside CD microchip within 450 s (inset) captured frames obtained from high speed camera.

3.2.3 Results and Discussion

3.2.3.1 eCD Design

To investigate the flow characteristic of a solution within a channel, the fluidic manipulation of Rose Bengal solutions inside the microfluidic platform was recorded using a high-speed CCD camera. Images of the solutions in the reservoir at each rotation speed are shown in Figure 3.2.2. When the rotation speed was increased (at 0-30 s), the solutions were forced by centrifugal force to flow toward the bottom side of reservoir No.1 and 2. At 30 s, the solution in reservoir No.1 and 2 flowed out and mixed at a critical rotation speed of 957 rpm. At 150 s, the solution was moved to the electrochemical detection zone while the washing solution was started to flow at 180 s with the same critical rotation speed. Finally, all of the solutions had completely flowed out and moved to the waste reservoir at 400 s. The mixing between solutions in reservoirs No.1 and 2 occurred simultaneously due to the similar distance between

the channel inlet and the center of the CD. Moreover, the washing solution in reservoir No.3 which was located at a shorter distance from the center of the CD, was subjected to a higher centrifugal force. Thus, the solution in reservoirs No.1 and 2 began to flow before the solution in reservoir No.3 with a calculated flow rate of 0.17 µL/s. In addition, the solution in reservoir No.1 and 2 can be completely mixed in 120 s within a spiral channel which is beneficial for the reaction time of glucose and glucose oxidase which require a mixing time of at least 2 min. As a result, our system is particularly suitable for use in an enzymatic assay in the microchip channel with a simple manual operation and substantially reduced reagent consumption.

3.2.3.2 H_2O_2 Detection of G-PANI/CoPc-CPE

Electrochemical enzymatic biosensor based on glucose oxidase (GOx) has played an important role in simple easy-to-use blood glucose testing. H_2O_2 product from the reaction between glucose and GOx was electrochemically measured at electrode. Therefore, the measurement of the H_2O_2 produced from GOx reaction can be used to determine glucose level indirectly. In this work, a G-PANI/CoPc-CPE was used for the sensitive detection of H_2O_2 and glucose using cyclic voltammetry and amperometry. Electrode modifier comprised of CoPc electrocatalyst and G-PANI nanocomposite. The role of the CoPc is to provide electrocatalytic activity by reducing the working potential of carbon-paste electrode as follows [111]. First, Co(III) was chemically reduced by H_2O_2 to Co(II). Then, Co(II) was electrochemically oxidized to Co(III). Moreover, G-PANI nanocomposite can enhance the electrochemical sensitivity of electrode due to large surface area of its nanostructure [5, 108]. Comparison of electrochemical performance between G-PANI/CoPc-CPE and bare CPE are illustrated in Figure 3.2.3a.
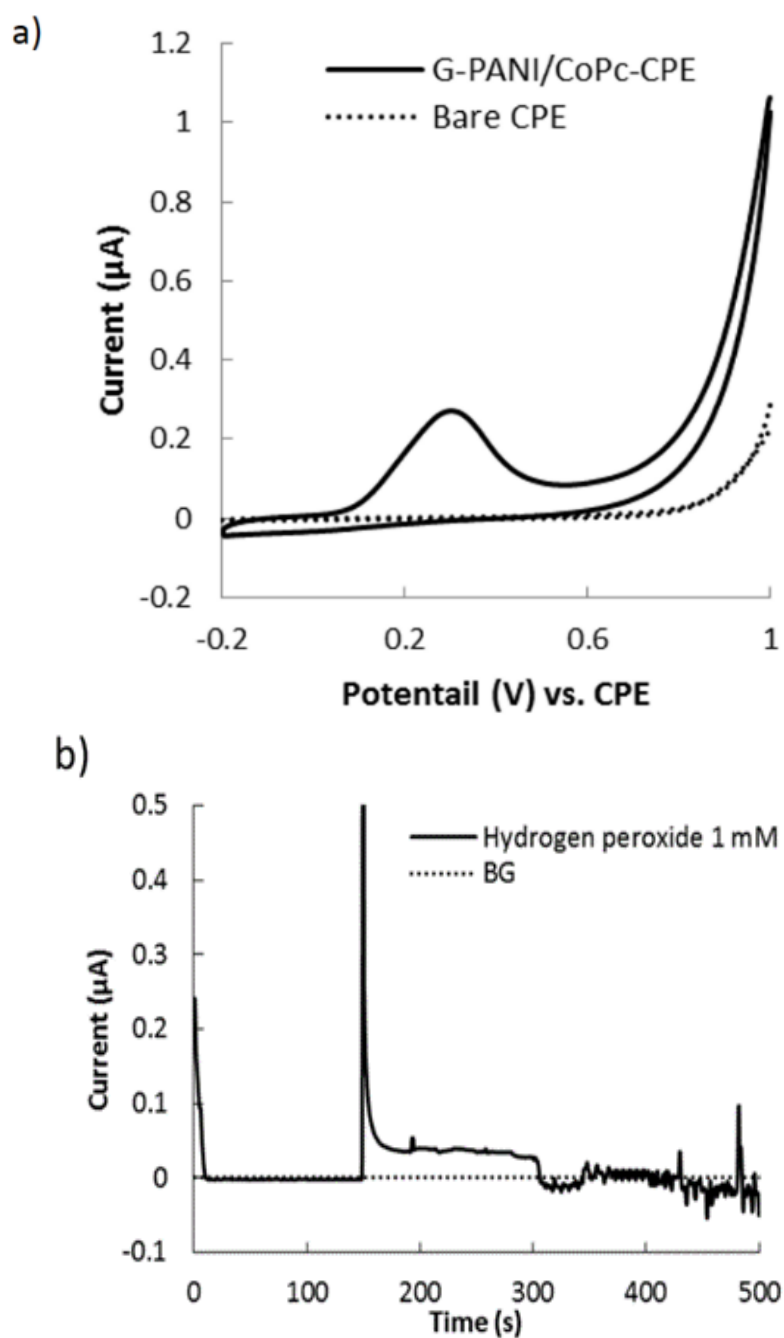
Figure 3.2.3 (a) Cyclic voltammograms of 1 mM H_2O_2 in 0.1 M PBS pH 7.4 measured in electrochemical batch cell based on a G-PANI/CoPc-CPE (solid line) and bare CPE (dash line) at a scan rate of 100 mV/s. (b) Amperogtram of 1 mM H_2O_2 in 0.1 M PBS pH 7.4 measured by eCD system based on a G-PANI/CoPc-CPE.

Compared to a bare CPE (dashed line), a well-defined irreversible anodic peak with a significant increase in anodic current of H_2O_2 by using G-PANI/CoPc-CPE was observed, indicating that G-PANI nanocomposite and CoPc electrocatalyst might be a promising electrode modifier for sensitive detection of glucose due to its excellent electrocatalytic activity. Figure 3.2.3b shows the amperometric response of 1 mM H_2O_2 in 0.1 M PBS pH 7.4, obtained from the eCD system based on a G-PANI/CoPc-CPE. According to the period of time required for the H_2O_2 solution to flow to the electrode surface (between 150 to 300 s), the anodic current decreased with time which is related to the Cottrel equation [112]. The anodic current then decreased because the washing solution passed through the electrode surface. For the further determination of glucose using the eCD system, the amperometric currents were recorded at a steady state current of 300 s (before the signal dropped) [113].

3.2.3.3. Optimization Conditions

Various optimization conditions were examined, including applied potential, rotating speed, and GOx concentration.

3.2.3.3.1. Applied Potential

To obtain the optimal potential for amperometric detection in the eCD system, the hydrodynamic voltammetry of 1 mM H_2O_2 was studied, as shown in Figure 3.2.4a. A hydrodynamic voltammetric *i–E* curve obtained at the G-PANI/CoPc-CPE electrode for 1 mM H_2O_2 (solid line) vs. 0.1 M PBS pH 7.4 (dash line). The anodic current of H_2O_2 obviously increased as a function of the detection potential; however, the background current increased as well. The *S/B* ratios were calculated from the data in Figure 3.2.4a at each potential. The resulting curve for the *S/B* ratios vs. potential is shown in Figure 3.2.4b. The result shows that the maximum *S/B* ratio was found to be 0.4 V vs. CPE. Higher potentials over 0.8 V. vs CPE were not investigated in order to reduce the tendency for interfering compounds (e.g. ascorbic acid (AA), uric acid (UA), and paracetamol (PA)) to be oxidized [107]. Therefore, this optimal applied potential of

+0.4 V vs. CPE was selected for quantitative amperometric detection in the eCD experiments.
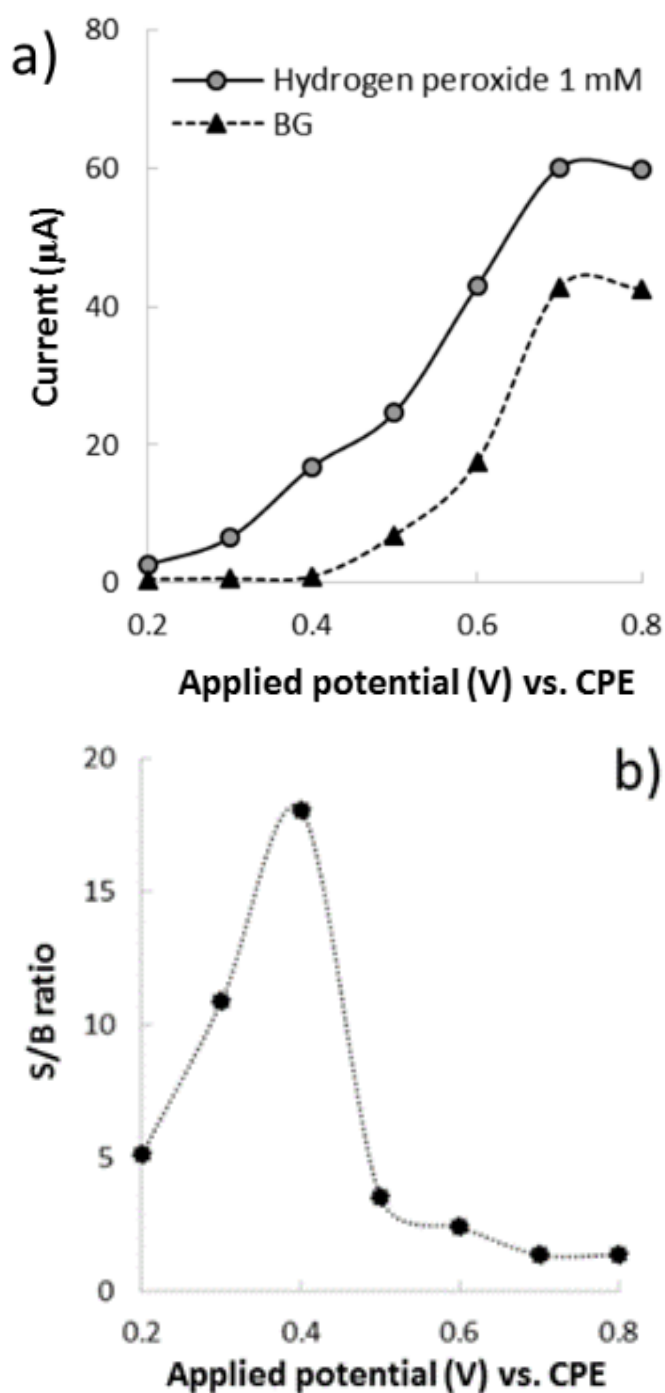
Figure 3.2.4 (a) A hydrodynamic voltammetric i–E curve obtained at the G-PANI/CoPc-CPE electrode for 1 mM H$_2$O$_2$ (solid line) versus 0.1 M PBS pH 7.4 (dash line). (b) A signal-to-background (S/N) ratios extracted from Figure 3.2.4a.

3.2.3.3.2. Rotating Speed

The speed of rotation of eCD is related to the flow rate of the solution. When the rotating speed is increased, the flow rate of a solution within the microfluidic platform also increases. Figure 3.2.5 displays displays amperograms for a 1 mM H_2O_2 solution obtained using different rotating speeds in the range of 957-1598 rpm.
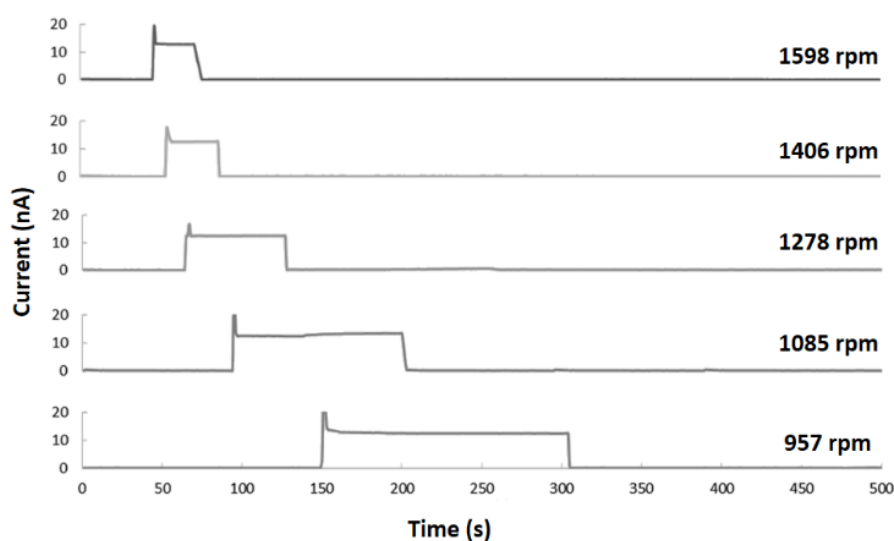
Figure 3.2.5 Effect of rotating speed for amperometric detection of 1 mM H_2O_2 in 0.1 M PBS pH 7.4 using eCD system based on a G-PANI/CoPc-CPE at applied potential of +0.4 V vs. CPE.

The results show that the peak width decreased with increasing flow rate. Lower flow rates below 957 rpm were not studied because the flow of all solutions through the electrochemical detection zone was incomplete. Although a rotating speed at 1085 rpm provided the highest oxidation current of H_2O_2, the mixing time is shorter than a rotating speed of 957 rpm. As a result, the optimal rotating speed in this eCD system was found to be 957 rpm.

3.2.3.3.3. GOx Concentration

The influence of GOx concentration in reservoir No.2 on the response to the 2 mM glucose substrate was investigated. The current increased rapidly when the GOx

concentration was increased from 0 U/mL to 100 U/mL, and then reached a plateau from 100 to 200 U/mL. We believe that this plateau phenomena is due to the complete consumption of glucose by an excess GOx concentration. Therefore, the optimal concentration was found to be 100 U/mL.
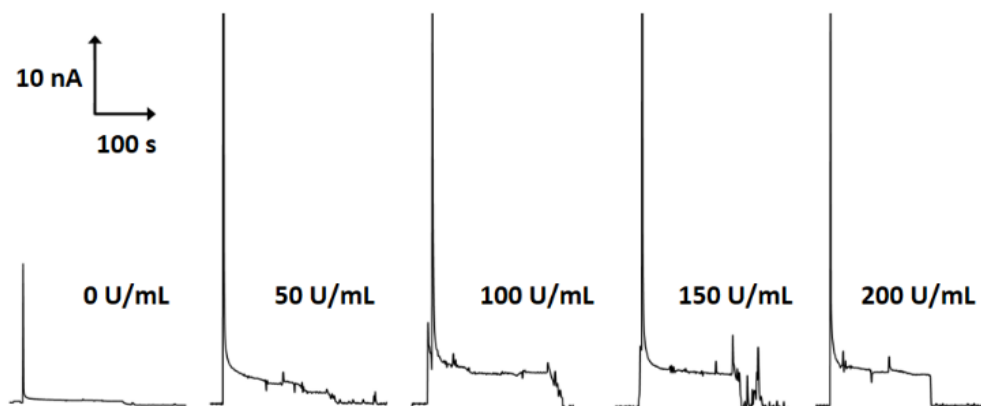
Figure 3.2.6 Amperogram of 2 mM glucose with different concentration of GOx (0-200 U/mL) in 0.1 M PBS pH 7.4 measured by eCD system based on a G-PANI/CoPc-CPE at applied potential of +0.4 V vs. CPE.

3.2.3.4. Analytical Performance

The optimized conditions for glucose detection using the eCD system consisting of 100 U/mL GOx, an applied potential of +0.4 V vs. CPE, and a rotating speed of 957 rpm were used to construct the calibration curve, which is shown in Figure 3.2.7. Using the optimal conditions, the linear calibration was in the range of 1 to 10 mM with a correlation coefficient of 0.996 and relative standard deviation (%RSD) of 4.26%
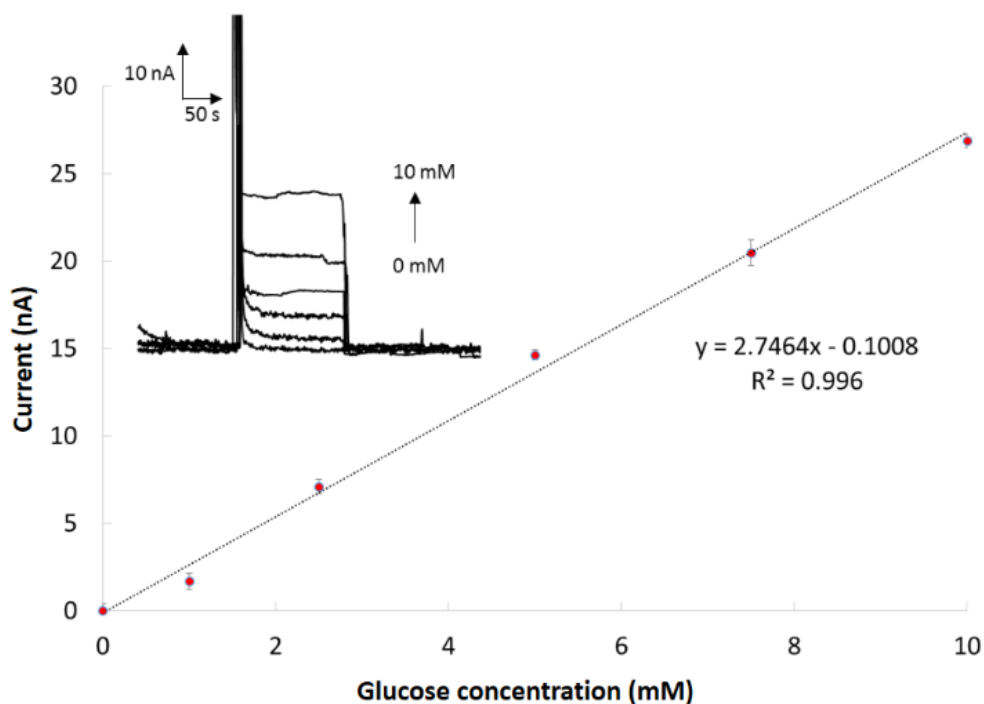
Figure 3.2.7 Calibration curve and amperogram (inset) for glucose assay using eCD system based on a G-PANI/CoPc-CPE at applied potential of +0.4 V vs. CPE.

The limit of detection (LOD, *S/N*=3) and limit of quantitation (LOQ, *S/N*=10) were found to be 0.29 mM and of 0.97 mM, respectively. These results indicate that our eCD system provided a low detection limit and a wide linear range for the determination of glucose. Usually, the normal glucose levels in whole blood and serum are in the range of 3.5-5.3 mM and 2.5-5.3 mM, respectively [86]. Our eCD can be effectively used for measurements in this range; therefore, this proposed system can be applied to the determination of glucose in both whole blood and serum within our linear calibration range.

Although the LOD and LOQ values reported here are higher than those reported in previous studies [111, 114-117], our eCD system requires an extremely low sample volume (only 10 μL) for each glucose assay. In addition, this proposed method included all of these steps, i.e., sample-enzyme mixing, electrochemical measurement, and washing steps; therefore, it provides more advantages than conventioncal electrochemical batch systems in that the for an analysis and reagent/sample consumption are reduced substantially.

3.2.3.5. Interference Study

In order to evaluate the selectivity of this eCD system, the effect of various foreign compounds on the determination of 2 mM glucose by the proposed method was investigated. Generally, for the electrochemical detection of glucose in biological fluids, some coexisting electroactive species including ascorbic acid (AA), uric acid (UA), paracetamol (PA), and L-cysteine (Cys) have been considered because these compounds can also be oxidized at an anodic potential similr to that for H_2O_2 [107, 111]. The results are summarized in Figure 3.2.8 and Table 3.2.1.   The tolerance limit was defined as the concentration of an interfering compound required to generate a change in the electrochemical response of more than or equal to 5% when compared to the response obtained from the standard concentration. The result shows that 5% tolerance concentration from adding interfering compounds was observed over their highest normal level found in human serum. This serves to confirm that there were no significant interferences in blood or plasma. Unfortunately, only PA appeared to have an impact on the selectivity of the proposed eCD system; therefore, PA needed to be diluted or removed to a level where it no longer influenced the analytical results.

Table 3.2.1 Influence of eletroactive interfering species on glucose assay

Interference	Highest normal level in serum (mM)	5% Tolerance concentration (mM)
Ascorbic acid	0.08	0.16
Uric acid	0.4	0.8
Paracetamol	0.1	0.1
L-cysteine	0.05	0.2
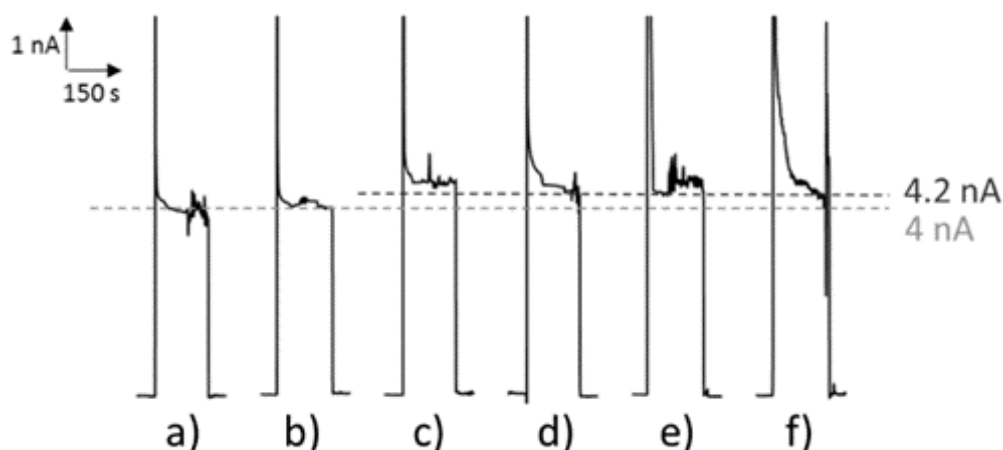
Figure 3.2.8 Amperograms of 2 mM glucose and 100 U/mL GOx with/without interfering compounds at highest concentration found in normal human serum and 5% tolerance concentration (mM). Conditions: (a) glucose without interfering compound, (b) glucose with 0.08 mM AA, 0.4 mM UA, 0.05 mM PA, and 0.2 mM Cys, (c) glucose with 0.16 mM AA, (d) glucose with 0.8 mM UA, (e) glucose with 0.1 mM PA, and (f) glucose with 0.2 mM Cys.

3.2.3.6. Determination of Glucose in Human Serum

To evaluate the eCD microfluidic system with actual samples, seven replicate determinations (n=7) of glucose in clinical control samples was performed. The control samples are common systems for evaluating the accuracy of diagnostic tests in a biologically relevant matrix without worry of blood borne pathogens. The results are shown in Table 2.

Table 3.2.2 Determination of glucose in control serum samples

Sample	Glucose concentration (mM ± SD[1])	
	Certified level	Proposed method
Human serum level I	4.77±0.39	4.62±0.09
Human serum level II	15.54±1.28	16.00±0.28

[1]SD, standard deviation (n=7)

The paired t-test was used to validate our method versus both control levels for glucose. No significant difference was found at the 95% confidence level. Thus, the analyzed values of glucose in human serum are acceptable. Therefore, it can be successfully applied to the determination of glucose in control samples.

3.2.4. Conclusions

We demonstrate the potential of using CD microfluidic biosensor to access quantitative measurement of critical diabetes markers in serum for the first time. Using G-PANI nanocomposite, significant electrochemical enhancement was achieved, along with an improvement in the selectivity due to a shift in less oxidation potential by using CoPc electrocatalyst. This spiral channel platform has been suitably designed for the optimal mixing between glucose and oxidase enzyme for 2 min. Eventually, this eCD system was accomplished for selective determination of glucose in human serums with a reasonable agreement corresponding to actual glucose level in the serum. Therefore, this practical eCD system has been valuable for various electrochemical detections required mixing step like enzymatic reaction. Additionally, this eCD model can be further extended to several applications such as point-of-care testing, quality control of foods and/or beverages, and environmental monitoring.

3.3 High-throughput Determination of 4-Aminophenol using a Graphene-Polyaniline Modified Electrochemical Droplet-Based Microfluidic Sensor

Poomrat Rattanarat[a], Akkapol. Suea-Ngam[b], Nipapon Ruecha[c], Weena Siangproh[d], Charles. S. Henry,[e,f], Monpichar Srisa-Art,[b,*] and Orawon Chailapakul[a,g,*]

[a]Electrochemistry and Optical Spectroscopy Research Unit (EOSRU), Department of Chemistry, Faculty of Science, Chulalongkorn University, Patumwan, Bangkok 10330, Thailand. E-mail: corawon@chula.ac.th

[b]Chromatography and Separation Research Unit (ChSRU), Department of Chemistry, Faculty of Science, Chulalongkorn University, Patumwan, Bangkok 10330, Thailand. E-mail: monpichar.s@chula.ac.th

[c]Program in Macromolecular Science, Faculty of Science, Chulalongkorn University, Patumwan, Bangkok 10330, Thailand.

[d]Department of Chemistry, Faculty of Science, Srinakharinwirot University, Sukhumvit 23, Wattana, Bangkok 10110, Thailand.

[e]Department of Chemistry, Colorado State University, Fort Collins, CO 80523, United States.

[f]School of Biomedical Engineering, Colorado State University, Fort Collins, CO 80523, United States.

[g]National Center of Excellent of Petroleum, Petrochemicals and Advanced Materials, Chulalongkorn University, Patumwan, Bangkok 10330, Thailand.

*Corresponding authors

Abstract

A droplet-based microfluidic device coupled with electrochemical detection using a graphene-polyaniline modified carbon paste electrode (G-PANI/CPE) was successfully developed for high-throughput detection of 4-aminophenol (4-AP) in paracetamol (PA) drug formulations. A simple T-junction microfluidic platform using an oil flow rate of 1.8 µL/min and an aqueous flow rate of 0.8 µL/min was used to continuously produce aqueous testing microdroplets within its microchannel. The microchannel was designed to allow the aqueous droplet to span all 3 electrode bands, allowing for electrochemical measurements in a single droplet. Parameters including G:PANI ratio, droplet flow rate, water fraction, and applied detection potential (E_{app}) were investigated to obtain optimal conditions. Using G-PANI/CPE significantly increased the detection current for both cyclic voltammetric detections of ferri/ferrocyanide $[Fe(CN)_6]^{3-/4-}$ ion (10 times) and 4-AP (2 times), compared to an unmodified electrode. Using the optimized conditions in the droplet system, 4-AP in the presence of PA was selectively determined. The linear range of 4-AP was 50-500 M (R^2 = 0.9972), limit of detection (LOD, S/N=3) was 53.77 µM, and limit of quantification (LOQ, S/N=10) was 170.94 µM. Finally, the system was used to determine 4-AP spiked in commercial PA liquid drugs and found good agreement with those obtained from conventional capillary zone electrophoresis/UV-Visible spectrophotometric (CZE/UV-Vis). The resulting microfluidic device could be employed for high-throughput screening tool for pharmaceutical purity requiring low sample and reagent consumption.

Keywords: droplet-based microfluidics, electrochemical detection, 4-aminophenol, paracetamol

3.3.1 Introduction

Since the mid-1940s, paracetamol (PA, acetaminophen or N-acetyl-p-aminophenol) has been commonly used as an antipyretic and analgesic drug around the world [118, 119]. Many paracetamol formulations, such as tablets, syrups, injections, and suppositories, have been available and highly effective for a variety of patients including children, pregnant women, and the elderly. Unfortunately, 4-AP residue might be present as an impurity in paracetamol formulations obtained from its synthesis or as a result of degradation [120]. Consuming 4-AP unintentionally can cause numerous pathologies (e.g. nephrotoxicity and hepatotoxicity). The European, United States, British, German, and Chinese Pharmacopoeias have set the maximum allowable limit of 4-AP in the paracetamol drug formulations at 50 ppm (0.005% w/w). Several analytical approaches to determine 4-aminophenol in paracetamol formulations have been developed, including high performance liquid chromatography (HPLC) coupled with UV-Visible [121, 122] or fluorescence detection [123], electrochemical detection [124], capillary electrophoresis [125, 126] and flow-based analytical techniques [127, 128]. Although highly, selective, and sensitive, these techniques are also time consuming, have high operation costs, and are available only in sophisticated laboratories.

Recently, droplet microfluidics have demonstrated promise for analytical measurements due to their portability, fast analysis time, low manufacturing cost, low reagent/sample consumption, and high-throughput screening [23]. Droplet microfluidics are capable of generating and manipulating small droplets encapsulated by an immiscible phase. Among other microfluidic platforms, droplet microfluidics have gained attention because of superior mixing efficiency and low dispersion adsorption of sample within the microchannel [129]. The utility of droplet-based technology has been demonstrated for many diagnostic applications including biomedical diagnosis [130, 131], food safety [132, 133], and environmental monitoring [134]. Other demonstrated applications include protein crystallization [135] and enzymatic kinetic assays [20], emulsion based polymerase chain reaction [136], chemical synthesis [35], and single cell-based analysis [34]. For detection in droplet

microfluidics, various detection methods have been used for content detection including laser-induced fluorescence [9], mass spectrometry [40], Raman spectroscopy [38], bright-field microscopy [137], and absorption spectroscopy [138]. Although these techniques offer highly selective, sensitive and accurate quantification, the main disadvantage of these techniques are high equipment cost and challenge of coupling them with miniaturized systems for on-site application.

Electrochemical detection is an attractive alternative for microfluidics because it is low cost, high speed, sensitive, cost-effective, and independent of sample turbidity or optical path length [139]. Currently, there have been a few reports on electrochemical detection for droplet microfluidic systems. For example, Liu et al. used chronoamperometry for the detection of droplet contents and characterization of droplet generation (e.g. frequency, size and velocity [113]. Han et al. [140] developed an amperometric droplet microfluidic device to investigate the kinetics of enzymatic decomposition of H_2O_2 using catalase. Gu et al. [21] used a Pt-black modified electrochemical droplet-based microfluidic sensor for enzymatic glucose assays in biological fluids. Itoh et al. demonstrated a novel droplet-based microdevice with an electrochemical ATP-sensing function for fish freshness determination [141].

The use of nanomaterials to improve electrode performance in microfluidic devices has drawn increasing attention in recent years. Numerous nanomaterials types (e.g. gold nanoparticles, silver nanoparticles, single-wall carbon nanotubes, and multi-wall carbon nanotubes) are currently available and can increase active surface area of working electrode, leading to enhanced electrochemical sensitivity and conductivity [71, 111, 115, 116]. Graphene (G) has received substantial attention for chemical modification of electrodes [142], owing to its large surface area, extraordinary electrical conductivity, high mechanical strength and potentially low manufacturing cost. In addition, G has been also used to modify electrode surface in order to improve the electrochemical properties of the electrodes. One problem with G-based electrode modification is the potential for self-agglomeration of pure G on the electrode surface. One solution is use of a nanocomposite consisting of conducting polymer and G to increase the distribution of graphene [143]. Among conducting

polymers, polyaniline (PANI) has been widely used for electrode modification because of its inherent electrochemical properties, biocompatibility and stability [108, 109]. Previous reports have used G-PANI hybrid modified electrochemical sensors for electrochemiluminescent detection of luminol [144], voltammetric determinations of dopamine [108] and dobutamine [145], and electrochemical immunoassays of estradiol [146] and salbutamol [147].

To the best of our knowledge, there are no previous reports combining droplet microfluidics and G-PANI modified electrodes for determination of 4-AP. As a result, the aim of this work is to develop a method using G-PANI modified electrochemical droplet-based microfluidic sensor for high-throughput and sensitive determination of 4-AP in pharmaceutical PA products. An improved selectivity for 4-AP was achieved using G-PANI modified carbon-paste electrodes (G-PANI/CPE) operating at the optimized potential for highly selective detection of 4-AP in the presence of PA. The advantages of this high-throughput system including ease of operation, less sample/reagent consumption, and cost were demonstrated. Finally, the method was successfully applied for the determination of 4-AP levels in commercial PA liquid drug samples giving high correlation with a CZE/UV-Vis method.

3.3.2 Experimental

3.3.2.1 Materials and Chemicals

The following materials were used as received: poly(dimethylsiloxane) (PDMS) Sylgard 184 eleastomer kit (Dow Corning, USA), mineral oil (Perkin Elmer, Thailand), silver paint (SPI supplies, USA), graphite powder (≤20 µm, Sigma-Aldrich, Singapore), and graphene (A.C.S Medford, USA). All chemicals were analytical grade: sodium chloride (NaCl: Merck, Thailand), disodium hydrogen phosphate (Na$_2$HPO$_4$: Merck, Thailand), potassium dihydrogen phosphate (KH$_2$PO$_4$: Carlo ERBA, Thailand), potassium chloride (KCl: Ajax Finechem, Thailand), and ethanol (Merck, Thailand). Potassium ferricyanide (K$_3$[Fe(CN)$_6$]) and potassium ferrocyanide (K$_4$[Fe(CN)$_6$]) were obtained from Sigma-Aldrich (Singapore). Polyaniline and camphor-10-sulfonic acid (C$_{10}$H$_{16}$O$_4$S) were purchased from Merck (Darmstadt, Germany). 4-Aminophenol (4-AP) and paracetamol

(PA) were purchased from Sigma-Aldrich (Singapore). Commercial paracetamol drugs consisting of Infants' Tylenol were purchased from local pharmacy in Thailand. For droplet generation, a 10:2 (v/v) mixture of perfluorodecalin (mixture of cis and trans, 95%, Sigma-Aldrich, Germany) and 1H, 1H, 2H, 2H-perfluoro-1-octanol (97%, Sigma-Aldrich, Germany) was used as an oil solution. All aqueous solutions were prepared with deionized water (18.0 MΩ cm. Milli-Q Gradient System, Millipore, Thailand). Phosphate buffer saline (PBS) pH 7.4 at a concentration of 0.1 M was used as a supporting electrolyte for all experiments. To prepare 0.1 M PBS, the mixture comprising of 2.0 g NaCl, 0.05 g KCl, 0.36 g Na_2HPO_4 and 0.06 g KH_2PO_4 was dissolved in a 250 mL volumetric flask using deionized water. All aqueous stock standards of 4-AP and PA were prepared in 0.1 M PBS.

3.3.2.2 Fabrication of Patterned PDMS

In this work, solutions were pumped through the device using syringe pumps (Harvard Apparatus 11 Plus). Both aqueous and oil phases was prepared and stored in 1 mL plastic syringes (Nipro, Thailand). Polyethylene tubing (0.38 mm I.D., 1.09 mm O.D., PORTEX, Belgium) connecting the inlets of microfluidic device with syringe pump was secured using commercial epoxy. For microfluidics experiments, a T-junction microchannel and electrode layout originally published by Liu et al. was used [113]. Briefly, the SU-8 negative photoresist was coated onto a silicon wafer using a spin coater and then baked at 95 °C for 45 min. Next, the transparency films containing the microchannel and electrode pattern were placed over the wafer, and exposed to ultra-violet (UV) light for pattern. The final SU-8 templates were obtained by washing with SU-8 developer and isopropanol, respectively. Microchannel platforms were fabricated using published soft lithography methods using a 10:1 ratio of Sylgard 184 to cross linking agent. The mixture was degassed under vacuum to remove dissolved air. The PDMS mixture was poured onto SU-8 masters and baked in the oven at 65 °C for 3 hrs. The cross-linked PDMS was peeled off the mold, and inlets created using a circular biopsy punch. Two PDMS replicas containing the microchannel layer and the electrode layer were obtained. The depth of all microchannels was 100 μm. For upper PDMS layer, the main channel of 500 μm width was narrowed to be a confined channel

(50 μm width and 1 cm length) with two inlets and one outlet. For lower electrode layer, three parallel electrode channels 100 μm deep and 500 μm wide with a spacing between each electrode of 500 μm was used according to previous reports

3.3.2.3 Fabrication and Modification of Electrode

Electrode fabrication was accomplished in two steps, screen-printing of the carbon-paste electrode and electrode modification using G-PANI nanocomposite. PDMS cross-linked carbon paste electrodes (CPEs) were created using the previously published method from Sameenoi et al. [6]. Briefly, a carbon paste containing graphite powder, mineral oil, and PDMS mixture in a ratio of 2:1:1 was spread over the electrode channels in the PDMS. Excess paste was removed using Scotch Magic Tape^{TM} until a well-defined carbon paste electrode was obtained.

For electrode modification, G-PANI nanocomposite was prepared using a simple physical mixing procedure [143]. G in NMP solution (2 mg mL-1) was prepared and dispersed using an ultrasonicate bath for 12 hours at room temperature. The conductive form of PANI was prepared by doping with camphor-10-sulfonic acid and dissolved in chloroform. Then, the G and PANI solutions were mixed and sonicated for 12 hrs to obtain a well-dispersed G-PANI nanocomposite solution. Next, 1 μL-aliquot of G-PANI nanocomposite was cast onto surface area of carbon-paste working electrode. The modified CPE was baked in the oven at 65 $^{\circ}$C in order to evaporate NMP solution. The morphology of G-PANI nanocomposite was observed using, a JEM-2100 transmission electron microscope (Japan Electron Optics Laboratory Co., Ltd, Japan). For electrochemical detection in batch and droplet-based systems, a second PDMS layer (containing 10 mm diameter hole or T-junction microchannel) was sealed over PDMS layer containing G-PANI/CPE using reversible ethanol bonding method. Ethanol was dropped onto both PDMS surfaces, the surfaces carefully aligned before baking at 65°C for 1 hour. For electrical connections were made using wires glued to the electrode using silver paste (SPI supplies, West Chester, PA) and epoxy. The actual working electrode area for the batch system was 5 mm^2 while droplet system was

0.025 mm^2. Example microfluidic device and batch cell devices are shown in the Figure 3.3.1a and b, respectively.
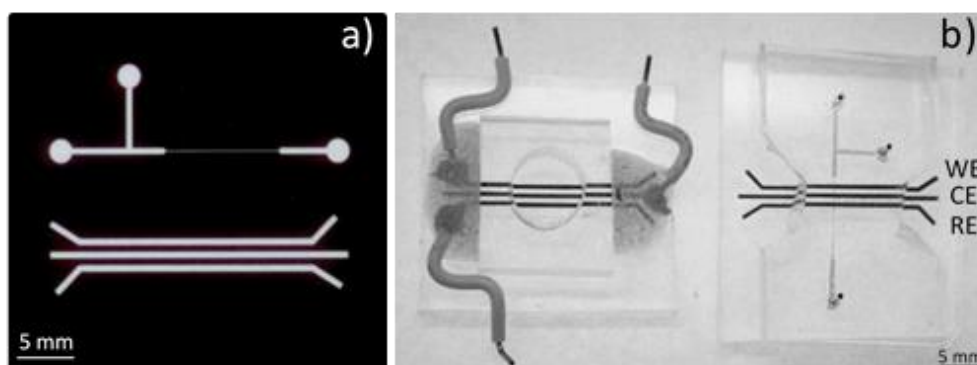
Figure 3.3.1 (a) Schematic of microchannel and electrode patterns, (b) An electrochemical batch cell (left) and a microfluidic device comprising of main channel and confined channel coupled with microband electrodes (WE-working electrode, CE-counter electrode, and RE-reference electrode).

3.3.2.4 Electrochemical Detection using G-PANI Modified CPE

Electrochemical measurements including cyclic voltammetry, square-wave voltammetry, and chronoamperometry were performed using a commercially available potentiostat (eDAQ, ED410, 410-088, Australia) using standard three-electrode configuration. The working electrode was a bare CPE or G-PANI/CPE. Both pseudo-reference and auxiliary electrodes were CPE. Cyclic voltammetry was used to compare electrochemical performance of each working electrode type using potential ranges of -0.60 to +0.60 V and -0.20 to +1.00 V vs. CPE for ferri/ferrocyanode and 4-AP, respectively. To study mass transfer of 4-AP on G-PANI/CPE, the dependence of scan rates was performed in the range of 0.01-0.20 V/s. To measure 4-AP and PA simultaneously, square-wave voltammetry with a potential range of –0.20 to +1.00 V vs. CPE was used. Voltammograms were recorded in the positive sweep direction to observe the anodic responses of both 4-AP and PA. All electrochemical experiments were done at room temperature.

3.3.2.5 Chronoamperometric Determination of 4-AP

In the microfluidic system, droplets were generated using an oil carrier phase (perfluorodecalin and 1H, 1H, 2H, 2H-perfluoro-1-octanol in a ratio of 10:2 (v/v) and an aqueous testing solution. Chronoamperometric detection was performed for the detection of 4-AP in the droplets. The oil phase flow rate was 0.8 μL/min while the aqueous phase flow rate was 1.8 μL/min. The water fraction (W_f) was calculated from $W_f = F_w/(F_w + F_o)$, where F_w and F_o are the aqueous- and oil-phase flow rates, respectively. [148]. Here, the total flow rate was 2.6 μL/min, corresponding to a linear flow velocity of 0.86 mm/s and a water fraction of 0.31. Chronoamperometric responses from droplet contents were measured while droplets passed through the three-electrode system. Data was collected for 1 min and average currents were plotted versus applied potential (E_{app}) to generate hydrodynamic voltammograms (HDVs) in the range of 0.00–0.40 V vs. CPE. HDVs were used to find the optimal detection potential as defined by the highest signal-to-noise ratio (S/N). The limits of detection (LOD) and quantitation (LOQ) were obtained from LOD=3(SD_{bl}/S) and LOQ=10(SD_{bl}/S), respectively, where SD_{bl} is the standard deviation of the blank measurement (n = 10) and S is the slope of the linear calibration. Finally, our method was applied for 4-AP determination in PA liquid drug. Prior to analysis, the PA liquid drug was diluted by 0.1 M PBS pH 7.4. The 4-AP levels in all samples were determined and compared with those obtained for standard CZE/UV-Vis method [149].

CZE separation was performed by a P/ACE 5500 automated CE system coupled with a diode array detector, fluid-cooled column cartridge and automatic injector. Fused-silica capillaries (Beckman) of 57 cm (length to detector 50 cm) × 75 μm i.d. and 375 μm o.d. were used. New capillaries were first rinsed with 0.1 M sodium hydroxide for 5 min at high pressure (20 psi), followed by rinsing with the running buffer. It was then equilibrated with the buffer for 10 min by applying a separation voltage of 18 kV. Between experiments, the capillary was rinsed with the running buffer for 1 min. Absorbance was monitored at 250 nm.

3.3.3 Results and Discussion

3.3.3.1 Morphology and Electrochemical Characterization of G-PANI/CPE.

Various reports have used G-PANI nanocomposites to improve the electrochemical sensitivity of carbon electrodes with the resulting performance improvement being attributed to the increase in electrode surface area [120, 150]. To observe the changes electrode morphology, transmission electron microscopy (TEM) was used to characterize G-PANI nanocomposite (Figure 3.3.2a). The images clearly show that the single sheet of G was well dispersed on the CPE. Next, cyclic voltammetry of standard ferri/ferrocyanide redox species was used to characterize the electrochemical properties of the bare CPE, PANI/CPE, and G-PANI/CPE electrodes (Figure 3.3.2b).
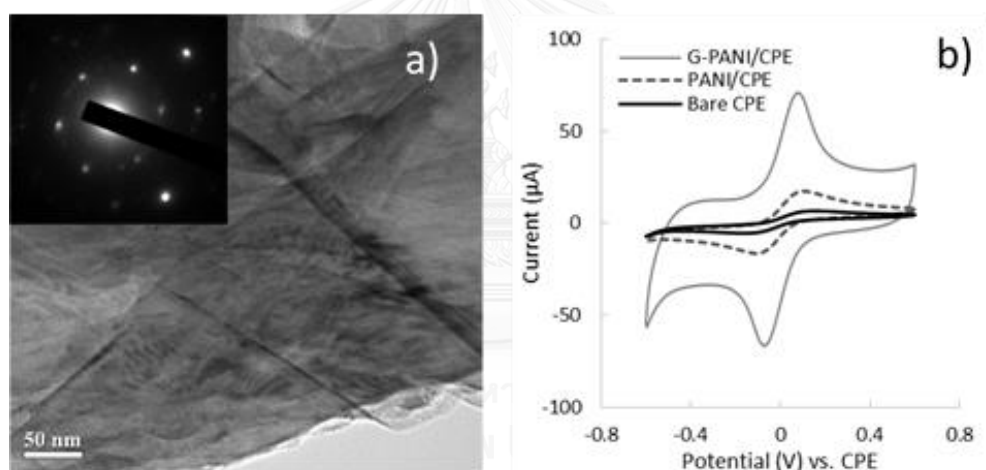
Figure 3.3.2 (a) TEM image of G-PANI nanocomposite with an electron diffraction pattern of G (inset of Figure 3.3.2a) and (b) cyclic voltammograms of 1 mM ferri/ferrocyanide in 0.1 M KCl at bare CPE (black solid line), PANI/CPE (dash line), and G-PANI/CPE (gray solid line).

Compared to the PANI/CPE and bare CPE, G-PANI/CPE exhibited well-defined anodic and cathodic ferri/ferrocyanide current responses which were 10-fold higher than bare CPE and 2-fold greater than PANI/CPE. Moreover, peak potential separation between anodic and cathodic peaks noticeably was reduced when using G-PANI/CPE compared to those measured from PANI/CPE and bare CPE, indicating that the G-PANI

nanocomposite can be also used as an electrode modifier to improve the electron transfer kinetics.

3.3.3.2 Electrochemcial Detection of 4-AP and PA using G-PANI/CPE.

Next, the electrochemical behaviour of 4-AP and PA using the G-PANI/CPE in batch cell was investigated using cyclic voltammetry with the comparison between G-PANI/CPE and bare CPE shown in Figure 3.3.3a. Cyclic voltammograms for the G-PANI/CPE exhibited quasi-reversible redox peaks with significantly increased redox current (2-fold) and reduced redox potentials (~100 mV) when compared to bare CPE. These results can be ascribed to good electrocatalytic activity of G-PANI nanocomposite towards 4-AP, demonstrating that the nanomodifier offers improved sensitivity for 4-AP relative to the CPE. Therefore, the G-PANI nanocomposite can be used a beneficial electrode modifier in the microfluidic systems.

To study the mass transfer process of 4-AP on G-PANI/CPE surface, the scan rate in range of 0.01-0.20 V/s was performed as shown in Figure 3.3.3b and c. A small shift of both anodic and cathodic peak potentials was observed owing to the adsorption of 4-AP on the electrode surface. Both anodic ($i_{p,a}$) and cathodic ($i_{p,c}$) peak currents increased linearly with the square root of scan rate ($V^{1/2}$) with correlation coefficients (R^2) over 0.9, verifying the redox process was controlled by diffusion of 4-AP.

Next, square-wave voltammetry was used to determine detection limits and linearity. Figure 3.3.3d displays representative square-wave voltammograms of 4-AP and PA between 50 and 200 μM. For the response from both 4-AP and PA, anodic peak currents are linearly proportional to their concentration with an LOD of 4.33 μM and 2.12 μM for 4-AP and PA, respectively. The peak potential separation between 4-AP and PA is clearly observed with potential difference (EPA-E4-AP) of ~400 mV. As a result, the selection of potential to use in further chronoamperometric experiment would be particularly useful for selective electrochemical detection of 4-AP in the presence of PA.
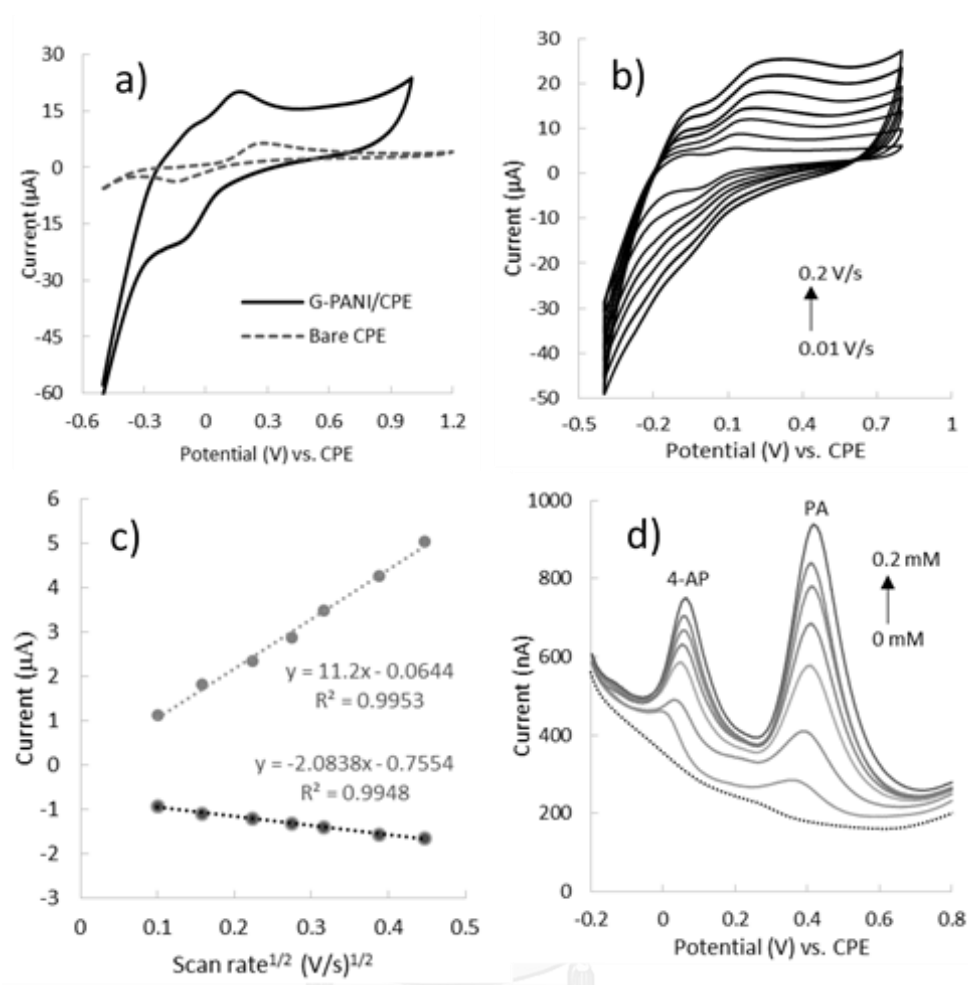
Figure 3.3.3 (a) comparison of electrode for cyclic voltammetric detection of 1 mM 4-AP at scan rate of 0.1 V/s, (b) cyclic voltammogram of 1 mM 4-AP at G-PANI/CPE with various scan rate in the range of 0.01-0.2 V/s, (c) current dependence on scan rate, and (d) square-wave voltammograms of 4-AP and PA (0-0.2 mM) at G-PANI/CPE with scanning potential range of -0.2 to 0.8 V vs. CPE.

3.3.3.3 Chronoamperometric Detection in Droplets

3.3.3.3.1 Selection of the Optimal Applied Potential (E_{app}).

Chronoamperometric detection has been broadly used in the various flow-based systems due to its ease of operation and low background current. Figure 3.3.4 shows a representative chronoamperogram of 300 µM 4-AP in droplets where each discrete peak corresponds to an individual droplet.
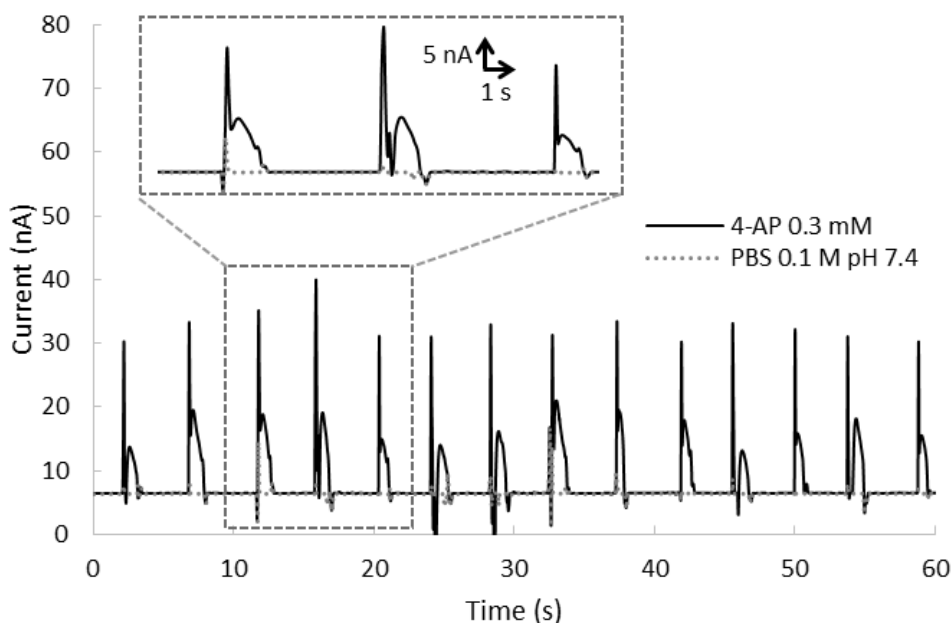
Figure 3.3.4 (a) Chronoamperogram of droplets containing 0.3 mM 4-AP in 0.1 M PBS pH 7.4. Conditions: an applied potential (E_{app}) of +0.2 V vs. CPE, total flow rate of 2.6 µL/min (0.016 mm/s) and W_f = 0.31.

When the droplet front began to pass through the electrode array, the current increased sharply, as a result of the oxidation of 4-AP and generation of the electrical double layer.   The subsequent drop in current is due to both reduction the 4-AP concentration as well as reaching steady state current for the double layer charging. Next, the current approaches a steady state level of 5.14±0.11 nA (n=10) which can be assigned to the diffusion-limited current of 4-AP. For quantification, the current was measured during this regime.

Selective detection of 4-AP in the presence of PA in the flow-based system was assessed. According to Figure 3.3.3d, the selection of E_{app} lower than +0.3 V vs. CPE should achieve selective detection of 4-AP in the presence of PA. To select an optimal Eapp for chronoamperometric detection of 4-AP and PA in droplet-based flow system, hydrodynamic voltammetry (Figure 3.3.5a) experiments were conducted.
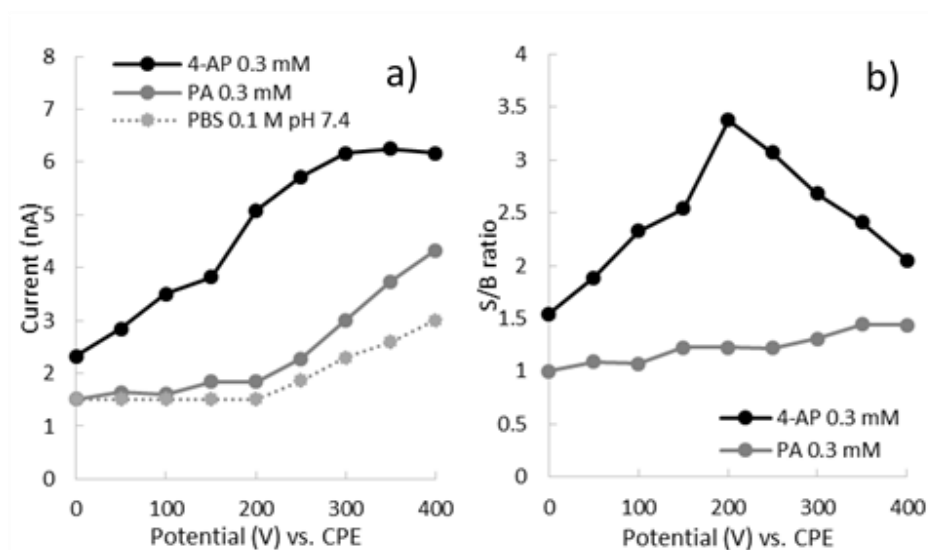
Figure 3.3.5 Hydrodynamic voltammograms and (b) signal to background ratio of 0.3 mM 4-AP and 0.3 mM PA. The measurements were carried out using a total flow rate of 2.6 µL/min (0.016 mm/s) and W_f = 0.31.

The anodic peak current of 4-AP increased with E_{app}. There is no signal response from PA and background (BG) solution (0.1 M PBS pH 7.4) in the range of 0.0-0.2 V vs. CPE while both anodic current signals of 300 µM PA and BG solution also increased with E_{app} over +0.2 V vs. CPE. Thus, the E_{app} for chronoamperometric detection in the range between 0.0-0.2 V vs. CPE can be used for selective detection of 4-AP without an interfering response from PA. To optimize the E_{app} for chronoamperometric detection of droplet contents, the signal-to-background (S/B) ratio of 4-AP and PA was plotted as a function of E_{app}. As seen from Figure 3.3.5b, an E_{app} of +0.2 V vs. CPE showed the highest S/B ratio for 4-AP detection; consequently, +0.2 V vs. CPE was chosen as the optimal chronoamperometric E_{app} for quantitative measurements of 4-AP for further experiment.

3.3.3.3.2 Effect of Water Fraction and Total Flow Rate.

The influence of water fraction (W_f) and total flow rate on chronoamperometric measurements were studied next. One of well-known factor strongly affecting droplet

size is W_f, with droplet size increasing with W_f. In this work, the droplet sizes at W_f values in the range of 0.15-0.46 were generated by adjusting the flow rates ratio between oil and aqueous solutions while the total flow rate was kept constant at 2.6 µL/min. As shown in Figure 3.3.6a, when the water fraction was lower than 0.31, small unstable droplets were produced, resulting in low anodic current. For W_f values over 0.38, droplet length is too long and the anodic steady-state current decreased exponentially. The highest current was measured at a water fraction of 0.31. Consequently, the water fraction of 0.31 was found to be optimal W_f to produce stable droplet and all subsequent experiments were performed at this condition.

Another important factor influencing on chronoampermetric response is total flow rate. The effect of total flow rate was investigated as shown in Figure 3.3.6b. While the water fraction was kept at a constant 0.31, total flow rate was varied between 1.30-3.90 µL/min, corresponding to a linear flow velocity in the range of 0.43-1.29 mm/s. The results show that for flow rates <2.6 µL/min (linear velocity = 0.43 mm/s), a low steady-state current was obtained due to the long residence time of a single droplet passing over the electrode surface. When the total flow rate was >3.25 µL/min (linear velocity = 1.08 mm/s), the current also reduced significantly. We believe that this high total flow rate provided short residence time for the electrochemical process to occur. The highest steady-state current values were obtained from the total flow rates at 2.6 and 3.25 µL/min; however, use of high flow rate to produce droplet increases reagent/sample consumption. Therefore, an optimal total flow rate of 2.6 µL/min (linear velocity = 0.86 mm/s) was selected to use in further experiments.
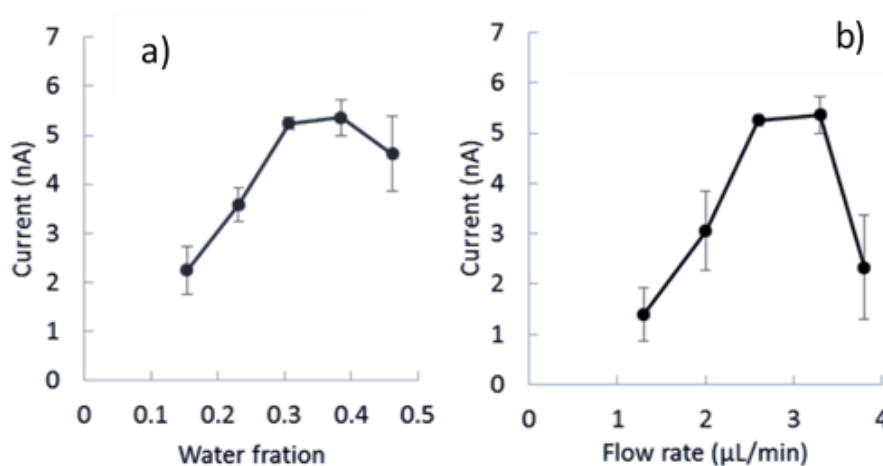
Figure 3.3.6 Effect of water fraction and total flow rate on chronoamperometric detection of 0.3 mM 4-AP. Conditions: an applied potential (E_{app}) of +0.2 V vs. CPE, total flow rate of 2.6 µL/min (0.016 mm/s) and W_f = 0.31.

3.3.3.4 Analytical performance of system.

The analytical performance of the droplet microfluidics coupled with G-PANI/CPE was investigated. Chronoamperometric detection of 4-AP at E_{app} of +0.2 V vs. CPE was performed using optimal conditions described above. Calibration curve of 4-AP was plotted between anodic current as a function of the standard 4-AP concentration as shown in Figure 3.3.7. Linear calibration range was found to be 50-500 µM with correlation coefficient (R^2) of 0.998. The limit of detection (LOD, S/N=3) was found to be 53.77 µM (5.87 ppm) while limit of quantitation (LOQ, S/N=10) was found to be 170.94 µM (18.65 ppm).

The European, United States, British, German, and Chinese Pharmacopoeias report the maximum allowable limit of 4-AP in PA products is 50 ppm (0.005% w/w); therefore, our system can determine 4-AP at relevant concentration in paracetamol drug samples. Although the LOD and LOQ values reported here are higher than those obtained previous publications, our approach offers simplicity and inexpensive operation. In addition, small aliquot (~1 mL) of testing sample/reagent was required to operate the droplet generation within microfluidic system, leading to provide a fast and high-throughput analysis of 4-AP.
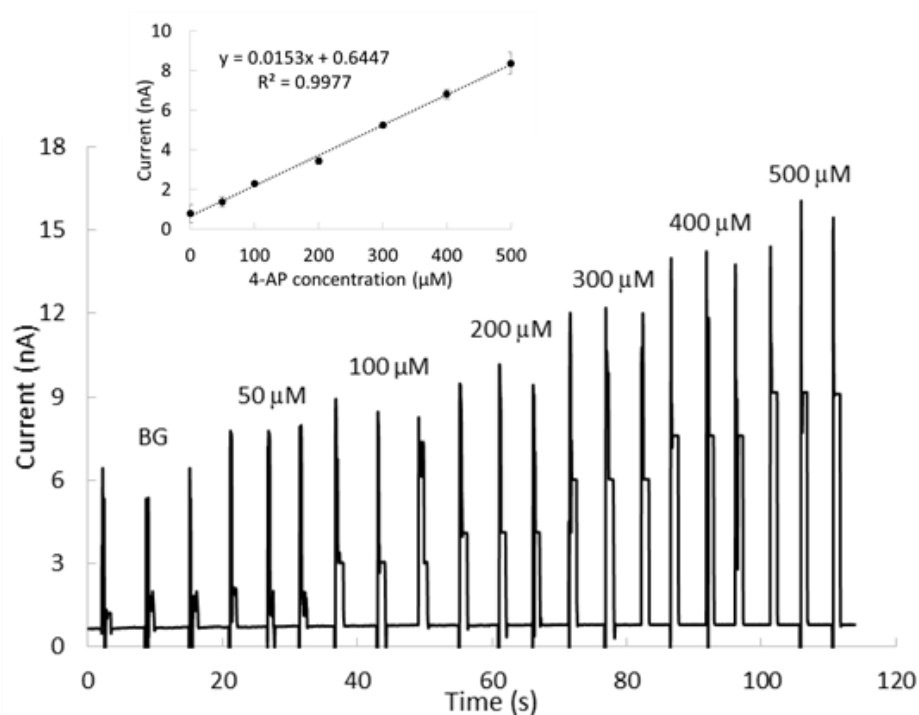
Figure 3.3.7 Chronoamperogram of 4-AP in the concentration range of 0-500 µM using the optimal Conditions: an applied potential (E_{app}) of +0.2 V vs. CPE, total flow rate of 2.6 µL/min (0.016 mm/s) and W_f = 0.31. (Inset) Linear calibration plot of 4-AP concentration vs. current.

In addition to assess the stability of this system, chronoamperometric detection of standard 4-AP at three different concentrations (100, 200, and 300 µM) by 20 successive measurements was performed for intra-day and inter-day precision. For intra-day and inter-day results, relative standard deviation (RSD) was found to be less than 5% (n = 20). Therefore, these results verify our proposed system had the good stability.

3.3.3.5 Determination of 4-AP in Commercial Drug Samples.

Since 4-AP is produced from the degradation of PA drug, the selectivity of this method towards the determination of 4-AP in the presence of PA in commercial samples was evaluated. The tolerance concentration is defined as the concentration

of 4-AP, generating a change in signal response of ±5%. The results show that 5000 µM PA gave a 5%change in the detection of 50 µM 4-AP; thus, PA sample was diluted to a lower concentration. Next, the application of our method was tested by measuring the spiked 4-AP concentrations (100, 200, 300, 400, and 500 µM) in each diluted PA sample. The % recovery of this system was found in the range of 91.21%-105.34% (n=20). Moreover, to validate our method, the results obtained from the proposed system was compared to those obtained from the conventional capillary zone electrophoresis/UV-Visible spectrophotometric technique (CZE/UV-Vis) using a paired t-test at 95% confidential interval. The results show there is no significant difference between the results obtained from our method and CZE/UV-Vis method. As a result, our electrochemical droplet system is an alternative, high-throughput method for determining the 4-AP contamination in commercial PA formulations.

3.3.4 Conclusions

In this work, we report a novel electrochemical droplet microfluidic device for determination of 4-AP in commercial PA formulations. The G-PANI/CPE was first coupled with droplet system to perform chronoamperometric detection of 4-AP. The improvement in electrochemical sensitivity was attributed to an enhancement of the active surface area of electrode and increased electrochemical conductivity. Our proposed method can perform a high-throughput and rapid measurement of 4-AP in commercial PA product with required small consumption of reagent/sample. Eventually, this system was successfully applied for the determination of 4-AP in PA liquid drugs with high precision and good recovery; therefore this system might be an alternative analytical device for routine analysis of 4-AP residue in pharmaceutical products.

CHAPTER IV

DEVELOPMENT OF PAPER-BASED COLRIMETRIC/ELECTROCHEMICAL DEVICE FOR DETERMINATION OF HEAVY METALS

4.1 A Microfluidic Paper-Based Analytical Device for Rapid Quantification of Particulate Chromium

Poomrat Rattanarat[a], Wijitar Dungchai[b], David M. Cate[d], Weena Siangproh[c], John Volckens[e,*], Orawon Chailapakul[a,f,*], Charles S. Henry[d,g,*]

[a]Electrochemistry and Optical Spectroscopy Research Unit (EOSRU), Department of Chemistry, Faculty of Science, Chulalongkorn University, Patumwan, Bangkok 10330, Thailand

[b]Department of Chemistry, Faculty of Science, King Mongkut's University of Technology Thonburi, 91 Prachautid Road, Thungkru, Bangkok 10140, Thailand

[c]Department of Chemistry, Faculty of Science, Srinakharinwirot University, Sukhumvit 23, Wattana, Bangkok 10110, Thailand

[d]School of Biomedical Engineering, Colorado State University, Fort Collins, Colorado 80523

[e]Department of Environmental and Radiological Health Sciences, Colorado State University, Fort Collins, Colorado 80523

[f]National Center of Excellence for Petroleum, Petrochemicals and Advanced Materials, Chulalongkorn University, Patumwan, Bangkok 10330, Thailand

[g]Department of Chemistry, Colorado State University, Fort Collins, Colorado 80523

*Corresponding authors

Abstract

Occupational exposure to Cr is concerning because of its myriad of health effects. Assessing chromium exposure is also cost and resource intensive because the analysis typically uses sophisticated instrumental techniques like Inductively-Coupled Plasma-Mass Spectrometry (ICP-MS). Here, we report a novel, simple, inexpensive microfluidic paper-based analytical device (μPAD) for measuring total Cr in airborne particulate matter. In the μPAD, tetravalent cerium (Ce(IV)) was used in a pretreatment zone to oxidize all soluble Cr to Cr(VI). After elution to the detection zone, Cr(VI) reacts with 1,5-diphenylcarbazide (1,5-DPC) forming 1,5-diphenylcarbazone (DPCO) and Cr(III). The resulting Cr(III) forms a distinct purple colored complex with the DPCO. As proof-of-principle, particulate matter (PM) collected on a sample filter was analyzed with the μPAD to quantify the mass of total Cr. A log-linear working range (0.23-3.75 μg; r^2=0.998) between Cr and color intensity was obtained with a detection limit of 0.12 μg. For validation, a certified reference containing multiple competing metals was analyzed. Quantitative agreement was obtained between known Cr levels in the sample and the Cr measured using the μPAD.

Keywords: paper-based analytical device, colorimetric detection, particulate chromium, 1,5-diphenylcarbazide

4.1.1 Introduction

There are many industrial uses of Cr, including pigment dyes, plastics, protective coatings, ferrochromium alloys, chromate production, tannery facilities, and steel alloys [151]. Chromium exists primarily in one of two oxidation states, trivalent (Cr(III)) and hexavalent (Cr(VI)). Trivalent chromium has an LD_{50} of 200-600 mg/kg and is suggested to play an important role in insulin action and glucose regulation in the human body [152-154]. Cr(VI) has an LD_{50} of 50-150 mg/kg and effects respiratory, gastrointestinal, immunological, hematological, reproductive, and developmental systems. In addition, Cr(VI) is a potent carcinogen [155]. Airborne exposure to both forms of chromates in dye pigments, anticorrosive agents, surface coatings, and welding is linked with lung, nasal, and stomach cancers [156]. The legal limit for airborne exposure to total Cr in U.S. workplaces is 0.05 $\mu g/m^3$, set by The Occupational Safety and Health Administration (OSHA) in 2012.

At present, occupational exposure to metals in particulate matter (PM) requires sampling onto filters, which are then transported to a centralized analytical laboratory for analysis. Many instrumental techniques have been used to measure Cr, including UV-Visible spectrophotometry [157], ion chromatography [158], inductively couple plasma-mass spectrometry [159], atomic absorption spectroscopy [160], and X-ray techniques [161]. Although highly sensitive, these approaches are time-consuming (approximately two weeks for assessment), expensive (over $100 per sample), and require trained operators. Consequently, there is a need for simple, sensitive methods for Cr analysis to enable more frequent assessment of exposures of 'at-risk' workers.

Paper-based microfluidic devices (µPADs) have emerged as a low-cost alternative for quantitative chemical measurement. Relative to traditional assays, µPADs are easy to operate, consume small reagent volumes, and provide rapid results (typically in min) [7, 13, 29, 57, 162, 163]. µPADs represent a new generation of lateral-flow chemical assays utilizing hydrophobic barriers printed on paper. These barriers direct flow so that specific chemical assays may be conducted rapidly and efficiently [8]. Paper substrates are easy to use because flow is generated via capillary action.

Reagents impregnated in 'detection zones' on the µPAD allow analytes to be quantified by visual assessment using an external optical reader (i.e. camera, scanner) [84, 162]. The utility of this technology has been demonstrated for applications in point-of-care [33, 43, 164], food safety [44, 165, 166], and environmental monitoring [10, 36, 167]. Several reports have focused on quantifying metals using µPADs. Hossain and Brennan used the enzymatic activity of beta-galactosidase and silver nanoparticle aggregation to detect metals in water [36]. Yang and Wang developed a method for determining Ag and Cu via an autocatalytic reaction with *o*-phenylenediamine followed by detection with fluorescence [168]. Ratnarathorn et al. used silver nanoparticles to detect Cu ions in water [10]. Our group demonstrated the use of µPADs for determination of Fe, Cu, and Ni in aerosolized incineration ash as a first step towards monitoring occupational exposure, with detection limits of 1 – 1.5 µg [84].

Here, a µPAD was developed for total Cr determination using tetravalent cerium Ce(IV) and 1,5-diphenylcarbazide (1,5-DPC) as oxidizing [169] and colorimetric [170] reagents, respectively. The µPAD approach is different from previous reports because it includes sample pretreatment on the device as well as addition of stabilizing agents to give the device long-term shelf life. Furthermore, the device includes four separate detection zones to provide an estimate of analytic precision and to ensure (statistical) reproducibility. Tetravalent cerium oxidizes all forms of soluble Cr to Cr(VI) for reaction with 1,5-DPC. We chose Ce(IV) over hydrogen peroxide [171], perchloric acid [172], and bromine [173] because these latter chemicals typically require multiple reagent additions, time-consuming steps, and precise temperature control. Alternatively, Ce(IV) does not require precise temperature control, is easy to use, and can be stored on paper. For colorimetric detection of Cr(VI), many published methods have been reported including the use of gold and silver nanoparticles [37, 153] and nanoparticle derivatives [174]. 1,5-diphenylcarbazide has been used as a selective Cr(VI) reagent for decades [175]. 1,5-DPC reduces Cr(VI) to Cr(III) and is itself oxidized to diphenylcarbazone (DPCO). DPCO complexes with the generated Cr(III) to form an intensely purple-colored complex [170]. Phthalic anhydride stabilizes 1,5-DPC on the µPADs [155]. Method viability was established using standardized metal-

containing baghouse dust samples. Dust collected on cellulose filters was digested using microwave-assisted wet digestion, followed by μPAD analysis. Quantitative evaluation showed good correlation with known Cr levels.

4.1.2 Experimental

4.12.1 Materials and Equipment

Ammonium dichromate (VI), lead(II) nitrate, cadmium(II) nitrate tetrahydrate, iron(III) chloride hexahydrate, nickel(II) sulfate hexahydrate, barium(II) chloride, manganese(II) chloride tetrahydrate, zinc(II) nitrate hexahydrate, vanadium(III) chloride, silver(II) nitrate, cobalt(II) chloride, aluminum(III) sulfate hydrate, copper(II) sulfate pentahydrate, phthalic anhydride, cerium (IV) ammonium nitrate, 1,5-diphenylcarbazide, and polydiallyldimethylammonium chloride (medium molecular weight) were obtained from Sigma-Aldrich (St. Louis, MO). Sodium acetate and glacial acetic acid were obtained from Fisher Scientific (Pittsburgh, PA). Metal-containing certified industrial incineration ash samples (RTC-CRM012) and pre-validated baghouse dust (RTC-CRM014) were purchased from LGC Standards (Teddington, UK). Milli-Q water from Millipore ($R \geq 18.2$ MΩ cm^{-1}) was used for all experiments. All chemicals were used as received.

4.2.2.2 Device Design and Fabrication

The μPADs described here were fabricated using wax printing [57]. Hydrophobic barriers were printed using a commercial wax printer (Xerox Phaser 8860, VWR) onto Whatman grade one filter paper, as described previously [44]. The μPAD design shown in Figure 4.1.1 was generated using graphics software (CorelDRAW). The RGB values 248-195-0 were selected as the barrier color, providing a high contrast background for subsequent image analysis. Printed wax was melted at 200 °C for 120 s on a hot plate. One side of the paper substrate was then covered with packing tape to prevent leakage of eluent through the bottom of the μPAD.
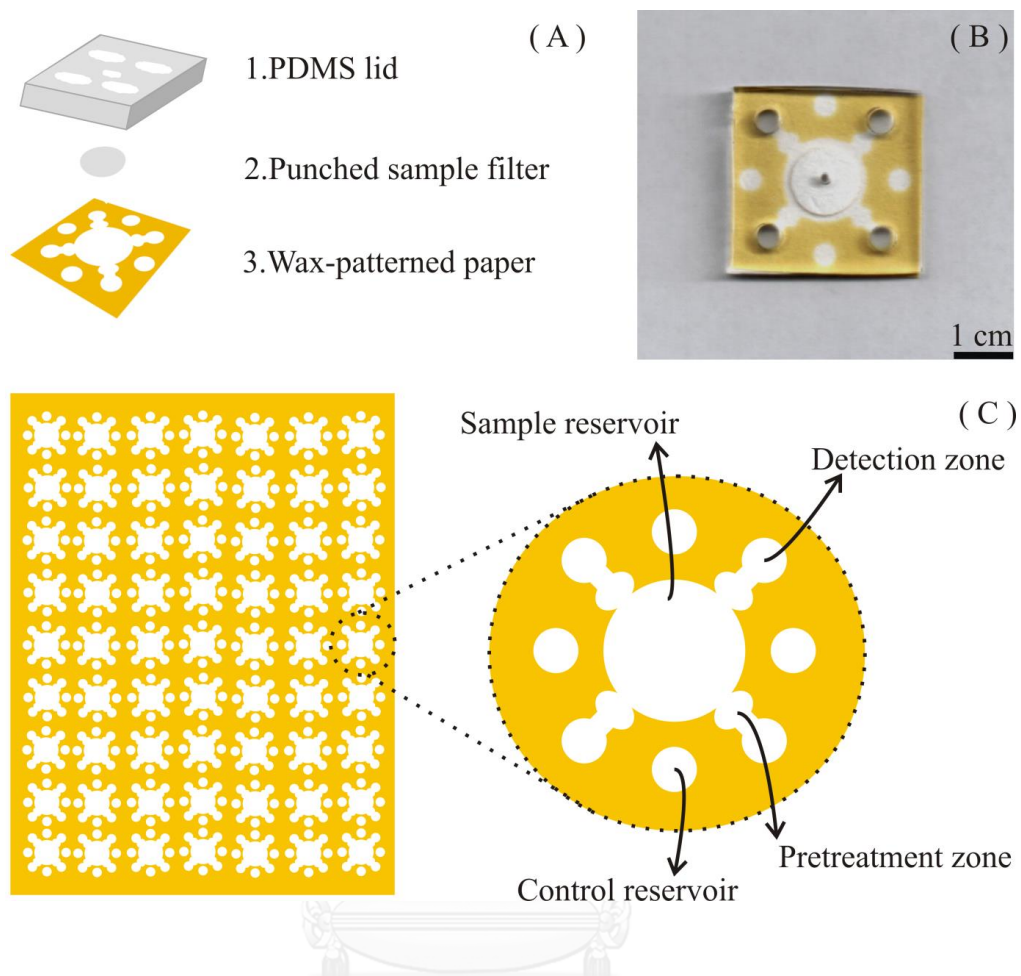
Figure 4.1.1 (a) Schematic of a μPAD, consisting of a PDMS lid for applying equal pressure across the paper surface, a 10 mm filter punch containing PM from baghouse dust, and a patterned filter paper treated with reagents for colorimetric analysis of total Cr. (b) The combined device. (c) Analytical devices can be mass-produced on a single sheet of filter paper (the figure shows 63 individual devices).

4.1.2.3 Colorimetric Detection of Total Chromium

For Cr detection, a solution containing 1.5 g of 1,5-diphenylcarbazide (1,5-DPC) and 4.0 g of phthalic anhydride was dissolved in 100 mL of acetone. The μPAD was prepared by adding 0.5 μL of ceric(IV) ammonium nitrate (0.35 mM) twice onto the pretreatment zone, followed by 0.5 μL of polydiallyldimethylammonium chloride (PDDA) (5% w/v). PDDA was added to stabilize the reaction product between Cr and

1,5-DPC and to prevent the complex from flowing to the edges of the hydrophilic channels [84]. Two 0.25 µL aliquots of the detection reagent solution (1,5-DPC and phthalic anhydride) were then added to the detection zone. The device was allowed to dry completely between each reagent addition.

4.1.2.4 Experimental Procedure

An overview of the experimental procedure is shown in Figure 4.1.2. For measurements, a 10 mm (diameter) circular punch was taken from an air sampling filter (described below).
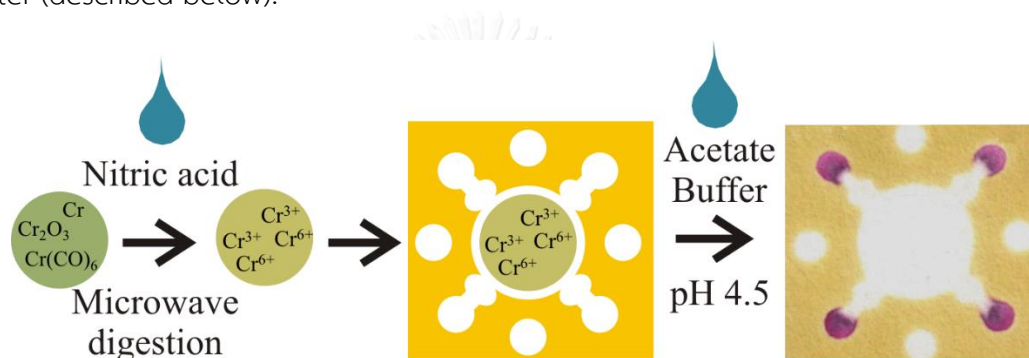
Figure 4.1.2 Acid digestion procedure for measuring total soluble Cr. HNO_3 is deposited on a 10 mm filter punch and digested using a commercial microwave. The digested punch is placed on the µPAD and acetate buffer (pH 4.5) is added to the paper substrate through the PDMS lid. The buffer elutes Cr ions from the MCE filter to the detection zones.

Calibration plots were generated by adding standard solutions to one 10 mm punch. When dry, the punch was placed on the µPAD sample reservoir. For method validation, a sample of baghouse PM was resuspended in the laboratory and onto mixed cellulose ester (MCE) filters. After sample collection, 20 µL of SDS was added to each 10 mm punch to enhance the elution of metal ions from the relatively hydrophobic MCE filter. Microwave-assisted acid digestion on the filter samples was performed by adding 5 µL of concentrated nitric acid, followed by 30 µL of water to the filter punch. The punch was then placed in a household microwave (1100 W) for

a total of 30 s (two 15 s intervals). Between each 15 s interval, 30 µL of deionized water was added to each punch to wet the filter. After digestion, 10 µL of sodium bicarbonate (0.5 M, pH 9.5) was added to neutralize the acid. To accelerate neutralization, the µPAD was heated in the microwave for an additional 15 s. Finally, a polydimethylsiloxane (PDMS) lid with holes punched over the sample reservoir (2 mm diameter) and detection zone (5 mm diameter) was placed on top of the µPAD. Acetate buffer (40 µL, 0.1 M, pH 4.5) was added to the center hole of the PDMS lid, eluting the digested metals from the filter through the pretreatment zones to the detection zones. A 300 g weight (a water filled Erlenmeyer flask) was placed on the PDMS lid to distribute pressure evenly across the device. Color formation was complete in less than 10 min. The device was allowed to dry before color intensity was measured.

4.1.2.5 Quantitative Image Processing

Color intensity was measured using a desktop scanner (XEROX DocuMate 3220). To quantify intensity, a color threshold window was applied to the Cr(III)-1,5-diphenylcarbazone product (0-180) using NIH ImageJ software, effectively removing all unwanted color channels. This method passes only the purple of the Cr(III)-1,5-DPC complex, and removes the wax background. After thresholding, images were converted to gray scale and inverted, yielding higher intensity values for darker (more concentrated) Cr samples [84]. For background measurements, color intensities for blank samples were measured using the same protocol described above. The background values were used to determine the baseline intensity for detection limit calculations.

4.1.2.6 Particulate Metal Collection and Digestion

A suspension of 0.1% (w/v %) incineration ash in deionized water was prepared and nebulized into a 0.8 m^3 plexiglass chamber. The average PM concentration in the chamber was 0.73 mg/m^3 as measured using an aerosol photometer (TSI, Model 8250). Relative humidity was not controlled but was monitored and remained below 50%

throughout all experiments. Resuspended dust was sampled onto Pallflex and mixed cellulose ester (MCE) filters (37 mm diameter) at a flow rate of 10 L/min for 4 hrs. Sampled PM mass was quantified using a Mettler-Toledo analytical microbalance (model MX5). These filters collected approximately 1.16 µg ash per mm^2 of exposed filter area (or 91.14 µg per punch). After sample collection, 10 mm diameter punches were taken from the filter, extracted, and prepared according to the procedure described above.

4.1.3. Results and Discussion

We first evaluated the ability to measure total Cr using the combination of Ce(IV) oxidation followed by colorimetric detection with 1,5-DPC. After the reaction was complete, the purple 1,5-DPCO product was readily visible in the detection zone. A log-linear calibration curve was obtained from standard chromium solutions added to 10 mm MCE punches (Figure 4.1.3). Intensities were linear with respect to total chromium mass (log scale) from 0.23-3.75 µg with a detection limit of 0.12 µg and a pooled relative standard deviation (RSD) for all measurements (n = 7 measures for each Cr level) of 4.9%. The detection limit was determined by the lowest Cr mass with an intensity three standard deviations above the background standard deviation. Above 3.75 µg, the paper surface saturated and no additional increase in intensity was measured. Although the overall linear range covers only one order of magnitude, this range should be sufficient for hazard evaluation, since higher exposures (once detected) will likely require further investigation. Analysis of smaller punch sizes can also be employed. The linear range of the assay is extendable by increasing the surface area of the detection zone; larger detection zones facilitate analysis of greater chromium mass. The minimum detectable levels of Cr using the µPAD were compared to the permissible exposure limit (PEL), stipulated by the OSHA. For method validation, minimum detectable limits were measured as a TWA, collected at sampling rate of 4 L/min. At the detection limit of 0.12 µg Cr, we calculated a minimum detectable level as a TWA of 0.72 µg/m^3.
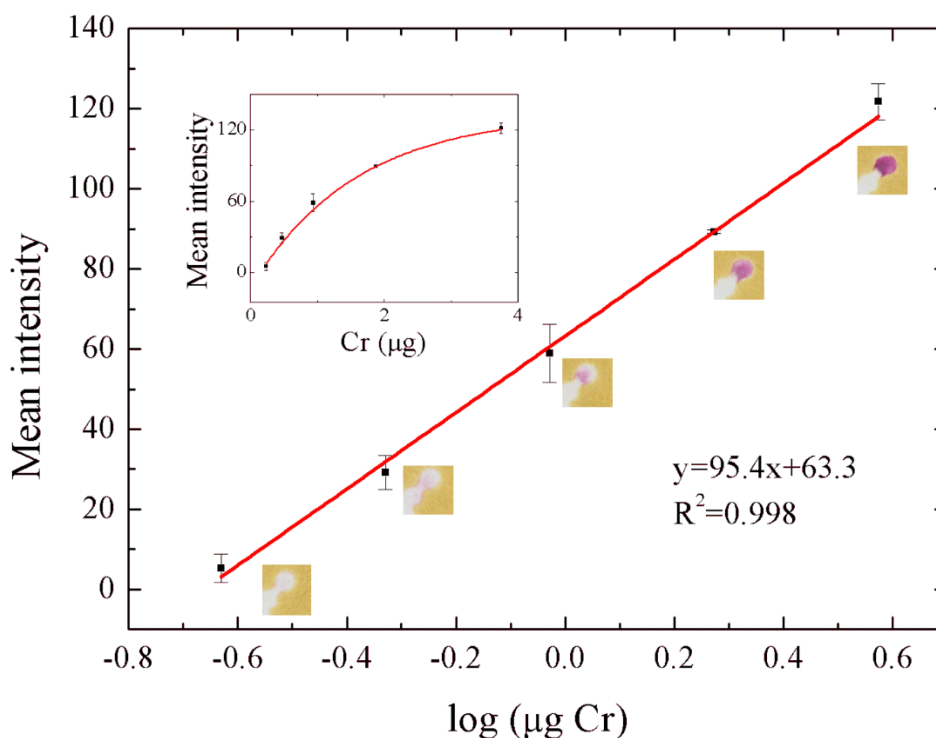
Figure 4.1.3 Colorimetric intensity as a function of log Cr mass added to the µPAD. The working range was 0.23-3.75 µg and is log-linear with measured intensity. The inset shows the same data plotted on a linear mass scale (n = 3).

Although this level exceeds the PEL for Cr, stacking MCE punches and analyzing multiple filters simultaneously can be used to further decrease detection sensitivity. As a result, this proposed method should be sufficient for monitoring occupational exposure to particulate Cr.

We found, from prior work in our laboratory, that the metal complex should be homogenously distributed over the detection zone to maximize accuracy and detection sensitivity [84]. If the reaction product migrates to the detection zone edge, quantification (via color intensity integration) is more challenging. The final Cr complex generated here was highly mobile on paper, and as a result, the reaction product flowed to the detection zone edge, reducing measurement accuracy and sensitivity (Figure 4.1.4a). Tricapylmethyl ammonium chloride has been used previously to prevent the Cr-DPCO complex from spreading on spot tests [176]. Unfortunately, this

surfactant must be dissolved in acetone. When applied to the device, the acetone caused dissolution of the wax and leaking of subsequent aqueous solutions. As a result, polydiallyldimethylammonium chloride (PDDA) was used to produce the same effect (Figure 4.1.4) [84]. The intensities of blank samples (0.1 M acetate buffer, pH 4.5) in the presence and absence of PDDA were measured to be 2.4 ± 1.1 and 10.8 ± 1.7 (n=7). The use of PDDA achieved a two-fold increase in signal strength; intensities of 3.75 µg Cr with and without PDDA were measured to be 121.4 ± 4.4 and 65.1 ± 1.1, respectively.
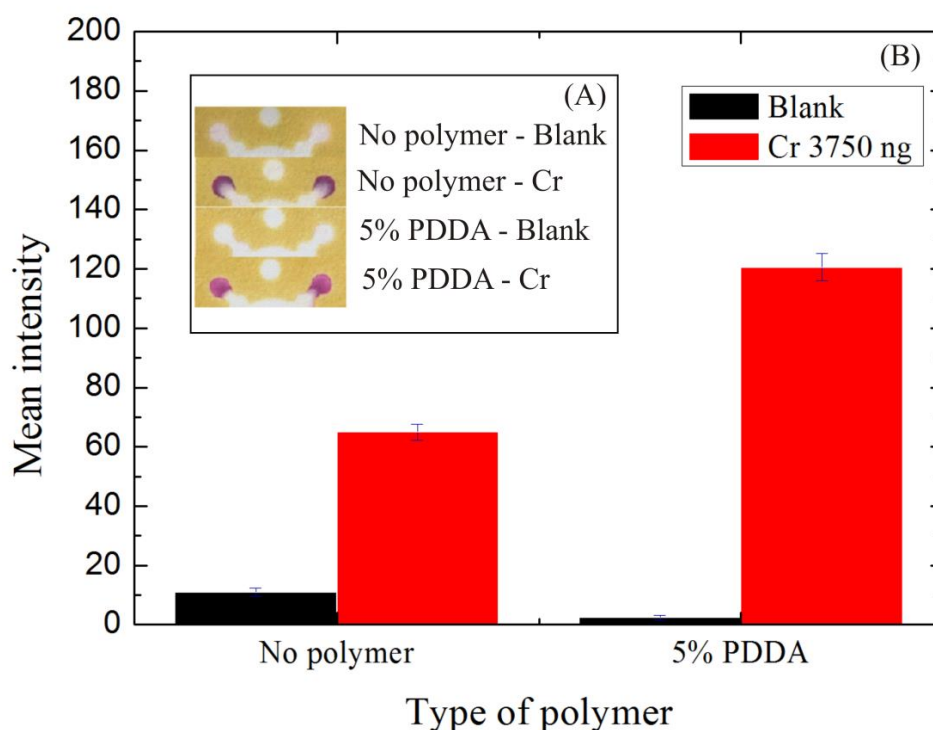
Figure 4.1.4 PDDA was investigated as a compound for retaining Cr the detection zone. (a) The devices were photographed, and (b) mean color intensity was measured in the presence and absence of PDDA in the detection zone.

We next investigated potential interferences from other metals. Cr(III) was added to the µPAD in the presence of Mg, Mn, Zn, Al, Ba, V, Co, Cu, Fe, and Ni (Figure 5) in metal:Cr ratios of 1:1 and 4:1. The measured levels of Cr were found to be 0.5 ±

0.1 and 1.8 ± 0.2 (n=7) g in the two samples. A paired t-Test confirmed that the presence of other metals did not significantly impact measurement (Figure 4.1.5).

	Presence of interference	Absence of interference
Cr 0.47 µg		
Cr 1.88 µg		

Figure 4.1.5 Representative µPADs for total Cr with and without potential interfering metals showing the ability to selectively measure Cr. Two different masses of Cr were analyzed in the presence of Mg, Mn, Zn, Al, Ba, V, Co, Cu, Fe, and Ni.

For method validation, a baghouse sample certified for Cd, Cr, and Pb, and containing unmeasured levels of Al, Sb, As, Ba, B, Be, Ca, Co, Cu, Fe, Mg, Mn, Hg, Mo, Ni, P, K, Ag, Se, Na, Sr, Tl, Sn, Ti, V, and Zn, was aerosolized and collected on filters. Total Cr mass was measured using combinations of two and three punches stacked over the sample zone (Figure 4.1.6). The measured Cr intensities were 31.8 ± 0.9 and 44.6 ± 2.1 (n=7), respectively. Gravimetric analysis was also performed on the filter punches to verify the Cr mass present. For two punches, the actual and measured Cr levels were 0.41 and 0.4 ± 0.1 (n=7) µg, respectively. For three punches, the absolute and measured Cr levels were 0.61 µg and 0.6 ± 0.1 (n=7) µg, respectively. These results suggest we can measure Cr concentrations from complex PM samples. Furthermore, detection limits and method sensitivity can be improved using multiple sample punches analyzed simultaneously on a single device.

Punch	Actual level (µg)[a]	Color product on the device	Measured level(µg)[b]
2 punches	0.41		0.4±0.1
3 punches	0.61		0.6±0.1

Figure 4.1.6 Detection of Cr from baghouse dust containing the Al, Sb, As, Ba, B, Be, Ca, Co, Cu, Fe, Mg, Mn, Hg, Mo, Ni, P, K, Ag, Se, Na, Sr, Tl, Sn, Ti, V, and Zn. Measured levels are shown in which multiple 10 mm punches were taken and stacked for simultaneous analysis to enhance the mean intensity of the colored product.

[a]The actual mass of Cr was calculated from gravimetric analysis of the filters after collection of baghouse dust.

[b]The measured mass of Cr was obtained from the paper-based colorimetric assay.

We also investigated the effects of long-term storage on device performance. A series of µPADs were stored at 4 and 22 ± 2℃ for 2, 3, 7, 14, 21, and 28 days. Colorimetric intensities as a function of storage time are shown in Figure 4.1.7 and 4.18 for samples with 0.0, 0.94, and 3.75 µg Cr. In the absence of Cr and phthalic anhydride, the indicator (1,5-DPC) changed color after two days, regardless of temperature. In the presence of phthalic anhydride, color formation was observed after three days only at 22℃. In the presence of phthalic anhydride, no significant color developed after 28 days when the device was covered and stored at 4℃. These results show that when storing the device it is important to cover and keep in a cold environment.
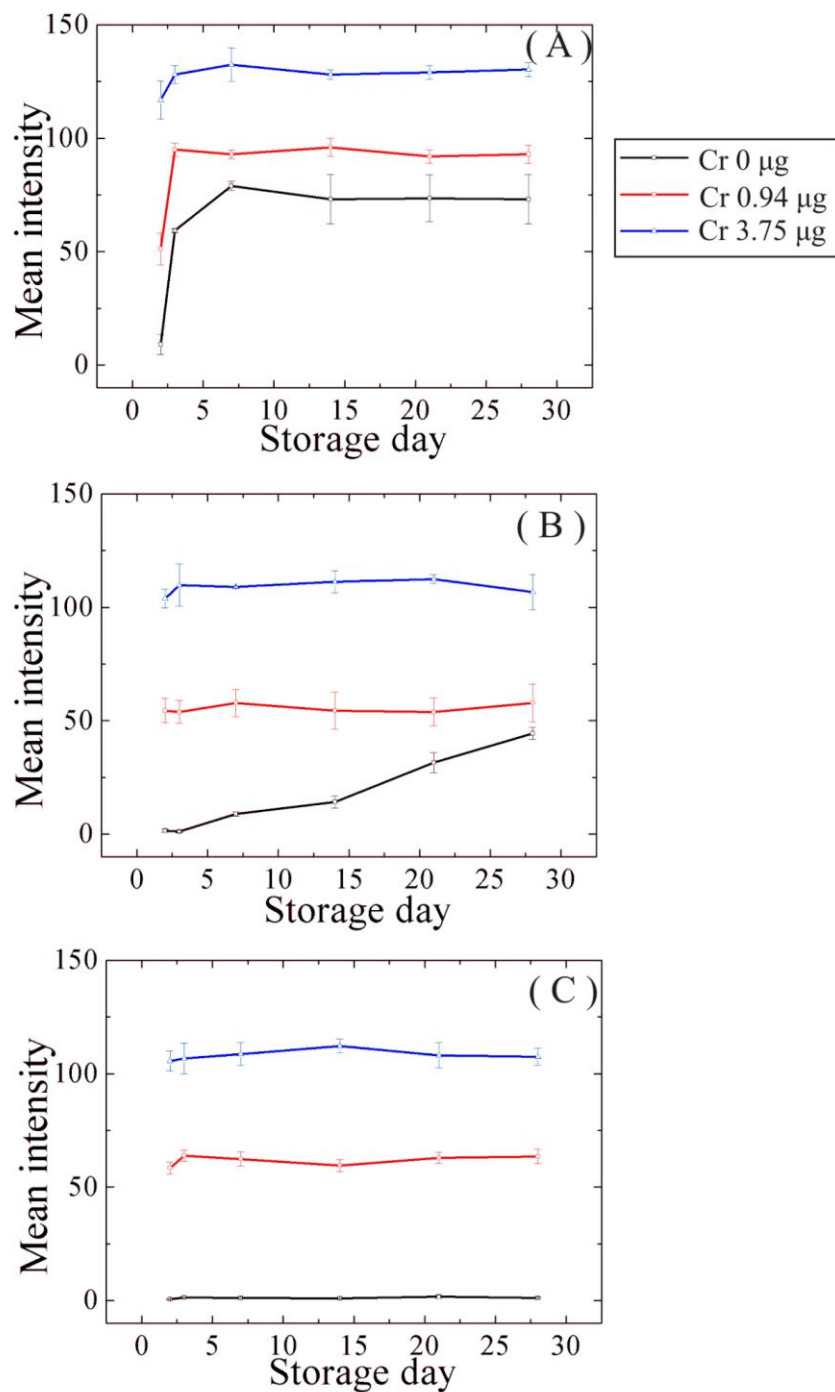
Figure 4.1.7 Effect of storage on µPAD performance in the presence and absence of pretreatment reagents. Cr masses of 0, 0.94, and 3.75 µg were measured using the µPAD with the following conditions: (a) devices stored at 4°C without phthalic anhydride (b) devices stored at 25°C with phthalic anhydride (c) devices stored at 4°C with phthalic anhydride. The µPADs were stored for 2, 3, 7, 14, 21, and 28 days.

Cr (ng)	Storage for 2 days			Storage for 3 days		Storage for 7 days	Storage for 14 days
	No phthalic anhydride	Room temperature	4°C	Room temperature	4°C	4°C	4°C
0							
230							
470							
940							
1880							
3750							

Figure 4.1.8 Effect of storage on µPAD performance. Devices were evaluated after 2, 3, 7, and 14-days. Background signals were obtained by adding acetate buffer pH 4.5 0.1 M.

4.1.4 Conclusions

A µPAD was developed for quantifying levels of particulate Cr. Colorimetric µPADs provide a simple, portable approach for measuring particulate Cr relative to traditional methods. Using our system, total Cr mass can be quantified using devices that are inexpensive (<$0.05/test) and easy to use. Ultimately, the goal of this work is to provide a system whereby the analysis is performed at the point of use to avoid transportation costs. Rapid sample analysis will lead to more effective risk communication, improved assessment, and a lower exposure to occupational aerosol hazards.

4.2 Multilayer Paper-based Device for Colorimetric and Electrochemical Quantification of Metals

Poomrat Rattanarat[a], Wijitar Dungchai[b], David M. Cate[d], John Volckens[d,*], Orawon Chailapakul[a,e,*], Charles S. Henry[d,f,*]

[a]Electrochemistry and Optical Spectroscopy Research Unit (EOSRU), Department of Chemistry, Faculty of Science, Chulalongkorn University, Patumwan, Bangkok 10330, Thailand

[b]Department of Chemistry, Faculty of Science, King Mongkut's University of Technology Thonburi, 91 Prachautid Road, Thungkru, Bangkok 10140, Thailand

[c]School of Biomedical Engineering, Colorado State University, Fort Collins, Colorado 80523

[d]Department of Environmental and Radiological Health Sciences, Colorado State University, Fort Collins, Colorado 80523

[e]National Center of Excellence for Petroleum, Petrochemicals and Advanced Materials, Chulalongkorn University, Patumwan, Bangkok 10330, Thailand

[f]Department of Chemistry, Colorado State University, Fort Collins, Colorado 80523

*Corresponding authors

Abstract

The release of metals and metal-containing compounds into the environment is a growing concern in developed and developing countries, as human exposure to metals is associated with adverse health effects in virtually every organ system. Unfortunately, quantifying metals in the environment is expensive; analysis costs using certified laboratories typically exceed $100/sample, making the routine analysis of toxic metals cost-prohibitive for applications such as occupational exposure or environmental protection. Here, we report on a simple, inexpensive technology with the potential to render toxic metals detection accessible for both the developing and developed world that combines colorimetric and electrochemical microfluidic paper-based analytical devices (mPAD) in a three-dimensional configuration. Unlike previous mPADs designed for measuring metals, the device reported here separates colorimetric detection on one layer from electrochemical detection on a different layer. Separate detection layers allow different chemistries to be applied to a single sample on the same device. To demonstrate the effectiveness of this approach, colorimetric detection is shown for Ni, Fe, Cu, and Cr and electrochemical detection for Pb and Cd. Detection limits as low as 0.12 µg (Cr) were achieved on the colorimetric layer while detection limits as low as 0.25 ng (Cd and Pb) were achieved on the electrochemical layer. Selectivity for the target analytes was demonstrated for common interferences. As an example of the device utility, particulate metals collected on air sampling filters were analyzed. Levels measured with the mPAD matched known values for the certified reference samples of collected particulate matter.

Keywords: paper-based analytical device, colorimetric detection, electrochemical detection, particulate metals

4.2.1 Introduction

Human exposure to particulate matter (PM) air pollution has been established as a leading cause of human morbidity and mortality. Indoor and outdoor air pollution each rank among the top 10 risk factors contributing to disability-adjusted life years - a metric used by the World Health Organization to quantify the global burden of disease. Both the size and composition of airborne particles have been shown to play a role in PM toxicity [62]. Despite the well-established link between exposure and disease, the cellular mechanisms of PM-induced health effects are still not well defined. Metals present in PM have been the subject of much research, as metals have known pathologies in many organ systems. In occupational settings, exposure to metal-containing PM is particularly concerning due to the tendency for higher exposures [62]. For example, metals exposures (e.g. Be, Cd, Cr, Cu, Fe, Pb, Ni, and Hg) have been linked to increased hospitalization and mortality and to a variety of serious respiratory disorders including cancers of the lung, nose, and sinus cavity [177-179]. The Occupational Safety and Health Administration (OSHA) mandates permissible exposure limits (PELs) for workplace exposure to metals across a range of levels. For example, worker exposure to Pb and Ni is regulated at 30 and 1 $\mu g/m^3$, respectively, for an 8-hr workshift [84]. As a result, methods to measure aerosolized metals are important to understand and mitigate exposure.

In occupational settings, the approach for PM exposure assessment prescribes collection of an 8-hour filter sample from within a worker's breathing zone followed by analysis using either inductively coupled plasma (ICP) [180] or atomic emission spectrometry (OES) [181]. These analytic methods give very low detection limits and selective detection of multiple metals in a single sample. However, ICP and OES analyses require tedious sample preparation, highly trained personnel, and the equipment is both expensive and complicated. As a result, analytic costs are high, often more than $100 per sample [84]. The high cost makes large-scale studies economically infeasible and also prevents small businesses from routinely assessing worker exposure. As a result, there is a strong need for new approaches that are

substantially less expensive and can be performed by minimally trained individuals or even everyday citizens.

Although many approaches have been proposed as point-of-need sensors, [182] paper-based analytical devices (PADs) have recently gained significant attention because they are simple, inexpensive, require minimal sample, and are readily disposable [7, 13, 30]. To date, PADs have been used for point-of-care diagnostic assays, food safety assessment [44], and environmental monitoring [10, 83, 84]. The most of common detection method used with PADs is colorimetry where specific reagents are applied to the device and the developed color intensity and/or hue correlates with analyte concentration [30]. Electrochemical detection has also been used with PADs to generate electrochemical paper-based analytical devices (ePADs). Electrochemistry is attractive due to its portability, sensitivity, and selectivity [86, 87, 91, 119, 167, 183]. The use of ePADs for environmental analysis has been reported but only for limited applications [87, 167].

Here, a paper-based analytical device was developed that combines colorimetric and electrochemical quantification of six metals using two separate detection layers. Colorimetric detection was used for Fe, Ni, Cr, and Cu while square-wave anodic stripping voltammetry was used to measure Pb and Cd. Separating the colorimetric and electrochemical detection areas allowed for different sample preparation methods to be applied for each technique. Following sample collection, microwave-assisted acid digestion was performed directly on a filter punch to solubilize metals [84]. For analysis, the digested punch was placed on the center of the PAD, a drop of buffer was added, and metals were eluted outwards to the colorimetric detection zones and downwards to the electrodes. Ferricyanide and bismuth were added to the electrode surface prior to analysis to reduce the impact of Cu on Cd electrochemistry and to create an amalgam, respectively. Using the optimized PADs, detection limits of 0.12, 0.75, 0.75, 0.75 µg for Cr, Fe, Cu, and Ni in colorimetric detection mode and detection limits of 0.25 ng (1 µg/L) were achieved for Pb and Cd were obtained when analysis was performed on 2-mm and 10-mm filter punches, respectively. Finally, the PADs were used to measure metal content in

resuspended baghouse dust samples, and results matched known quantities of each metal deposited on the filter.

4.2.2 Experimental

4.2.2.1 Materials and Methods.

Standards for the six metals assays were prepared from lead(II) nitrate, cadmium(II) nitrate tetrahydrate, ammonium dichromate(VI), iron(III) chloride hexahydrate, nickel(II) sulfate hexahydrate, and copper(II) sulfate pentahydrate (Sigma-Aldrich, St. Louis, MO). Potential interferences (i.e., metals commonly found in PM) were prepared from barium(II) chloride, manganese(II) chloride tetrahydrate, zinc(II) nitrate hexahydrate, vanadium(III) chloride, silver(II) nitrate, cobalt(II) chloride, and aluminum(III) sulfate hydrate (Sigma-Aldrich, St. Louis, MO). For colorimetric assays, phthalic anhydride, cerium (IV) ammonium nitrate, 1,5-diphenylcarbazide, dimethylglyoxime, ammonium hydroxide, sodium chloride, bathocuproine, polydiallyl-dimethylammonium chloride (medium molecular weight) and sodium fluoride (Sigma-Aldrich, St. Louis, MO) were used as received. Hydroxylamine (Fisher Scientific, Pittsburgh, PA), 1,10-phenanthroline (Acros Organics, Fair Lawn, NJ), poly(acrylic acid) (Polysciences, Warrington, PA), polyethylene glycol (PEG) (Calbiochem, LaJolla, CA), and chloroform (Macron,) were used as received. For electrochemical detection, carbon ink (E3178, Ercon Incorporated, Wareham, MA) and Graphite powder (diameter <20 μm, Sigma-Aldrich, St. Louis, MO) were used for electrode materials. Multiwalled carbon nanotubes (MWCNT), 1000 ppm Bi standard solution (Sigma-Aldrich, St. Louis, MO) and potassium ferricyanide (Fisher Scientific, Pittsburgh, PA) were used for electrode modification. The transparency film used for electrode fabrication was purchased from Apollo Presentation Products (Booneville, MS). Sodium acetate and glacial acetic acid were obtained from Fisher Scientific (Pittsburgh, PA). The certified metal sample of baghouse dust (RTC-CRM014) was purchased from LGC Standards (Teddington, UK). Milli-Q water from Millipore (R ≥ 18.2 MΩ cm^{-1}) was used throughout these experiments. All chemicals were used as received without further purification.

4.2.2.2 Design and Fabrication of the PAD.

A wax-printing technique was used to create PADs because this fabrication process is simpler, less expensive, and faster than other reported methods [56, 57]. CorelDRAW software was used to create the device design shown in Figure 4.2.1. The patterned paper consisted of 3 colors: blue, yellow, and black. The RGB color code for blue was 0-153-255. The RGB color code for yellow was 248-195-0. The RGB color code for black was 22-24-25. The black portion of the pattern was used as a supporting layer for the PAD. The Blue zone was used for Fe and Cu assays while the yellow zone was used for Cr and Ni assays. Figure 4.2.1 was drawn to fill a letter size (8.5 x 11 inches) of Whatman grade 1 filter paper, which consists of 35 individual devices.
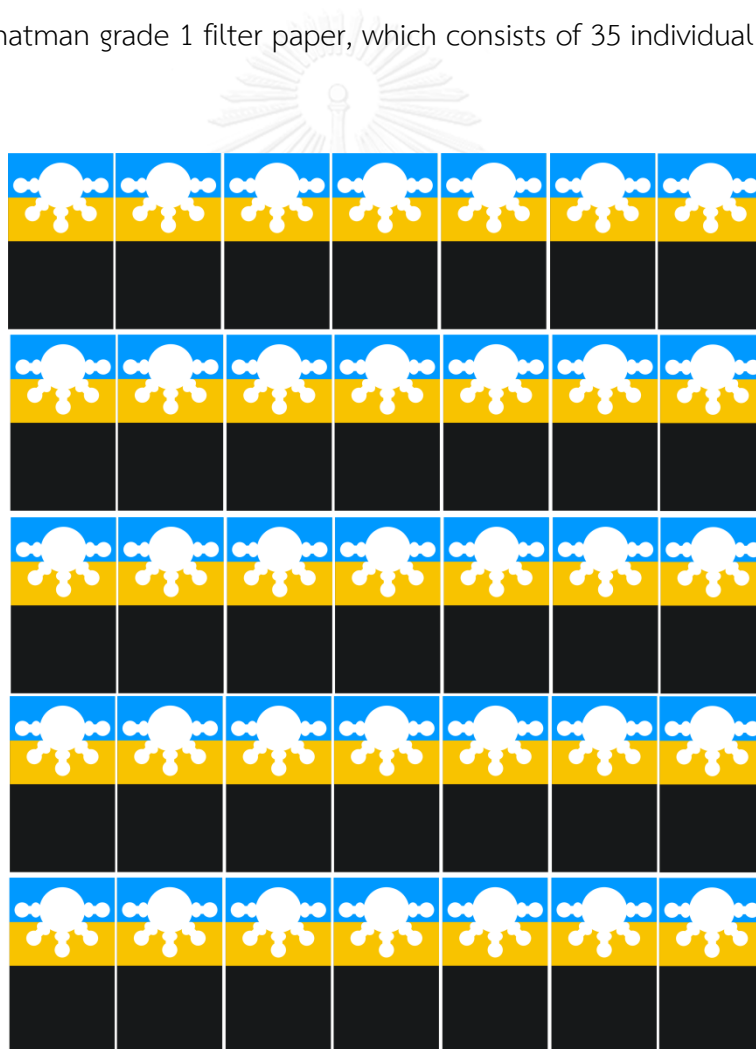
Figure 4.2.1 Layout of the wax-patterned paper design for an 8.5 x 11 inch sheet of Whatman filter paper.

The colors were selected to be complimentary to the colorimetric reactions. The wax-pattern was printed onto Whatman Grade 1 filter paper (VWR) using a wax printer (Xerox Phaser 8860). The wax pattern was melted at 200 °C for 120 s on a hot plate to define the hydrophobic barriers and hydrophilic channels. The hydrophilic area consisted of sample reservoir, pretreatment zone, and detection zone with diameters of 1.2, 0.3, and 0.3 cm, respectively. One side of the device was covered with clear packing tape to prevent solution leakage through the device and to add structural integrity. Finally, a 6 mm diameter hole was punched in the middle of sample reservoir using a biopsy punch to provide a solution connection between the sample and the electrode surfaces. For electrochemical detection, a three-electrode system was screen printed onto polyester film. Unmodified carbon ink (Gwent) was printed onto the substrate to make a conductive pads and a pseudo reference electrode. Ink modified with a mixture of MWCNTs, graphite powder, and carbon ink (5:5:200) was printed three times onto the substrate to make the working and counter electrodes. To cure the inks, the transparency film was baked at 65 °C for 30 min after each screen-printing step. To complete the device, patterned paper, double sided adhesive tape, a screen-printed electrode, and 6 mm-punched double-sided adhesive tape was assembled by folding as shown in Figure 4.2.2 [184].

4.2.2.3 Colorimetric Detection of Fe, Ni, Cr, and Cu.

Previously reported methods for Fe, Ni, Cr, and Cu detection on PADs were combined here [84, 185]. These methods employ addition of non-volatile reagents direct to the paper to define sample pretreatment and detection zones as described previously [84]. For colorimetric detection of Fe, the detection zone was prepared by adding 1 µL of hydroxylamine (0.1 g/mL) in 6.3 M acetate buffer. Next, 0.5 µL of poly(acrylic acid) (0.7 mg/mL) was added, followed by two 0.5 µL aliquots of 1,10-phenanthroline (8 mg/mL) in 6.3 M acetate buffer. The poly(acrylic acid) was added to immobilize the Fe-phenanthroline complex. For Ni detection, devices were prepared by adding two 0.5 µL aliquots of NaF in DI water (0.5 M), followed by 0.4 µL of acetic acid (6.3 M, pH 4.5) to define a sample pretreatment zone. Five 0.5 µL

aliquots of DMG in methanol were then added to the colorimetric detection zone, followed by two 0.5 µL aliquots of ammonium hydroxide (0.03 mM pH 9.5). For Cr detection, the PAD was prepared by adding two 0.5 µL of ceric(IV) ammonium nitrate (0.35 mM), followed by 0.5 µL of poly(diallyldimethylammonium chloride) (PDDA) (5% w/v) to the pretreatment zone. Two 0.25 µL aliquots of a 1,5-diphenylcarbazide (1,5-DPC) and phthalic anhydride (15 mg and 40 mg, respectively, in acetone 1 mL) mixture were also added to the colorimetric detection zone.
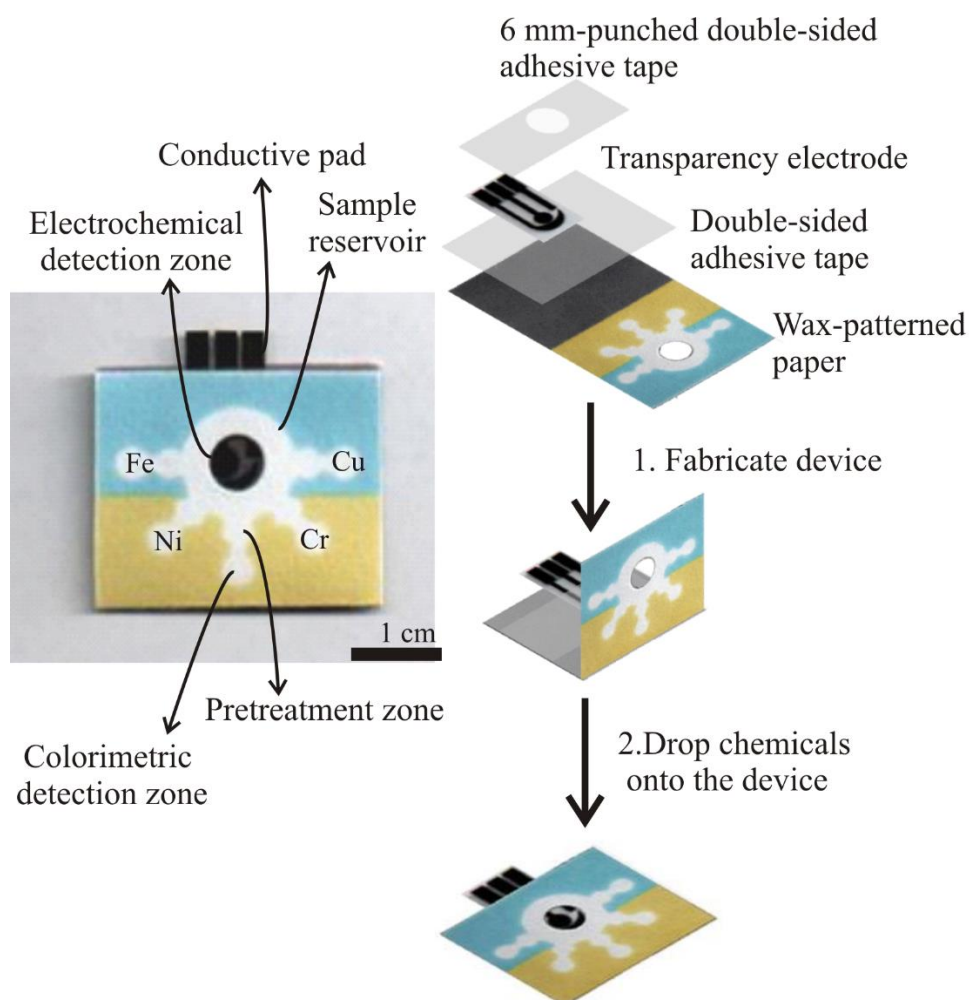
Figure 4.2.2 Left) Photograph of a microfluidic paper-based analytical device with the different regions labeled. Right) Schematic drawing of the fabrication procedure for the PAD.

For Cu, a 1 µL aliquot of hydroxylamine (0.1 g/mL), followed by a 0.5 µL aliquot of acetic acid/NaCl buffer (10 mM, pH 4.5) was first added to the colorimetric detection zone. The Cu detection solution was prepared from 50 mg/mL bathocuproine and 40 mg/mL PEG 400 dissolved in chloroform. Two 0.5 µL aliquots of the bathocuproine/PEG detection solution were then added to the colorimetric detection zone. Between each addition of reagent, the device was allowed to dry at room temperature (22±1°C).

4.2.2.4 Electrode Modification of Bi and ferricyanide.

A mixture of Bi (100 ppm) and potassium ferricyanide (5 mM) was prepared in acetate buffer pH 4.5 (0.1 M). A 2.5 µL aliquot of this mixture was added directly to the screen-printed carbon nanotube electrode surface and allowed to dry. The final device is shown in Figure 4.2.2.

4.2.2.5 Analytical Procedure.

For calibration, a series of 10 mm diameter punches were cut from either Whatman #1 filter paper or mixed cellulose ester (MCE) filters using a CO_2 laser cutter (Zing). Standards were added to punches and allowed to dry. The punch was placed at the center of the sample reservoir. As shown in Figure 4.2.3, a polydimethylsiloxane (PDMS) lid consisting of one 2 mm-diameter hole over the sample reservoir and five 5 mm-diameter holes over the colorimetric detection zones was then aligned over the device and the device connected to the potentiostat. The PDMS lid was prepared using 10:1 Sylgard 184 elastomer and curing agent (Dow Corning, Midland, MI), respectively. PDMS was poured onto an unpatterned 100 mm silicon wafer (100) and allowed to cure at 95 °C for at least 30 min. Biopsy punches were used to create a hole over each colorimetric detection zone (5 mm diameter) and in the center of the sample inlet (3 mm diameter). The center hole allows for the addition of the eluent to the device; the holes at each detection zone allow for faster evaporation and thus

quicker drying in those areas. As a result, sample will flow continuously from the sampling filter though each detection zones.

Figure 4.2.3 A representative photograph of the PAD and PDMS cover.

The lid reduced evaporation during analyte transport from the sample to detection zones. The PDMS cover also provides consistent pressure across the surface of the device, maintaining conformal contact between the filter and device across the entire filter punch. 50 µL of 0.1 M acetate buffer (pH 4.5) was added to the center hole of PDMS lid causing the soluble metals to flow through the channels to the colorimetric detection zones and down to the electrodes.

4.2.2.6 Square-wave Anodic Stripping Voltammetric Detection.

Electrochemical measurements were made at room temperature (22 ± 1 °C) using a potentiostat (CHI 660B, CH Instruments, Austin, TX). Square-wave anodic stripping voltammetry was performed for sample measurement using the following (optimized) conditions: conditioning potential (E_{cond}) +0.0 V for 5 s, deposition potential (E_{dep}) −1.5 V for 240 s, equilibration time (t_{eq}) 5 s, SW amplitude (E_{amp}) 15 mV, step potential (E_{step}) 5 mV, frequency (f) 15 Hz, and scanning potential -1.5 to 0.0 V. All

measurements were made against a carbon pseudo-reference counter electrode on the PAD.

4.2.2.7 Image Processing.

After electrochemical detection, a scanner (XEROX DocuMate 3220) was used to capture the device image for colorimetric measurements. Collected images were saved in JPEG format at 600 dpi and analyzed using ImageJ software (National Institutes of Health) using previously developed methods from our laboratory [44, 84]. The software was used to measure the mean intensity of the color for each colorimetric reaction. As shown in Figure 4.2.4, the hue of interest was selected by applying a color threshold window specific for each metal/reagent complex.
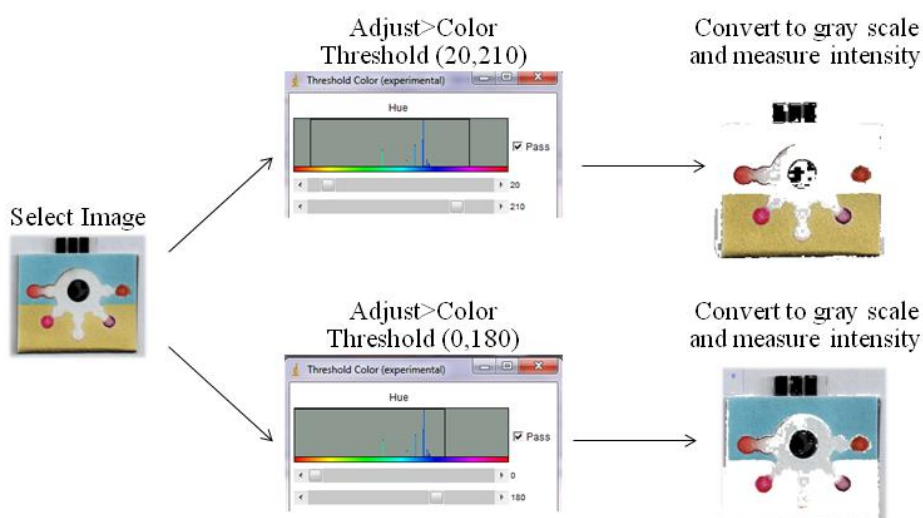
Figure 4.2.4 Image processing with hue adjustment for eliminating background color.

After JPEG images were opened with ImageJ in RGB color, adjustment of the color threshold was performed first. Briefly, the "Color Threshold" window is accessed through the ImageJ menu by selecting "Image", "Adjust", and "Color Threshold", respectively. Then, the HSB option is selected to adjust image hue, saturation, and brightness. The hue was tuned by changing the sliders directly below the "Hue" spectrum until the color of interest is visible and the wax-patterned barrier

disappeared. The hue threshold range set for each metal assay was kept consistent throughout all experiments. The optimum threshold color ranges for removing hydrophobic wax barrier were found to be (20,210) and (0,180) for blue and yellow, respectively. Images were next converted to 8-bit grey scale ("Image", "Type", and "8-bit", respectively) and inverted ("Edit" and "Invert"). As a result, the intensity measurement, when plotted versus metal amounts, yields a positive slope. The mean intensity was then measured and imported into Origin (v 8.0, MicroCal) for analysis. Alternative methods that do not rely on conversion to grayscale are also available and gave similar results [85, 186].

4.2.2.8 Particulate Metal Collection and Digestion.

Dust samples were generated in a 1 m^3 chamber. Using an aerosol photometer (TSI, Model 8250), the average concentration in the chamber was measured at 0.73 mg m^{-3}. The relative humidity (RH) was monitored and remained <50% RH during all experiments. The dust was reaerosolized and collected at a flow rate of 10 L/min for 4 h onto 37 mm Pallflex or mixed cellulose ester (MCE) filters. For the Pallflex filter, gravimetric analysis was used to measure the dust mass by weighing the filter before and after sampling using a Mettler-Toledo analytical microbalance (MX5), yielding an average of 1.25 mg ash per cm2 on the filter. A 20 μL aliquot of sodium dodecyl sulfate (1 mM) was added to each 10 mm MCE punch to make it more hydrophilic prior to metal digestion. Microwave-assisted acid digestion was performed by adding 5 μL of concentrated nitric acid followed by 30 μL of water to the filter punches. The punches were placed in a household microwave on high power (1100 W). The filter was heated for 15 s three times, and 30 μL of water was added to the punches between each heating step. Finally, 10 μL of sodium bicarbonate (0.5 M pH 9.5) was added to neutralize the digested sample. After adding the sodium bicarbonate, the filter was heated again for 15 s. Finally, the digested filter was placed on the center of the PAD and analyzed as described above.

4.2.3 Results and discussion

4.2.3.1 Device Design.

Simultaneous profiling of multiple metals using both colorimetric and electrochemical methods is challenging because each method requires different sample pretreatment steps. As a result, it is more common to analyze a small sub-set of metal species using any one technique when applying these detection modalities. To reduce overall analysis cost and complexity, a PAD was designed to allow detection of multiple metals using both modalities simultaneously. Key to this development is the ability to isolate each colorimetric step from the electrochemical detection steps to allow distinct chemical reactions to occur for each analysis. The PAD design and fabrication steps used to accomplish this goal are shown in Figure 4.2.2 and the operational procedure is shown in Figure 4.2.5. The top layer contains five wax-defined channels extending outward from an open sample reservoir. Each channel contains unique sample pretreatment and detection zones that give both metal selectivity and sensitivity. For electrochemistry, MWCNT modified carbon inks were screen-printed onto polyester and then modified with Bi and ferricyanide to enhance stripping signals and reduce Cu interference, respectively [187, 188]. The electrodes were aligned below the colorimetric detection layer and isolated by double sided adhesive tape. Upon sample addition, solution moved downwards to wet the electrodes in the bottom layer while also moving outwards to wet the colorimetric detection channels. The device shown here represents the first integration of all four colorimetric methods along with electrochemical methods for Pb and Cd.
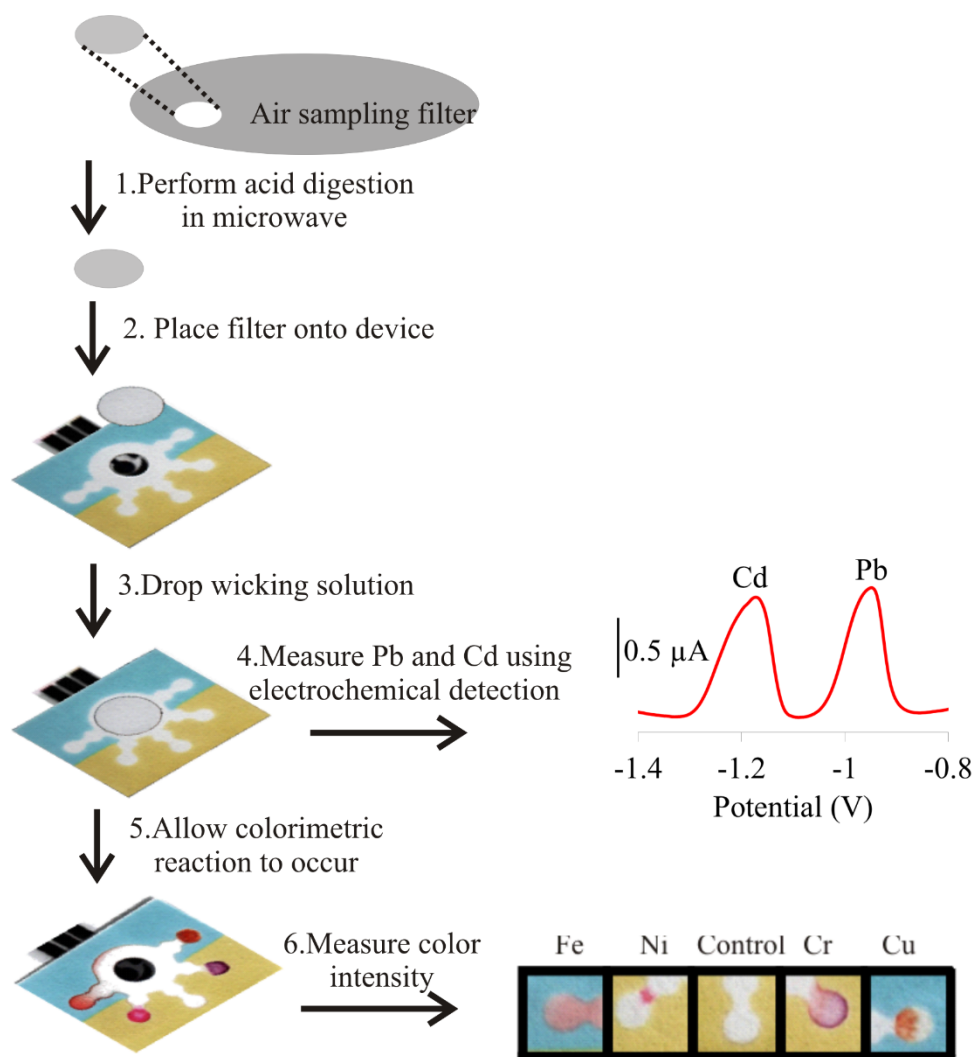
Figure 4.2.5 Analytical procedure for metal assays using the PADs. The assay requires three steps, (i) microwave-assisted acid digestion, (ii) Anodic stripping voltammetric detection of Pb and Cd, and (iii) Colorimetric detection of Fe, Ni, Cr, and Cu.

4.2.3.2 Colorimetric Detection of Fe, Ni, Cr, and Cu.

On-device images of colorimetric reaction products and associated calibration curves for all four species are shown in Figure 4.2.6a and 4.2.6b, respectively. The specifics of the chemistry for each analysis have already been reported.
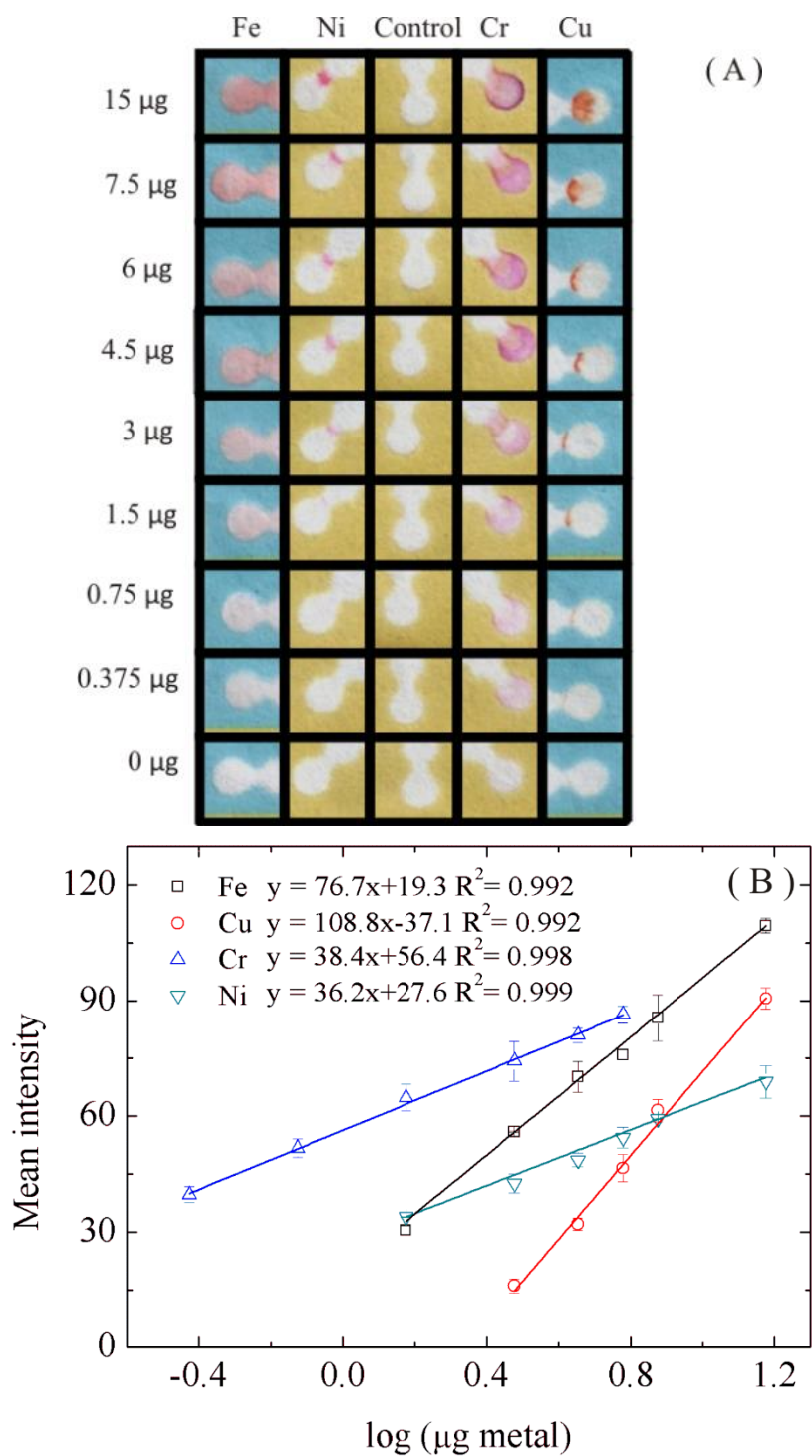
Figure 4.2.6 (a) Visual color changes obtained from detection of Fe, Cu, Cr, and Ni. (b) representative calibration graph for each metal using a logarithmic metal concentrations and mean intensity.

For Fe, Fe(III) was reduced to Fe(II) at the sample pretreatment zone using ascorbic acid. The resulting linear range of 1.5-15 µg was established for total on-filter Fe, and a visual detection limit of 0.75 µg was achieved. For Ni, we adjusted the pH to ~9.0 and added NaF and acetic acid as masking agents for Fe to the pretreatment zone. The resulting linear range for Ni was 1.5-15 µg for total on-filter Ni with a visible detection limit of 0.75 µg. The visible detection limit is defined as the lowest mass for which the complexation product was still visible against the substrate background with the unaided eye. To control user bias, untrained individuals were asked to identify which device contained a colored product with the lowest (yet still visible) intensity. Detection of Cu was performed at acidic pH 4.5 and the surface of the detection zone was modified with polyethylene glycol to trap the hydrophobic Cu-bathocuproine complex. The operating range and detection limit of Cu were 3.0-15 µg and 0.75 µg, respectively. For Cr, soluble Cr(III) was oxidized to Cr(VI) using Ce(IV) on the PAD and then reacted with 1,5-diphenylcarbazide. A linear calibration curve was obtained in the range of 0.38-6.0 µg and the visible detection limit was found to be 0.12 µg. The linear working ranges and detection limits reported here are appropriate for measuring integrated 4- to 8-hr filter samples from occupational settings. Variability in the detection limits is largely the result of the molar absorptivity of each final complex. The upper end of each range occurred where the paper became saturated with the complex and additional complexation did not result in additional increases in color intensity.

4.2.3.3 Electrochemical Detection of Cd and Pb.

For monitoring low levels of heavy metals in biological, food, fuel, and/or environmental samples, anodic stripping voltammetry (ASV) is frequently used [189, 190]. Due to the low levels Pb and Cd in most types of PM, ASV was used in conjunction with Bi and ferricyanide additives. Bi improves ASV performance because it forms a metal-Bi alloy at the electrode surface during preconcentration and allows for the stripping measurement to be performed without deoxygenation [188]. Furthermore, Bi-modified electrodes have lower toxicity than mercury-modified

electrodes. Under optimized conditions, anodic peaks for Cd and Pb were obtained at -1.10±0.04 V and -0.91±0.04 V (n=4) versus pseudo-reference carbon electrode. Under the optimized conditions, the anodic peak currents were proportional to Cd and Pb levels in the range of 0.25 – 7.5 ng (5 -150 µg/L) with regression coefficients of 0.990 and 0.995, respectively (Figure 4.2.7a and 4.2.7b).
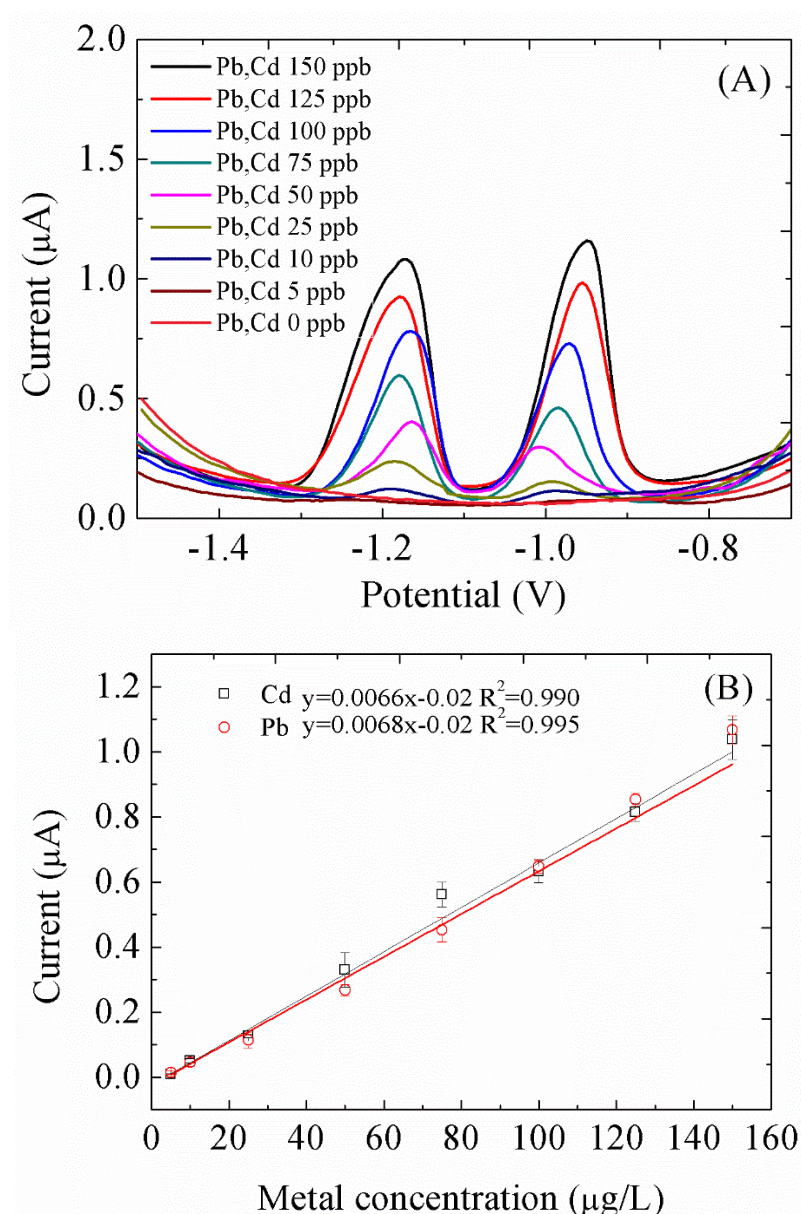
Figure 4.2.7 (a) Square-wave voltammogram showing electrochemical detection of Cd and Pb. (b) Representative calibration graph between metal and anodic current of Cd and Pb.

The relative standard deviation for the method was found to be 9.79% and 7.02% for Cd and Pb, respectively. The detection limit was found to be 0.25 ng (1 µg/L) for both Cd and Pb. Analytical performance data for all six metals are summarized in Table 4.2.1 and that the multilayer PAD can provide sensitive, selective analysis of multiple metals simultaneously. Furthermore this system has the ability to isolate each analytical reaction so that simultaneous detection of multiple metals can be conducted in a single device.

Table 4.2.1 Summarized analytical performance of proposed mPAD for each metal assay.

Metal	Linearity	MDL[1]	%RSD (n=3)[2]	Detection mode
Fe	1.5-15 µg	0.75 µg	8.84%	Colorimetric detection
Cu	3.0-15 µg	0.75 µg	9.54%	Colorimetric detection
Ni	1.5-15 µg	0.75 µg	8.52%	Colorimetric detection
Cr	0.38-6.0 µg	0.12 µg	4.01%	Colorimetric detection
Pb	5 -150 µg/L	0.25 ng (1 µg/L)	7.02%	Electrochemical detection
Cd	5 -150 µg/L	0.25 ng (1 µg/L)	9.79%	Electrochemical detection

[1]Minimum detectable level (MDL) was observed from the lowest level of metals detected on a 10 mm filter punch.

[2]Relative standard deviation (%RSD) was calculated from triplicate (n=3) calibration curves

Table 4.2.2 provides a comparison of mPAD performance versus existing methods as well as the reported minimum detectable level (MDL) and minimum detectable level for an 8-h time-weighted average [84, 191-194]. The results clearly show our ability to make measurements in relevant concentration ranges.

Table 4.2.2 the comparison between the minimal detectable levels using various analytical methods and permissible exposure limits set by OHSA.

Metal	Cr		Fe		Ni		Cu		Pb		Cd	
Methods	MDL[a]	TWA[b]	MDL[a]	TWA[b]	MDL[a]	TWA[b]	MDL[a]	TWA[b]	MDL[a]	TWA[b]	MDL[a]	TWA[b]
UE-ASV[c,1]	-	-	-	-	-	-	-	-	2 µg	-	-	-
FP-XRF[d,2]	-	-	-	-	-	-	-	-	6.2 µg	-	-	-
ICP-MS[e,3]	-	6 ng/m^3	-	-	-	3 ng/m^3	-	10 ng/m^3	-	15 ng/m^3	-	-
IC[f,4]	-	-	15 µg/L	0.007 µg/m^3	10 µg/L	0.006 µg/m^3	10 µg/L	0.006 µg/m^3	60 µg/L	0.030 µg/m^3	30 µg/L	0.020 µg/m^3
ASV[g,5]	-	-	-	-	-	0.4 ng/m^3	-	0.3 ng/m^3	-	0.8 ng/m^3	-	0.1 ng/m^3
ASV[g,6]	-	-	-	-	-	-	0.2 µg/L	-	0.8 µg/L	-	0.05 µg/L	-
OSHA 8-h PEL[i,7]	-	1 mg/m^3	-	10 mg/m^3	-	1 mg/m^3	-	1 mg/m^3	-	30 µg/m^3	-	2.5 µg/m^3
Previous µPADs[h,8]	-	-	1.5 µg	9 µg	1 µg	6 µg	1 µg	6 µg	-	-	-	-
This mPAD	0.12 µg	0.72 µg/m^3	0.75 µg	0.45 µg/m^3	0.75 µg	4.5 µg/m^3	0.75 µg	4.5 µg/m^3	1 µg/L	1.5 ng/m^3	1 µg/L	1.5 ng/m^3

[a]MDL: minimum detectable level. [b]TWA: minimum detectable air concentrations as an 8-h time-weighted average. [c]UE-ASV: ultrasonic extraction and field-portable anodic stripping voltammetry. [d]FP-XRF: field-portable X-ray fluorescence. [e]ICP-MS: inductively coupled plasma-mass spectrometry. [f]IC: ion chromatography. [g]ASV-HMDE: anodic stripping voltammetry using hanging mercury drop electrode. [h]µPADs: microfluidic paper-based analytical device. [i]OSHA 8-h PEL: permissible exposure limit based on an 8-h sample with 4 L/min collection rate.

4.2.3.3 Interference Study for Cd and Pb.

Because airborne PM contains many different metals that could interfere with ASV, the tolerance ratio for interfering metal species was measured. The tolerance ratio is defined as the concentration of metals ions that generates a change in the peak height of less than 5% for Pb and Cd anodic peaks [195]. The maximum concentrations of interfering metals are shown in Table 2 when using 2.5 ng (50 µg/L) of Pb and Cd as the sample. From the results, it was concluded that Mn(II), Mg(II), Zn(II), Fe(III), Fe(II), Al(III), Ba(II), and V(III) ions did not affect Pb and Cd detection. On the other hand, Ni(II), Co(II), Cu(II), and Cr(VI) significantly impacted sensitivity. To minimize this problem, two solutions are possible, (i) diluting the aerosol sample by decreasing the size of the sampling filter while simultaneously maintaining extraction volume and (ii) complexation of Cu(II) using ferricyanide. Dilution represents a simple solution for ASV since the deposition step allows for preconcentration and was used for Ni(II), Co(II), and Cr(VI) interferences. Furthermore, these ions should be at very low levels in the proposed samples [196]. Cu levels are anticipated to be much higher, however, and thus additional optimization was required.

Table 4.2.3 Tolerance ratio of interfering ions in the electrochemical determination of 2.5 ng (50 µg/L) of Pb(II) and Cd(II).

Interfering ion	5% Tolerance ratio	
	Cd	Pb
Mn(II)	10000	10000
Mg(II)	1000	1000
Zn(II)	1000	1000
Fe(II)	1000	1000
Fe(III)	1000	100
Al(III)	100	100
Ba(II)	100	100
V(III)	100	100

Ni(II)	100	10
Cr(VI)	50	50
Co(III)	10	10
Cu(II)	2	5

4.2.3.4 Minimizing the Cu(II) Interference using Ferricyanide.

The well-known Cu(II) interference has been previously described and attributed to the formation of intermetallic compounds of the target metals with deposited Cu [54]. The suppression of the ASV signal for Pb and Cd in the presence of Cu results from competition between electrodeposited bismuth and copper intermetallic compounds at the electrode surface because the reduction potential of Cu is close to reduction potential of Bi. In the absence of Cu(II), well-defined Pb(II) and Cd(II) peaks were observed as shown in Figure 4.2.8a.
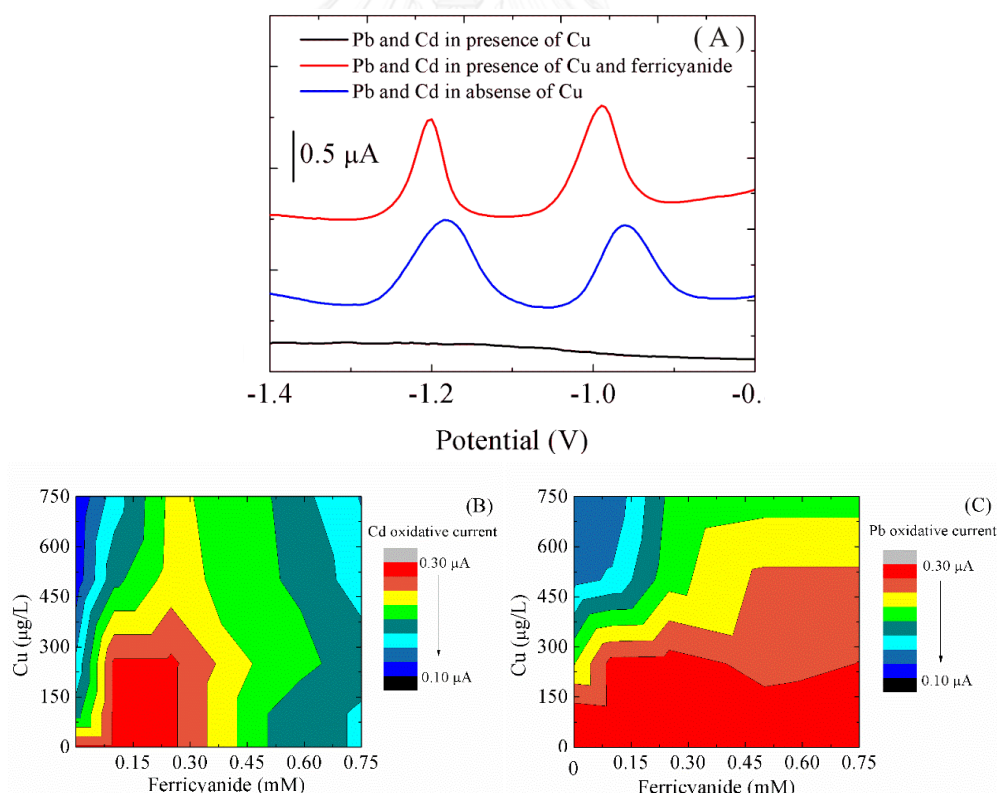
Figure 4.2.8 (a) Influence of ferricyanide concentration for elimination of Cu effect in square-wave anodic stripping voltametric detection of Cd and Pb (b) Contour plot

between Cu concentration and ferricyanide affecting to Cd detection and (c) Pb detection electrochemically.

In the presence of 25 ng (500 µg/L) of Cu(II), ASV responses for both Pb(II) and Cd(II) were significantly diminished. To suppress the effect of Cu(II) on Pb and Cd detection, various compounds have been used to complex the Cu(II) including ferrocyanide [197] and cyanide [191]. In our experiment, ferricyanide was selected to complex with Cu(II) because it is less toxic than cyanide [198]. Suppression of the Cu signal was presumably due to the strong complexation between Cu and cyanide, leading to shift of the Cu oxidation potential to more negative potential over potential range of -1.5 V to 0.0 V. The optimum ferricyanide concentration was determined from contour plots of Cu and ferricyanide concentrations shown in Figures 4.2.8b and c. In the presence of 30 µg (500 µg/L) of Cu(II), complete recovery of Pb(II) and Cd(II) anodic peak currents was achieved when 0.25 mM of ferricyanide was added to the device prior to Pb and Cd measurements. These results demonstrate the importance of separating the detection modes because the highly colored ferricyanide would interfere with any of the colorimetric reactions.

4.2.3.5 Metal Determination in Resuspended Baghouse Dust.

To validate the multi-level PAD approach, a baghouse dust sample certified for Cd, Cr, and Pb, and containing unknown amounts of Al, Sb, As, Ba, B, Be, Ca, Co, Cu, Fe, Mg, Mn, Hg, Mo, Ni, P, K, Ag, Se, Na, Sr, Tl, Sn, Ti, V, and Zn was analyzed from a filter sample. To generate a PM sample filter, dust was nebulized in an aerosol chamber and collected onto MCE filters at 10 L/min for 4 h. Sodium dodecyl sulfate (SDS) was used to pretreat the hydrophobic MCE filter after sample collection but before acid digestion [83]. Adding SDS to the MCE punch reduced its hydrophobicity allowing aqueous solutions to penetrate through the MCE punch for elution. Metal concentrations measured from resuspended baghouse dust samples are shown in Figure 4.2.9b. As shown in the Figure 4.2.9a, a single 2 mm punch could be used for electrochemical detection, while three 10 mm punches were needed for colorimetric

detection. The measured values were not statistically different from the known masses on the filters and demonstrate the accuracy of the system reported here.

(A)

Three MCE punches with diameter of 10 mm for colorimetric detection

MCE punch with diameter of 2 mm for electrochemical detection
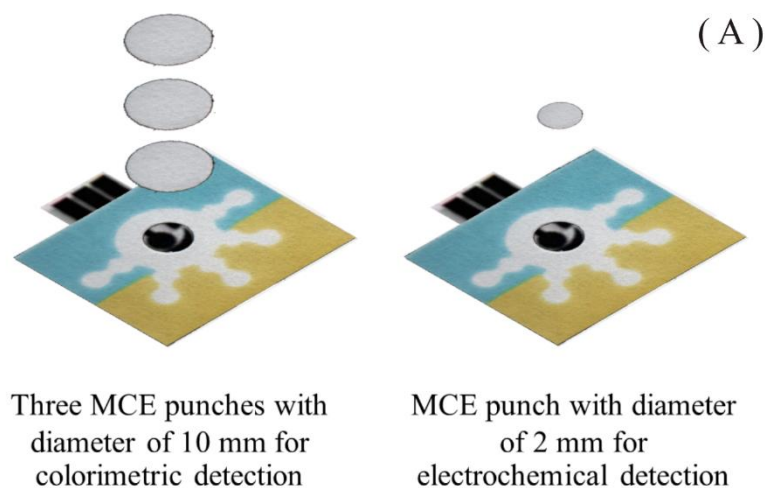
Metal	Results	Punch size (mm)	Punch Piece (piece)	Actual level (µg/ng)	Measured level[1] (µg/ng)
					(B)
Cd	0.5 µA / -1.2 -1.0	2	1	1.86 ng	1.96±0.04 ng
Pb		2	1	6.97 ng	6.25±0.11 ng
Ni		10	3	3.83 ng	ND[2]
Fe		10	3	1.60 µg	1.61±0.01 µg
Cr		10	3	0.61 µg	0.64±0.03 µg
Cu		10	3	0.03 µg	ND[2]

Figure 4.2.9 (a) Variation of the size and number of filter punches for determination of metals using the PAD. A single 2 mm punch was used for electrochemical methods while three 10 mm punches were best suited for colorimetric measurements. (b) Results from electrochemical and colorimetric detection by our proposed 3DPAD. [1]Measured level obtained from three dependent measurement (n=3), [2]ND; Not detectable.

4.2.4 Conclusions

A PAD was developed to measure particulate metals as part of an effort to reduce the overall cost and operation complexity of this measurement. The key development reported here is the use of two separate detection layers, one for colorimetric detection and one for electrochemical detection. Separating detection layers allowed for each layer to contain unique chemistries to improve sensitivity and selectivity. Using the method, six metals (Cd, Pb, Fe, Cu, Ni, and Cr) were determined simultaneously from PM collected on sample filters. Metal levels measured using the PAD matched those using traditional approaches.

CHAPTER V

CONCLUSIONS AND FUTURE PERSPECTIVE

5.1 Conclusions

The main objective of this dissertation is to develop the miniaturized analytical systems coupled with colorimetric/electrochemical detection for the determination of organic compounds and heavy metals in biomedical, pharmaceutical, and environmental applications. Using optimal conditions, analytical figures of merit of these systems were assessed. The results indicate that these systems provided an acceptable detection limit and a wide linear range which is sufficiently sensitive to measure in relevant concentration ranges.

Moreover, various outstanding strategies to improve sensitivity and selectivity for each method were evaluated following;

1. A novel ePAD was demonstrated for dopamine (DA) determination in serum. The selective enhancement of the DA signal is primarily due to electrostatic interactions between the positively charged dopamine and the negatively charged SDS, leading to shift in the oxidation potential. A significant preconcentration was achieved by adding multiple aliquots of the testing DA-containing sample.

2. The potential of using CD microfluidic biosensor to access quantitative measurement of diabetes biomarkers in human serum was demonstrated for the first time. The pattern of spiral channel was appropriately designed to allow the well-mixing between glucose and oxidase enzyme in order to produce H_2O_2. A significant electrochemical enhancement was accomplished using G-PANI nanocomposite modified electrode. Furthermore, the selectivity in H_2O_2 detection can be improved by using CoPc electrocatalyst.

3. A novel electrochemical droplet-based microfluidics for determination of 4-AP in commercial PA products was successfully developed. The improvement in electrochemical sensitivity was attributed to in fact that the outstanding G-PANI nanocomposite can enhance the active surface area of an electrode and increase the electrochemical conductivity. The selective detection of 4-AP can be achieved by selecting the applied potential in amperometry while minimizing the PA response.

4. A simple and portable colorimetric µPAD was developed to quantify particulate Cr level. The ability to measure total Cr using the combination between Ce(IV) oxidation and selectively colorimetric detection using 1,5-DPC was introduced. This system is inexpensive (<\$0.05/test) and easy to use.

5. A multilayer paper-based analytical device was developed for simultaneous measurement of particulate metals. The key development reported here is the use of two separated detection layers (colorimetric and electrochemical detections), allowed unique chemistries in each layer to improve sensitivity and selectivity of both detections. Using specific condition, the colorimetric reagent used to react with the metal of interest to produce color product which summarized as shown in Table 5.1.1. For electrochemical detection, in situ bismuth-modified electrode was used to improve ASV performance because of the formation of a metal-bismuth alloy at the electrode surface during preconcentration. The effect of Cu interference on ASV performance was suppressed by using the complexing reaction between ferricyanide and Cu.

Table 5.1.1 Summerized colorimetric reagent for selective detection of Fe, Ni, Cr, and Cu

Metal	Colorimetric reagent	Color of product
Fe	1,10-phenanthroline	Red
Ni	dimethylglyoxime	Pink
Cr	1,5-diphenylcarbazide	Pink
Cu	bathocuproine	Orange

In addition, the developed systems were successfully used to determine target analytes in real life samples with satisfactory results, matched those obtained from traditional approaches.

5.2 Future Perspective

Miniaturization of analytical system will have a significant impact on all aspects of testing. The complicated analytical testing can be miniaturized which permit testing to move from the conventional laboratory towards limited-resource setting. These miniaturized analytical models can be further extended to detect various target analytes in the several applications such as point-of-care testing, quality control of pharmaceutical product, and environmental monitoring.

REFERENCES

[1]   Rios, A., Escarpa, A., and Simonet, B. Miniaturization in Analytical Chemistry. in
        Miniaturization of Analytical Systems, pp. 1-38: John Wiley & Sons, Ltd, 2009.

[2]   Janasek, D., Franzke, J., and Manz, A. Scaling and the design of miniaturized
        chemical-analysis systems. Nature 442(7101) (2006): 374-380.

[3]   Liu, J.-S., Liu, C., Guo, J.-H., and Wang, L.-D. Electrostatic bonding of a silicon
        master to a glass wafer for plastic microchannel fabrication. Journal of
        Materials Processing Technology 178(1–3) (2006): 278-282.

[4]   Poenar, D.P., Iliescu, C., Carp, M., Pang, A.J., and Leck, K.J. Glass-based
        microfluidic device fabricated by parylene wafer-to-wafer bonding for
        impedance spectroscopy. Sensors and Actuators A: Physical 139(1–2) (2007):
        162-171.

[5]   Ruecha, N., Siangproh, W., and Chailapakul, O. A fast and highly sensitive
        detection of cholesterol using polymer microfluidic devices and
        amperometric system. Talanta 84(5) (2011): 1323-1328.

[6]   Sameenoi, Y., et al. Poly(dimethylsiloxane) cross-linked carbon paste
        electrodes for microfluidic electrochemical sensing. Analyst 136(15) (2011):
        3177-3184.

[7]   Ballerini, D.R., Li, X., and Shen, W. Patterned paper and alternative materials
        as substrates for low-cost microfluidic diagnostics. Microfluidics and
        Nanofluidics 13(5) (2012): 769-787.

[8]   Martinez, A.W., Phillips, S.T., Butte, M.J., and Whitesides, G.M. Patterned paper
        as a platform for inexpensive, low-volume, portable bioassays. Angewandte
        Chemie-International Edition 46(8) (2007): 1318-1320.

[9]   Lin, S.-W., Chang, C.-H., and Lin, C.-H. High-throughput Fluorescence
        Detections in Microfluidic Systems. Genomic Medicine, Biomarkers, and Health
        Sciences 3(1) (2011): 27-38.

[10]   Ratnarathorn, N., Chailapakul, O., Henry, C.S., and Dungchai, W. Simple silver nanoparticle colorimetric sensing for copper by paper-based devices. Talanta 99 (2012): 552-557.

[11]   Ho, J., Tan, M.K., Go, D.B., Yeo, L.Y., Friend, J.R., and Chang, H.-C. Paper-Based Microfluidic Surface Acoustic Wave Sample Delivery and Ionization Source for Rapid and Sensitive Ambient Mass Spectrometry. Analytical Chemistry 83(9) (2011): 3260-3266.

[12]   Modick, H., Schütze, A., Pälmke, C., Weiss, T., Brüning, T., and Koch, H.M. Rapid determination of N-acetyl-4-aminophenol (paracetamol) in urine by tandem mass spectrometry coupled with on-line clean-up by two dimensional turbulent flow/reversed phase liquid chromatography. Journal of Chromatography B 925(0) (2013): 33-39.

[13]   Liana, D.D., Raguse, B., Gooding, J.J., and Chow, E. Recent Advances in Paper-Based Sensors. Sensors 12(9) (2012): 11505-11526.

[14]   Ren, K., Zhou, J., and Wu, H. Materials for Microfluidic Chip Fabrication. Accounts of Chemical Research 46(11) (2013): 2396-2406.

[15]   Land, K.J., Mbanjwa, M.B., Govindasamy, K., and Korvink, J.G. Low cost fabrication and assembly process for re-usable 3D polydimethylsiloxane (PDMS) microfluidic networks. Biomicrofluidics 5(3) (2011): 36502-365026.

[16]   Dhayal, M., Jeong, H.G., and Choi, J.S. Use of plasma polymerisation process for fabrication of bio-MEMS for micro-fluidic devices. Applied Surface Science 252(5) (2005): 1710-1715.

[17]   Iliescu, C., Chen, B., and Miao, J. On the wet etching of Pyrex glass. Sensors and Actuators A: Physical 143(1) (2008): 154-161.

[18]   Brown, S.S., Kendrick, T.C., McVie, J., and Thomas, D.R. 4 - Silicones. in Wilkinson, E.W.A.G.A.S. (ed.)Comprehensive Organometallic Chemistry II, pp. 111-135. Oxford: Elsevier, 1995.

[19]   Sameenoi, Y., et al. Microfluidic Electrochemical Sensor for On-Line Monitoring of Aerosol Oxidative Activity. Journal of the American Chemical Society 134(25) (2012): 10562-10568.

[20]   Bui, M.-P.N., Li, C.A., Han, K.N., Choo, J., Lee, E.K., and Seong, G.H. Enzyme
Kinetic Measurements Using a Droplet-Based Microfluidic System with a
Concentration Gradient. Analytical Chemistry 83(5) (2011): 1603-1608.

[21]   Gu, S., et al. A droplet-based microfluidic electrochemical sensor using
platinum-black microelectrode and its application in high sensitive glucose
sensing. Biosensors and Bioelectronics 55(0) (2014): 106-112.

[22]   Ji, J., Zhao, Y., Guo, L., Liu, B., Ji, C., and Yang, P. Interfacial organic synthesis in
a simple droplet-based microfluidic system. Lab on a Chip 12(7) (2012): 1373-
1377.

[23]   Zhu, Y. and Fang, Q. Analytical detection techniques for droplet
microfluidics—A review. Analytica Chimica Acta 787(0) (2013): 24-35.

[24]   Hemmi, A., et al. A surface plasmon resonance sensor on a compact disk-type
microfluidic device. Journal of Separation Science 34(20) (2011): 2913-2919.

[25]   Lai, S., Wang, S., Luo, J., Lee, L.J., Yang, S.T., and Madou, M.J. Design of a
compact disk-like microfluidic platform for enzyme-linked immunosorbent
assay. Anal Chem 76(7) (2004): 1832-7.

[26]   Ghanim, M.H. and Abdullah, M.Z. Integrating amperometric detection with
electrophoresis microchip devices for biochemical assays: Recent
developments. Talanta 85(1) (2011): 28-34.

[27]   Lu, Q., Copper, C.L., and Collins, G.E. Ultraviolet absorbance detection of
colchicine and related alkaloids on a capillary electrophoresis microchip.
Analytica Chimica Acta 572(2) (2006): 205-211.

[28]   Siangproh, W., Chailapakul, O., Laocharoensuk, R., and Wang, J. Microchip
capillary electrophoresis/electrochemical detection of hydrazine compounds
at a cobalt phthalocyanine modified electrochemical detector. Talanta 67(5)
(2005): 903-907.

[29]   Martinez, A.W., Phillips, S.T., Whitesides, G.M., and Carrilho, E. Diagnostics for
the Developing World: Microfluidic Paper-Based Analytical Devices. Analytical
Chemistry 82(1) (2010): 3-10.

[30]   Nery, E.W. and Kubota, L.T. Sensing approaches on paper-based devices: a
review. Analytical and Bioanalytical Chemistry 405(24) (2013): 7573-7595.

[31]   Llopis, M., Sánchez, J., Priego, T., Palou, A., and Picó, C. Maternal Fat Supplementation during Late Pregnancy and Lactation Influences the Development of Hepatic Steatosis in Offspring Depending on the Fat Source. Journal of Agricultural and Food Chemistry 62(7) (2014): 1590-1601.

[32]   Apilux, A., Siangproh, W., Praphairaksit, N., and Chailapakul, O. Simple and rapid colorimetric detection of Hg(II) by a paper-based device using silver nanoplates. Talanta 97 (2012): 388-394.

[33]   Dungchai, W., Chailapakul, O., and Henry, C.S. Use of multiple colorimetric indicators for paper-based microfluidic devices. Analytica Chimica Acta 674(2) (2010): 227-233.

[34]   Konry, T., Dominguez-Villar, M., Baecher-Allan, C., Hafler, D.A., and Yarmush, M.L. Droplet-based microfluidic platforms for single T cell secretion analysis of IL-10 cytokine. Biosensors and Bioelectronics 26(5) (2011): 2707-2710.

[35]   Lignos, I., et al. Facile Droplet-based Microfluidic Synthesis of Monodisperse IV–VI Semiconductor Nanocrystals with Coupled In-Line NIR Fluorescence Detection. Chemistry of Materials 26(9) (2014): 2975-2982.

[36]   Hossain, S.M.Z. and Brennan, J.D. beta-Galactosidase-Based Colorimetric Paper Sensor for Determination of Heavy Metals. Analytical Chemistry 83(22) (2011): 8772-8778.

[37]   Ravindran, A., Elavarasi, M., Prathna, T.C., Raichur, A.M., Chandrasekaran, N., and Mukherjee, A. Selective colorimetric detection of nanomolar Cr (VI) in aqueous solutions using unmodified silver nanoparticles. Sensors and Actuators B-Chemical 166 (2012): 365-371.

[38]   Cecchini, M.P., et al. Ultrafast Surface Enhanced Resonance Raman Scattering Detection in Droplet-Based Microfluidic Systems. Analytical Chemistry 83(8) (2011): 3076-3081.

[39]   Chailapakul, O., Korsrisakul, S., Siangproh, W., and Grudpan, K. Fast and simultaneous detection of heavy metals using a simple and reliable microchip-electrochemistry route: An alternative approach to food analysis. Talanta 74(4) (2008): 683-689.

[40]   Lee, J., Musyimi, H.K., Soper, S.A., and Murray, K.K. Development of an Automated Digestion and Droplet Deposition Microfluidic Chip for MALDI-TOF MS. Journal of the American Society for Mass Spectrometry 19(7) (2008): 964-972.

[41]   Grundmann, M., Rothenhoefer, M., Bernhardt, G., Buschauer, A., and Matysik, F.-M. Fast counter-electroosmotic capillary electrophoresis-time-of-flight mass spectrometry of hyaluronan oligosaccharides. Analytical and Bioanalytical Chemistry 402(8) (2012): 2617-2623.

[42]   Hu, Y., Xu, W., Li, J., and Li, L. Determination of 5-hydroxytryptamine in serum by electrochemiluminescence detection with the aid of capillary electrophoresis. Luminescence 27(1) (2012): 63-68.

[43]   Ge, L., Yan, J., Song, X., Yan, M., Ge, S., and Yu, J. Three-dimensional paper-based electrochemiluminescence immunodevice for multiplexed measurement of biomarkers and point-of-care testing. Biomaterials 33(4) (2012): 1024-1031.

[44]   Jokerst, J.C., Adkins, J.A., Bisha, B., Mentele, M.M., Goodridge, L.D., and Henry, C.S. Development of a Paper-Based Analytical Device for Colorimetric Detection of Select Foodborne Pathogens. Analytical Chemistry 84(6) (2012): 2900-2907.

[45]   Bakker, E. and Qin, Y. Electrochemical Sensors. Analytical Chemistry 78(12) (2006): 3965-3984.

[46]   Kimmel, D.W., LeBlanc, G., Meschievitz, M.E., and Cliffel, D.E. Electrochemical Sensors and Biosensors. Analytical Chemistry 84(2) (2011): 685-707.

[47]   Bleam, W.F. Chapter 8 - Redox Chemistry. in Bleam, W.F. (ed.)Soil and Environmental Chemistry, pp. 321-370. Boston: Academic Press, 2012.

[48]   Panero, S. ELECTROCHEMICAL THEORY | Thermodynamics. in Garche, J. (ed.)Encyclopedia of Electrochemical Power Sources, pp. 1-7. Amsterdam: Elsevier, 2009.

[49]   Sohail, M. and De Marco, R. ELECTRODES | Ion-Selective Electrodes. in Reference Module in Chemistry, Molecular Sciences and Chemical Engineering: Elsevier, 2013.

[50]   Laborda, E., González, J., and Molina, Á. Recent advances on the theory of pulse techniques: A mini review. Electrochemistry Communications 43(0) (2014): 25-30.

[51]   Tiwari, I., Singh, M., Pandey, C.M., and Sumana, G. Electrochemical genosensor based on graphene oxide modified iron oxide–chitosan hybrid nanocomposite for pathogen detection. Sensors and Actuators B: Chemical 206(0) (2015): 276-283.

[52]   Lovrić, M. and Komorsky-Lovrić, Š. Theory of square wave voltammetry of three step electrode reaction. Journal of Electroanalytical Chemistry 735(0) (2014): 90-94.

[53]   Adeloju, S.B. AMPEROMETRY. in Poole, P.W.T. (ed.)Encyclopedia of Analytical Science (Second Edition), pp. 70-79. Oxford: Elsevier, 2005.

[54]   Kokkinos, C., Economou, A., Raptis, I., and Efstathiou, C.E. Lithographically fabricated disposable bismuth-film electrodes for the trace determination of Pb(II) and Cd(II) by anodic stripping voltammetry. Electrochimica Acta 53(16) (2008): 5294-5299.

[55]   Rogers, J.A. and Nuzzo, R.G. Recent progress in soft lithography. Materials Today 8(2) (2005): 50-56.

[56]   Lu, Y., Shi, W., Jiang, L., Qin, J., and Lin, B. Rapid prototyping of paper-based microfluidics with wax for low-cost, portable bioassay. Electrophoresis 30(9) (2009): 1497-1500.

[57]   Carrilho, E., Martinez, A.W., and Whitesides, G.M. Understanding Wax Printing: A Simple Micropatterning Process for Paper-Based Microfluidics. Analytical Chemistry 81(16) (2009): 7091-7095.

[58]   Jakel, R.J. and Maragos, W.F. Neuronal cell death in Huntington's disease: a potential role for dopamine. Trends in Neurosciences 23(6) (2000): 239-245.

[59]   Heien, M., et al. Real-time measurement of dopamine fluctuations after cocaine in the brain of behaving rats. Proceedings of the National Academy of Sciences of the United States of America 102(29) (2005): 10023-10028.

[60]   Bugamelli, F., Marcheselli, C., Barba, E., and Raggi, M.A. Determination of L-dopa, carbidopa, 3-O-methyldopa and entacapone in human plasma by

HPLC-ED. <u>Journal of Pharmaceutical and Biomedical Analysis</u> 54(3) (2011): 562-567.

[61] Liu, L., et al. Simultaneous determination of catecholamines and their metabolites related to Alzheimer's disease in human urine. <u>Journal of Separation Science</u> 34(10) (2011): 1198-1204.

[62] Lim, S.S., et al. A comparative risk assessment of burden of disease and injury attributable to 67 risk factors and risk factor clusters in 21 regions, 1990-2010: a systematic analysis for the Global Burden of Disease Study 2010. <u>Lancet</u> 380(9859) (2012): 2224-2260.

[63] Zhao, Y., Zhao, S., Huang, J., and Ye, F. Quantum dot-enhanced chemiluminescence detection for simultaneous determination of dopamine and epinephrine by capillary electrophoresis. <u>Talanta</u> 85(5) (2011): 2650-2654.

[64] Huang, H., Gao, Y., Shi, F., Wang, G., Shah, S.M., and Su, X. Determination of catecholamine in human serum by a fluorescent quenching method based on a water-soluble fluorescent conjugated polymer-enzyme hybrid system. <u>Analyst</u> 137(6) (2012): 1481-1486.

[65] Li, L., Liu, H., Shen, Y., Zhang, J., and Zhu, J.-J. Electrogenerated Chemiluminescence of Au Nanoclusters for the Detection of Dopamine. <u>Analytical Chemistry</u> 83(3) (2011): 661-665.

[66] Naccarato, A., Gionfriddo, E., Sindona, G., and Tagarelli, A. Development of a simple and rapid solid phase microextraction-gas chromatography–triple quadrupole mass spectrometry method for the analysis of dopamine, serotonin and norepinephrine in human urine. <u>Analytica Chimica Acta</u> 810(0) (2014): 17-24.

[67] Guan, Q. and Henry, C.S. Improving MCE with electrochemical detection using a bubble cell and sample stacking techniques. <u>Electrophoresis</u> 30(19) (2009): 3339-3346.

[68] Kumbhat, S., Shankaran, D.R., Kim, S.J., Gobi, K.V., Joshi, V., and Miura, N. Surface plasmon resonance biosensor for dopamine using D3 dopamine receptor as a biorecognition molecule. <u>Biosensors & Bioelectronics</u> 23(3) (2007): 421-427.

[69]   Herrasti, Z., Martínez, F., and Baldrich, E. Electrochemical detection of dopamine using streptavidin-coated magnetic particles and carbon nanotube wiring. Sensors and Actuators B: Chemical 203(0) (2014): 891-898.

[70]   Zhong, M., Teng, Y., Pang, S., Yan, L., and Kan, X. Pyrrole–phenylboronic acid: A novel monomer for dopamine recognition and detection based on imprinted electrochemical sensor. Biosensors and Bioelectronics 64(0) (2015): 212-218.

[71]   Siangproh, W., Dungchai, W., Rattanarat, P., and Chailapakul, O. Nanoparticle-based electrochemical detection in conventional and miniaturized systems and their bioanalytical applications: A review. Analytica Chimica Acta 690(1) (2011): 10-25.

[72]   Lakshmi, D., et al. Electrochemical Sensor for Catechol and Dopamine Based on a Catalytic Molecularly Imprinted Polymer-Conducting Polymer Hybrid Recognition Element. Analytical Chemistry 81(9) (2009): 3576-3584.

[73]   Hou, S., Kasner, M.L., Su, S., Patel, K., and Cuellari, R. Highly Sensitive and Selective Dopamine Biosensor Fabricated with Silanized Graphene. Journal of Physical Chemistry C 114(35) (2010): 14915-14921.

[74]   Baldrich, E. and Munoz, F.X. Carbon Nanotube Wiring: A Tool for Straightforward Electrochemical Biosensing at Magnetic Particles. Analytical Chemistry 83(24) (2011): 9244-9250.

[75]   Domenech, A., Garcia, H., Domenech-Carbo, M.T., and Galletero, M.S. 2,4,6-triphenylpyrylium ion encapsulated into zeolite Y as a selective electrode for the electrochemical determination of dopamine in the presence of ascorbic acid. Analytical Chemistry 74(3) (2002): 562-569.

[76]   Sathisha, T.V., Kumara Swamy, B.E., Chandrashekar, B.N., Thomas, N., and Eswarappa, B. Selective determination of dopamine in presence of ascorbic acid and uric acid at hydroxy double salt/surfactant film modified carbon paste electrode. Journal of Electroanalytical Chemistry 674(0) (2012): 57-64.

[77]   dos Reis, A.P., Tarley, C.R.T., Maniasso, N., and Kubota, L.T. Exploiting micellar environment for simultaneous electrochemical determination of ascorbic acid and dopamine. Talanta 67(4) (2005): 829-835.

[78]   Liu, S.-Q., Sun, W.-H., and Hu, F.-T. Graphene nano sheet-fabricated electrochemical sensor for the determination of dopamine in the presence of ascorbic acid using cetyltrimethylammonium bromide as the discriminating agent. Sensors and Actuators B: Chemical 173(0) (2012): 497-504.

[79]   Shahrokhian, S. and Zare-Mehrjardi, H.R. Cobalt salophen-modified carbon-paste electrode incorporating a cationic surfactant for simultaneous voltammetric detection of ascorbic acid and dopamine. Sensors and Actuators B: Chemical 121(2) (2007): 530-537.

[80]   Niranjana, E., Kumara Swamy, B.E., Raghavendra Naik, R., Sherigara, B.S., and Jayadevappa, H. Electrochemical investigations of potassium ferricyanide and dopamine by sodium dodecyl sulphate modified carbon paste electrode: A cyclic voltammetric study. Journal of Electroanalytical Chemistry 631(1–2) (2009): 1-9.

[81]   Zheng, J. and Zhou, X. Sodium dodecyl sulfate-modified carbon paste electrodes for selective determination of dopamine in the presence of ascorbic acid. Bioelectrochemistry 70(2) (2007): 408-415.

[82]   Atta, N.F., Galal, A., and Ahmed, R.A. Poly(3,4-ethylene-dioxythiophene) electrode for the selective determination of dopamine in presence of sodium dodecyl sulfate. Bioelectrochemistry 80(2) (2011): 132-141.

[83]   Sameenoi, Y., et al. Microfluidic Paper-Based Analytical Device for Aerosol Oxidative Activity. Environmental Science & Technology 47(2) (2013): 932-940.

[84]   Mentele, M.M., Cunningham, J., Koehler, K., Volckens, J., and Henry, C.S. Microfluidic Paper-Based Analytical Device for Particulate Metals. Analytical Chemistry 84(10) (2012): 4474-4480.

[85]   Shen, L., Hagen, J.A., and Papautsky, I. Point-of-care colorimetric detection with a smartphone. Lab on a Chip 12(21) (2012): 4240-4243.

[86]   Dungchai, W., Chailapakul, O., and Henry, C.S. Electrochemical Detection for Paper-Based Microfluidics. Analytical Chemistry 81(14) (2009): 5821-5826.

[87]   Nie, Z., et al. Electrochemical sensing in paper-based microfluidic devices. Lab on a Chip 10(4) (2010): 477-483.

[88]   Dossi, N., et al. An electrochemical gas sensor based on paper supported room temperature ionic liquids. Lab on a Chip 12(1) (2012): 153-158.

[89]   Tan, S.N., Ge, L., and Wang, W. Paper Disk on Screen Printed Electrode for One-Step Sensing with an Internal Standard. Analytical Chemistry 82(21) (2010): 8844-8847.

[90]   Bugamelli, F., Marcheselli, C., Barba, E., and Raggi, M.A. Determination of l-dopa, carbidopa, 3-O-methyldopa and entacapone in human plasma by HPLC–ED. Journal of Pharmaceutical and Biomedical Analysis 54(3) (2011): 562-567.

[91]   Rattanarat, P., Dungchai, W., Siangproh, W., Chailapakul, O., and Henry, C.S. Sodium dodecyl sulfate-modified electrochemical paper-based analytical device for determination of dopamine levels in biological samples. Analytica Chimica Acta 744 (2012): 1-7.

[92]   Alarcon-Angeles, G., Corona-Avendano, S., Palomar-Pardave, M., Rojas-Hernandez, A., Romero-Romo, M., and Teresa Ramirez-Silva, M. Selective electrochemical determination of dopamine in the presence of ascorbic acid using sodium dodecyl sulfate micelles as masking agent. Electrochimica Acta 53(6) (2008): 3013-3020.

[93]   Rusling, J.F. Molecular aspects of electron transfer at electrodes in micellar solutions. Colloids and Surfaces A: Physicochemical and Engineering Aspects 123–124(0) (1997): 81-88.

[94]   Huang, S.-H., Liao, H.-H., and Chen, D.-H. Simultaneous determination of norepinephrine, uric acid, and ascorbic acid at a screen printed carbon electrode modified with polyacrylic acid-coated multi-wall carbon nanotubes. Biosensors & Bioelectronics 25(10) (2010): 2351-2355.

[95]   Hinoue, T., Kuwamoto, N., and Watanabe, I. Voltammetry using an electrode surface continuously renewed by laser ablation and its demonstration on electro-oxidation of L-ascorbic acid. Journal of Electroanalytical Chemistry 466(1) (1999): 31-37.

[96]   Pumera, M. Microchip-based electrochromatography: designs and applications. Talanta 66(4) (2005): 1048-1062.

[97]   Sundberg, S.A., Chow, A., Nikiforov, T., and Wada, H.G. Microchip-based systems for target validation and HTS. Drug Discovery Today 5(12, Supplement 1) (2000): 92-103.

[98]   Hugon, O., et al. Cell imaging by coherent backscattering microscopy using frequency-shifted optical feedback in a microchip laser. Ultramicroscopy 108(6) (2008): 523-528.

[99]   Liu, R., Ishimatsu, R., Yahiro, M., Adachi, C., Nakano, K., and Imato, T. Photometric flow injection determination of phosphate on a PDMS microchip using an optical detection system assembled with an organic light emitting diode and an organic photodiode. Talanta 132(0) (2015): 96-105.

[100]   He, X., Chen, Q., Zhang, Y., and Lin, J.-M. Recent advances in microchip-mass spectrometry for biological analysis. TrAC Trends in Analytical Chemistry 53(0) (2014): 84-97.

[101]   Nolte, D.D. Invited Review Article: Review of centrifugal microfluidic and bio-optical disks. Rev Sci Instrum 80(10) (2009): 3236681.

[102]   Vázquez, M., Brabazon, D., Shang, F., Omamogho, J.O., Glennon, J.D., and Paull, B. Centrifugally-driven sample extraction, preconcentration and purification in microfluidic compact discs. TrAC Trends in Analytical Chemistry 30(10) (2011): 1575-1586.

[103]   Hwang, H., Kim, Y., Cho, J., Lee, J.-y., Choi, M.-S., and Cho, Y.-K. Lab-on-a-Disc for Simultaneous Determination of Nutrients in Water. Analytical Chemistry 85(5) (2013): 2954-2960.

[104]   Kim, N., Dempsey, C.M., Zoval, J.V., Sze, J.-Y., and Madou, M.J. Automated microfluidic compact disc (CD) cultivation system of Caenorhabditis elegans. Sensors and Actuators B: Chemical 122(2) (2007): 511-518.

[105]   Trojanowicz, M. Recent developments in electrochemical flow detections—A review: Part I. Flow analysis and capillary electrophoresis. Analytica Chimica Acta 653(1) (2009): 36-58.

[106]   Heller, A. and Feldman, B. Electrochemical Glucose Sensors and Their Applications in Diabetes Management. Chemical Reviews 108(7) (2008): 2482-2505.

[107] Jia, W.-Z., Wang, K., and Xia, X.-H. Elimination of electrochemical interferences in glucose biosensors. TrAC Trends in Analytical Chemistry 29(4) (2010): 306-318.

[108] Rodthongkum, N., Ruecha, N., Rangkupan, R., Vachet, R.W., and Chailapakul, O. Graphene-loaded nanofiber-modified electrodes for the ultrasensitive determination of dopamine. Analytica Chimica Acta 804(0) (2013): 84-91.

[109] Ruecha, N., Rangkupan, R., Rodthongkum, N., and Chailapakul, O. Novel paper-based cholesterol biosensor using graphene/polyvinylpyrrolidone/polyaniline nanocomposite. Biosensors and Bioelectronics 52(0) (2014): 13-19.

[110] Hao, Q., Wang, H., Yang, X., Lu, L., and Wang, X. Morphology-controlled fabrication of sulfonated graphene/polyaniline nanocomposites by liquid/liquid interfacial polymerization and investigation of their electrochemical properties. Nano Research 4(4) (2011): 323-333.

[111] Wang, K., Xu, J.-J., and Chen, H.-Y. A novel glucose biosensor based on the nanoscaled cobalt phthalocyanine–glucose oxidase biocomposite. Biosensors and Bioelectronics 20(7) (2005): 1388-1396.

[112] Castro Júnior, J.G.M., Ferreira, G.M.M., de Oliveira, F.G., Damos, F.S., and Luz, R.d.C.S. A novel platform based on graphene/poly(3,4-ethylenedioxythiophene)/iron (III) hexacyanoferrate (II) composite film for electrocatalytic reduction of H2O2. Journal of Electroanalytical Chemistry 732(0) (2014): 93-100.

[113] Liu, H. and Crooks, R.M. Highly reproducible chronoamperometric analysis in microdroplets. Lab on a Chip 13(7) (2013): 1364-1370.

[114] Tian, K., Prestgard, M., and Tiwari, A. A review of recent advances in nonenzymatic glucose sensors. Materials Science and Engineering: C 41(0) (2014): 100-118.

[115] Lin, K.-C., Lin, Y.-C., and Chen, S.-M. A highly sensitive nonenzymatic glucose sensor based on multi-walled carbon nanotubes decorated with nickel and copper nanoparticles. Electrochimica Acta 96(0) (2013): 164-172.

[116] Sun, C.-L., Cheng, W.-L., Hsu, T.-K., Chang, C.-W., Chang, J.-L., and Zen, J.-M. Ultrasensitive and highly stable nonenzymatic glucose sensor by a

CuO/graphene-modified screen-printed carbon electrode integrated with flow-injection analysis. Electrochemistry Communications 30(0) (2013): 91-94.

[117] Park, S., Boo, H., and Chung, T.D. Electrochemical non-enzymatic glucose sensors. Analytica Chimica Acta 556(1) (2006): 46-57.

[118] Vijayakaran, K., et al. Arsenic reduces the antipyretic activity of paracetamol in rats: Modulation of brain COX-2 activity and CB1 receptor expression. Environmental Toxicology and Pharmacology 37(1) (2014): 438-447.

[119] Shiroma, L.Y., Santhiago, M., Gobbi, A.L., and Kubota, L.T. Separation and electrochemical detection of paracetamol and 4-aminophenol in a paper-based microfluidic device. Analytica Chimica Acta 725(0) (2012): 44-50.

[120] Yin, H., Ma, Q., Zhou, Y., Ai, S., and Zhu, L. Electrochemical behavior and voltammetric determination of 4-aminophenol based on graphene–chitosan composite film modified glassy carbon electrode. Electrochimica Acta 55(23) (2010): 7102-7108.

[121] Brega, A., Prandini, P., Amaglio, C., and Pafumi, E. Determination of phenol, m-, o- and p-cresol, p-aminophenol and p-nitrophenol in urine by high-performance liquid chromatography. Journal of Chromatography A 535(0) (1990): 311-316.

[122] Zou, C.-M., Yu, H., and Wang, M.-Y. Determination of tetraethyl ammonium by ion-pair chromatography with indirect ultraviolet detection using 4-aminophenol hydrochloride as background ultraviolet absorbing reagent. Chinese Chemical Letters 25(2) (2014): 201-204.

[123] Schultz, B. Determination of 4-aminophenol in water by high-performance liquid chromatography with fluorescence detection. Journal of Chromatography A 299(0) (1984): 484-486.

[124] Lourenção, B.C., Medeiros, R.A., Rocha-Filho, R.C., Mazo, L.H., and Fatibello-Filho, O. Simultaneous voltammetric determination of paracetamol and caffeine in pharmaceutical formulations using a boron-doped diamond electrode. Talanta 78(3) (2009): 748-752.

[125] Chu, Q., Jiang, L., Tian, X., and Ye, J. Rapid determination of acetaminophen and p-aminophenol in pharmaceutical formulations using miniaturized

capillary electrophoresis with amperometric detection. Analytica Chimica Acta 606(2) (2008): 246-251.

[126]   Pérez-Ruiz, T., Martínez-Lozano, C., Tomás, V., and Galera, R. Migration behaviour and separation of acetaminophen and p-aminophenol in capillary zone electrophoresis: Analysis of drugs based on acetaminophen. Journal of Pharmaceutical and Biomedical Analysis 38(1) (2005): 87-93.

[127]   Bloomfield, M.S. A sensitive and rapid assay for 4-aminophenol in paracetamol drug and tablet formulation, by flow injection analysis with spectrophotometric detection. Talanta 58(6) (2002): 1301-1310.

[128]   Vishnikin, A.B., et al. Highly sensitive sequential injection determination of p-aminophenol in paracetamol formulations with 18-molybdodiphosphate heteropoly anion based on elimination of Schlieren effect. Talanta 96(0) (2012): 230-235.

[129]   Yang, C.-G., Xu, Z.-R., and Wang, J.-H. Manipulation of droplets in microfluidic systems. TrAC Trends in Analytical Chemistry 29(2) (2010): 141-157.

[130]   Ramaswamy, B., Yeh, Y.-T.T., and Zheng, S.-Y. Microfluidic device and system for point-of-care blood coagulation measurement based on electrical impedance sensing. Sensors and Actuators B: Chemical 180(0) (2013): 21-27.

[131]   Park, S., Zhang, Y., Lin, S., Wang, T.-H., and Yang, S. Advances in microfluidic PCR for point-of-care infectious disease diagnostics. Biotechnology Advances 29(6) (2011): 830-839.

[132]   Atalay, Y.T., et al. Microfluidic analytical systems for food analysis. Trends in Food Science & Technology 22(7) (2011): 386-404.

[133]   Safavieh, M., Nahar, S., Zourob, M., and Ahmed, M.U. 15 - Microfluidic biosensors for high throughput screening of pathogens in food. in Bhunia, A.K., Kim, M.S., and Taitt, C.R. (eds.),High Throughput Screening for Food Safety Assessment, pp. 327-357: Woodhead Publishing, 2015.

[134]   Guo, Z.-X., et al. Valve-based microfluidic droplet micromixer and mercury (II) ion detection. Sensors and Actuators A: Physical 172(2) (2011): 546-551.

[135]   Teychené, S. and Biscans, B. Crystal nucleation in a droplet based microfluidic crystallizer. Chemical Engineering Science 77(0) (2012): 242-248.

[136]   Tsuchiya, H., Okochi, M., Nagao, N., Shikida, M., and Honda, H. On-chip polymerase chain reaction microdevice employing a magnetic droplet-manipulation system. Sensors and Actuators B: Chemical 130(2) (2008): 583-588.

[137]   Clausell-Tormos, J., et al. Droplet-Based Microfluidic Platforms for the Encapsulation and Screening of Mammalian Cells and Multicellular Organisms. Chemistry & Biology 15(5) (2008): 427-437.

[138]   Aubry, G., Méance, S., Couraud, L., Haghiri-Gosnet, A.M., and Kou, Q. Intracavity microfluidic dye laser droplet absorption. Microelectronic Engineering 86(4–6) (2009): 1368-1370.

[139]   Wang, J. Electrochemical detection for microscale analytical systems: a review. Talanta 56(2) (2002): 223-231.

[140]   Han, Z., Li, W., Huang, Y., and Zheng, B. Measuring Rapid Enzymatic Kinetics by Electrochemical Method in Droplet-Based Microfluidic Devices with Pneumatic Valves. Analytical Chemistry 81(14) (2009): 5840-5845.

[141]   Itoh, D., Sassa, F., Nishi, T., Kani, Y., Murata, M., and Suzuki, H. Droplet-based microfluidic sensing system for rapid fish freshness determination. Sensors and Actuators B: Chemical 171–172(0) (2012): 619-626.

[142]   Wu, S., He, Q., Tan, C., Wang, Y., and Zhang, H. Graphene-Based Electrochemical Sensors. Small 9(8) (2013): 1160-1172.

[143]   Thammasoontaree, N., Rattanarat, P., Ruecha, N., Siangproh, W., Rodthongkum, N., and Chailapakul, O. Ultra-performance liquid chromatography coupled with graphene/polyaniline nanocomposite modified electrode for the determination of sulfonamide residues. Talanta 123(0) (2014): 115-121.

[144]   Dong, Y.-P., Zhang, J., Ding, Y., Chu, X.-F., and Chen, J. Electrogenerated chemiluminescence of luminol at a polyaniline/graphene modified electrode in neutral solution. Electrochimica Acta 91(0) (2013): 240-245.

[145]   Asadian, E., Shahrokhian, S., zad, A.I., and Jokar, E. In-situ electro-polymerization of graphene nanoribbon/polyaniline composite film:

Application to sensitive electrochemical detection of dobutamine. Sensors and Actuators B: Chemical 196(0) (2014): 582-588.

[146] Li, J., et al. Electrochemical immunosensor based on graphene–polyaniline composites and carboxylated graphene oxide for estradiol detection. Sensors and Actuators B: Chemical 188(0) (2013): 99-105.

[147] Huang, J., et al. Electrochemical immunosensor based on polyaniline/poly (acrylic acid) and Au-hybrid graphene nanocomposite for sensitivity enhanced detection of salbutamol. Food Research International 44(1) (2011): 92-97.

[148] Tice, J.D., Lyon, A.D., and Ismagilov, R.F. Effects of viscosity on droplet formation and mixing in microfluidic channels. Analytica Chimica Acta 507(1) (2004): 73-77.

[149] Németh, T., Jankovics, P., Németh-Palotás, J., and Kőszegi-Szalai, H. Determination of paracetamol and its main impurity 4-aminophenol in analgesic preparations by micellar electrokinetic chromatography. Journal of Pharmaceutical and Biomedical Analysis 47(4–5) (2008): 746-749.

[150] Fan, Y., Liu, J.-H., Yang, C.-P., Yu, M., and Liu, P. Graphene–polyaniline composite film modified electrode for voltammetric determination of 4-aminophenol. Sensors and Actuators B: Chemical 157(2) (2011): 669-674.

[151] Abdolmohammad-Zadeh, H. and Sadeghi, G.H. A nano-structured material for reliable speciation of chromium and manganese in drinking waters, surface waters and industrial wastewater effluents. Talanta 94 (2012): 201-208.

[152] Han, Z., Qi, L., Shen, G., Liu, W., and Chen, Y. Determination of chromium(VI) by surface plasmon field-enhanced resonance light scattering. Analytical Chemistry 79(15) (2007): 5862-5868.

[153] Zhao, L., Jin, Y., Yan, Z., Liu, Y., and Zhu, H. Novel, highly selective detection of Cr(III) in aqueous solution based on a gold nanoparticles colorimetric assay and its application for determining Cr(VI). Analytica Chimica Acta 731 (2012): 75-81.

[154] Katz, S.A. and Salem, H. THE TOXICOLOGY OF CHROMIUM WITH RESPECT TO ITS CHEMICAL SPECIATION - A REVIEW. Journal of Applied Toxicology 13(3) (1993): 217-224.

[155] Sedman, R.M., Beaumont, J., McDonald, T.A., Reynolds, S., Krowech, G., and Howd, R. Review of the evidence regarding the carcinogenicity of hexavalent chromium in drinking water. Journal of Environmental Science and Health Part C-Environmental Carcinogenesis & Ecotoxicology Reviews 24(1) (2006): 155-182.

[156] Hayes, R.B. The carcinogenicity of metals in humans. Cancer Causes & Control 8(3) (1997): 371-385.

[157] Wang, J., Ashley, K., Kennedy, E.R., and Neumeister, C. Determination of hexavalent chromium in industrial hygiene samples using ultrasonic extraction and flow injection analysis. Analyst 122(11) (1997): 1307-1312.

[158] Talebi, S.M. Determination of total and hexavalent chromium concentrations in the atmosphere of the city of Isfahan. Environmental Research 92(1) (2003): 54-56.

[159] Powell, M.J., Boomer, D.W., and Wiederin, D.R. DETERMINATION OF CHROMIUM SPECIES IN ENVIRONMENTAL-SAMPLES USING HIGH-PRESSURE LIQUID-CHROMATOGRAPHY DIRECT-INJECTION NEBULIZATION AND INDUCTIVELY-COUPLED PLASMA-MASS SPECTROMETRY. Analytical Chemistry 67(14) (1995): 2474-2478.

[160] Huang, Y.L., Chuang, I.C., Pan, C.H., Hsiech, C., Shi, T.S., and Lin, T.H. Determination of chromium in whole blood and urine by graphite furnace AAS. Atomic Spectroscopy 21(1) (2000): 10-16.

[161] Tsuyumoto, I. and Maruyama, Y. X-ray Fluorescence Analysis of Hexavalent Chromium Using K beta Satellite Peak Observed as Counterpart of X-ray Absorption Near-Edge Structure Pre-Edge Peak. Analytical Chemistry 83(19) (2011): 7566-7569.

[162] Martinez, A.W., et al. Programmable diagnostic devices made from paper and tape. Lab on a Chip 10(19) (2010): 2499-2504.

[163] Parolo, C. and Merkoci, A. Paper-based nanobiosensors for diagnostics. Chemical Society Reviews 42(2) (2013): 450-457.

[164]   Vella, S.J., et al. Measuring Markers of Liver Function Using a Micropatterned Paper Device Designed for Blood from a Fingerstick. Analytical Chemistry 84(6) (2012): 2883-2891.

[165]   Hossain, S.M.Z., Luckham, R.E., McFadden, M.J., and Brennan, J.D. Reagentless Bidirectional Lateral Flow Bioactive Paper Sensors for Detection of Pesticides in Beverage and Food Samples. Analytical Chemistry 81(21) (2009): 9055-9064.

[166]   Hossain, S.M.Z., et al. Multiplexed paper test strip for quantitative bacterial detection. Analytical and Bioanalytical Chemistry 403(6) (2012): 1567-1576.

[167]   Apilux, A., Dungchai, W., Siangproh, W., Praphairaksit, N., Henry, C.S., and Chailapakul, O. Lab-on-Paper with Dual Electrochemical/Colorimetric Detection for Simultaneous Determination of Gold and Iron. Analytical Chemistry 82(5) (2010): 1727-1732.

[168]   Yang, X. and Wang, E. A Nanoparticle Autocatalytic Sensor for Ag+ and Cu2+ Ions in Aqueous Solution with High Sensitivity and Selectivity and Its Application in Test Paper. Analytical Chemistry 83(12) (2011): 5005-5011.

[169]   Whitaker, M.J. Determination of total chromium by flow injection analysis. Analytica Chimica Acta 174(0) (1985): 375-378.

[170]   Kong, F. and Ni, Y. DEVELOPMENT OF CELLULOSIC PAPER-BASED TEST STRIPS FOR Cr(VI) DETERMINATION. Bioresources 4(3) (2009): 1088-1097.

[171]   Andersen, J.E.T. Introduction of hydrogen peroxide as an oxidant in flow injection analysis: speciation of Cr(III) and Cr(VI). Analytica Chimica Acta 361(1-2) (1998): 125-131.

[172]   Lichtin, J.J. Perchloric acid as oxidizing agent in the determination of chromium. Industrial & Engineering Chemistry Analytical Edition 2(1) (1930): 126-127.

[173]   Balasubramanian, N. and Maheswari, V. Indirect spectrophotometric determination of chromium. Journal of Aoac International 79(4) (1996): 989-994.

[174]   Lai, Y.-J. and Tseng, W.-L. Role of 5-thio-(2-nitrobenzoic acid)-capped gold nanoparticles in the sensing of chromium(VI): remover and sensor. Analyst 136(13) (2011): 2712-2717.

[175]   Stover, N.M. DIPHENYLCARBAZIDE AS A TEST FOR CHROMIUM. <u>Journal of the American Chemical Society</u> 50(9) (1928): 2363-2366.

[176]   Saha, B., Gill, R.J., Bailey, D.G., Kabay, N., and Arda, M. Sorption of Cr(VI) from aqueous solution by Amberlite XAD-7 resin impregnated with Aliquat 336. <u>Reactive & Functional Polymers</u> 60 (2004): 223-244.

[177]   Brook, R.D. and Rajagopalan, S. Particulate matter, air pollution, and blood pressure. <u>Journal of the American Society of Hypertension</u> 3(5) (2009): 332-350.

[178]   Di Pietro, A., et al. Oxidative damage in human epithelial alveolar cells exposed in vitro to oil fly ash transition metals. <u>International Journal of Hygiene and Environmental Health</u> 212(2) (2009): 196-208.

[179]   Hou, L., et al. Airborne particulate matter and mitochondrial damage: a cross-sectional study. <u>Environmental Health</u> 9 (2010).

[180]   Kuhn, H.R. and Gunther, D. Elemental fractionation studies in laser ablation inductively coupled plasma mass spectrometry on laser-induced brass aerosols. <u>Analytical Chemistry</u> 75(4) (2003): 747-753.

[181]   Kuvarega, A.T. and Taru, P. Ambiental dust speciation and metal content variation in TSP, PM10 and PM2.5 in urban atmospheric air of Harare (Zimbabwe). <u>Environmental Monitoring and Assessment</u> 144(1-3) (2008): 1-14.

[182]   Gubala, V., Harris, L.F., Ricco, A.J., Tan, M.X., and Williams, D.E. Point of Care Diagnostics: Status and Future. <u>Analytical Chemistry</u> 84(2) (2012): 487-515.

[183]   Lankelma, J., Nie, Z., Carrilho, E., and Whitesides, G.M. Paper-Based Analytical Device for Electrochemical Flow-Injection Analysis of Glucose in Urine. <u>Analytical Chemistry</u> 84(9) (2012): 4147-4152.

[184]   Liu, H. and Crooks, R.M. Three-Dimensional Paper Microfluidic Devices Assembled Using the Principles of Origami. <u>Journal of the American Chemical Society</u> 133(44) (2011): 17564-17566.

[185]   Rattanarat, P., et al. A microfluidic paper-based analytical device for rapid quantification of particulate chromium. <u>Analytica Chimica Acta</u> 800 (2013): 50-55.

[186]   Murdock, R.C., Shen, L., Griffin, D.K., Kelley-Loughnane, N., Papautsky, I., and
Hagen, J.A. Optimization of a Paper-Based ELISA for a Human Performance
Biomarker. Analytical Chemistry 85(23) (2013): 11634-11642.

[187]   Hwang, G.-H., Han, W.-K., Park, J.-S., and Kang, S.-G. An electrochemical sensor
based on the reduction of screen-printed bismuth oxide for the
determination of trace lead and cadmium. Sensors and Actuators B-Chemical
135(1) (2008): 309-316.

[188]   Wang, J., Lu, J.M., Hocevar, S.B., Farias, P.A.M., and Ogorevc, B. Bismuth-coated
carbon electrodes for anodic stripping voltammetry. Analytical Chemistry
72(14) (2000): 3218-3222.

[189]   Keawkim, K., Chuanuwatanakul, S., Chailapakul, O., and Motomizu, S.
Determination of lead and cadmium in rice samples by sequential
injection/anodic stripping voltammetry using a bismuth film/crown
ether/Nafion modified screen-printed carbon electrode. Food Control 31(1)
(2013): 14-21.

[190]   Martiniano, L.C., et al. Direct simultaneous determination of Pb(II) and Cu(II) in
biodiesel by anodic stripping voltammetry at a mercury-film electrode using
microemulsions. Fuel 103 (2013): 1164-1167.

[191]   Ashley, K., Mapp, K.J., and Millson, M. Ultrasonic extraction and field portable
anodic stripping voltammetry for the determination of lead in workplace air
samples. American Industrial Hygiene Association Journal 59(10) (1998): 671-
679.

[192]   Buzica, D., Gerboles, M., Borowiak, A., Trincherini, P., Passarella, R., and
Pedroni, V. Comparison of voltammetry and inductively coupled plasma-mass
spectrometry for the determination of heavy metals in PM10 airborne
particulate matter. Atmospheric Environment 40(25) (2006): 4703-4710.

[193]   Shaw, M.J. and Haddad, P.R. The determination of trace metal pollutants in
enviromental matrices using ion chromatography. Environment International
30(3) (2004): 403-431.

[194]   Barcelo-Quintal, M.H., Manzanilla-Cano, J.A., Reyes-Salas, E.O., and Flores-
Rodriguez, J. Implementation of a differential pulse anodic stripping

voltammetry (DPASV) at a hanging mercury drop electrode (HMDE) procedure for the analysis of airborne heavy metals. Analytical Letters 34(13) (2001): 2349-2360.

[195]   Chaiyo, S., Chailapakul, O., Sakai, T., Teshima, N., and Siangproh, W. Highly sensitive determination of trace copper in food by adsorptive stripping voltammetry in the presence of 1,10-phenanthroline. Talanta 108 (2013): 1-6.

[196]   Nieboer, E., Thomassen, Y., Chashchin, V., and Odland, J.O. Occupational exposure assessment of metals. Journal of Environmental Monitoring 7(5) (2005): 412-415.

[197]   Hwang, G.H., Han, W.K., Park, J.S., and Kang, S.G. Determination of trace metals by anodic stripping voltammetry using a bismuth-modified carbon nanotube electrode. Talanta 76(2) (2008): 301-308.

[198]   Kadara, R.O. and Tothill, L.E. Resolving the copper interference effect on the stripping chronopotentiometric response of lead(II) obtained at bismuth film screen-printed electrode. Talanta 66(5) (2005): 1089-1093.

VITA

Mr. Poomrat Rattanarat was born in August 4, 1987. He is the eldest son of Mr. Udorn Rattanarat and Mrs. Ranee Rattanarat. He studied his elementary school at Bangbua School. He finished high school from Horwang School and received his Bachelor Degree in Science, majoring in Chemistry with 2nd Honor, from Srinakarinwirot University. He received Bachelor Degree's full scholarships from Science Achievement Scholarship of Thailand (SAST) from Office of the Higher Education Commission. During his Ph.D., he also received scholarship from Thailand Research Fund through The Royal Golden Jubilee Ph.D. Program (RGJ-Ph.D.). Mr. Poomrat was a visiting scholar at Henry's research lab, Chemistry Department, Colorado University, USA. He was also internship student at Imato Research Group, Kyushu University, Japan. His research interest areas focus on a miniaturized analytical system, paper-based analytical device, polymer microfluidics, colorimetric and electrochemical sensors, point-of-care testing and environmental monitoring.

AWARD

2014   Silver Metal Award at 2014 Taipei International Invention Show & Technomart, Taipei, Taiwan.

2014   Honor of Invention Award from World Invention Intellectual Property Associations (WIIPA) at 2014 Taipei International Invention Show & Technomart, Taipei, Taiwan.

2014   Outstanding poster presentation at Pure and Applied Chemistry International Conference 2014 (PACCON2014), Khonkhen, Thailand.

2013   Analytical Sciences Poster Presentation Award at ASIANALYSIS XII Conference, Fukuoka, Japan.

PUBLICATIONS

1.   **Rattanarat, P.**, Suea-Ngam, A., Ruecha, N., Siangproh, W., Henry, C. S., Srisa-Art, M., and Chailapakul, O. High-throughput Determination of 4-Aminophenol

using a Graphene-Polyaniline Modified Electrochemical Droplet-Based Microfluidic Sensor. Analyst (2014) *submitted*.

2. **Rattanarat, P.**, Teengam, P., Siangproh, W., Ishimatsu, R., Nakano, K., Chailapakul, O., and Imato, T. An Electrochemical Compact Disk-type for Use as an Enzymatic Biosensor. Electroanalysis (2014) *in press*.

3. Promphet, N., **Rattanarat, P.**, Rangkupan, R., Chailapakul, O., and Rodthongkum, N. An electrochemical sensor based on graphene/polyaniline/polystyrene nanoporous fibers modified electrode for simultaneous determination of lead and cadmium. Sensors and Actuators B: Chemical 207 (2015): 526-534.

4. Ekabutr, P., Sangsanoh, P., **Rattanarat, P.**, Monroe, C. W., Chailapakul, O., and Supaphol, P. Development of a Disposable Electrode Modified with Carbonized, Graphene-Loaded Nanofiber for the Detection of Dopamine in Human Serum. Journal of Applied Polymer Science 131 (2014): 40858.

5. Kiatkumjorn, T., **Rattanarat, P.**, Siangproh, W., Chailapakul, O., and Praphairaksit, N. Glutathione and l-cysteine modified silver nanoplates-based colorimetric assay for a simple, fast, sensitive and selective determination of nickel. Talanta 128 (2014): 215-220.

6. **Rattanarat, P.**, Dungchai, W., Cate, D. M., Volckens, J., Chailapakul, O., and Henry, C. S. Multilayer Paper-Based Device for Colorimetric and Electrochemical Quantification of Metals. Analytical Chemistry 86 (2014): 3555-3562.

7. Thammasoontaree, N., **Rattanarat, P.**, Ruecha, N., Siangproh, W., Rodthongkum, N., and Chailapakul, O. Ultra-performance liquid chromatography coupled with graphene/polyaniline nanocomposite modified electrode for the determination of sulfonamide residues Talanta, 123 (2014): 115-121.

8. **Rattanarat, P.**, Dungchai, W., Siangproh, W., Cate, D. M., Volckens, J., Chailapakul, O., and Henry, C. S. A Microfluidic Paper-based Analytical Device

for Rapid Quantification of Particulate Chromium. <u>Analytica Chimica Acta</u> 800 (2013): 50-55.

9.   Tee-ngam, P., Nunant, N., **Rattanarat, P.**, Siangproh, W., and Chailapakul, O. Simple and Rapid Determination of Ferulic Acid Levels in Food and Cosmetic Samples using Paper-based Platforms. <u>Sensors</u> 13 (2013): 13039-13053.

10.   **Rattanarat, P.**, Dungchai, W., Siangproh, W., Chailapakul, O., and Henry, C. S. Sodium Dodecyl Sulfate-modified Electrochemical Paper-based Analytical Device for Determination of Dopamine Levels in Biological samples. <u>Analytica Chimica Acta</u> 744 (2012): 1-7.

11.   Siangproh, W., Dungchai, W., **Rattanarat, P.**, and Chailapakul, O. Nanoparticle-based Electrochemical Detection in Conventional and Miniaturized Systems and Their Bioanalytical Application: A Review. <u>Analytica Chimica Acta</u> 690 (2011): 10-25.

12.   Siangproh, W., **Rattanarat, P.**, and Chailapakul, O. Reverse-phase Liquid Chromatographic Determination of α-lipoic Acid in Dietary Supplements using Boron-Doped Diamond Electrode. <u>Journal of Chromatography A</u> 1217 (2010): 7699-7705.